REPORT DOCUMENTATION PAGE

AFOSR-TR-97

0513

1. AGENCY USE ONLY *(Leave Blank)*	2. REPORT DATE	3. REPORT TYPE AND DATES COVERED
	September 1997	Final Technical Report 04/15/94-09/14/97

4. TITLE AND SUBTITLE

Rate Dependent Cohesive Zones

5. FUNDING NUMBERS

C F49620-94-C-0030

4. AUTHOR(S)

B.N. Cox

7. PERFORMING ORGANIZATION NAME(S) AND ADDRESS(ES)

ROCKWELL SCIENCE CENTER, LLC
1045 CAMINO DOS RIOS
THOUSAND OAKS, CA 91360

7. PERFORMING ORGANIZATION REPORT NUMBER

SC 71100

9. SPONSORING / MONITORING AGENCY NAME(S) AND ADDRESS(ES)

Air Force Office of Scientific Research/NA
Directorate of Aerospace and Engineering
110 Duncan Ave., Room B115
Bolling AFB, DC 20332-001

9. SPONSORING / MONITORING AGENCY REPORT NUMBER

11. SUPPLEMENTARY NOTES

12a. DISTRIBUTING/AVAILABILITY STATEMENT

Distribution Statement A. Approved for public release; distribution is unlimited.

12b. DISTRIBUTION CODE

13. ABSTRACT *(Maximum 200 Words)*

In work under another contract, we had studied the initiation of mode I tensile cracks (not delamination cracks) that tunnel down individual plies in brittle matrix laminates or woven textiles and then turn into plane cracks spreading across many plies en route to part failure. Under this contract, we unified this modeling with our models of cracks bridged by creeping fibers. In the absence of fiber creep, the plane strain phase of crack propagation often (and desirably) ends in crack arrest, because the plane strain crack grows into a lengthening bridging zone as the crack traverses plies. However, fiber creep relaxes the bridging and allows crack growth to resume, which leads to failure at undesirable low stresses. We developed comprehensive solutions to this mode of crack growth. Our predicted crack growth rates are in excellent agreement with trends seen in our own experiments (conducted under DoE funding) and experiments conducted at Pacific Northwest National Laboratory (Henager and Jones). We are very confident that we have the mechanics essentially right.

14. SUBJECT TERMS	15. NUMBER OF PAGES 94
	16. PRICE CODE

17. SECURITY CLASSIFICATION OF REPORT	18. SECURITY CLASSIFICATION OF THIS PAGE	19. SECURITY CLASSIFICATION OF ABSTRACT	20. LIMITATION OF ABSTRACT
UNCLASSIFIED	UNCLASSIFIED	UNCLASSIFIED	

TABLE OF CONTENTS

1. Objectives

Our original goals were the following.

1. Lay the mathematical foundations and formulate efficient numerical methods for life prediction for high temperature materials containing bridged cracks.

2. Map out possible classes of solutions, modes of fracture, asymptotic limits, and characterizing scales for crack propagation in the presence of rate dependent bridging phenomena.

3. Determine rate dependent constitutive laws based on micromechanics for rate dependent process zones in brittle composites at high temperature.

4. Advance optimal composite design by linking bridging constitutive laws to the microscopic properties of bridging ligaments via micromechanics.

5. Develop a practical methodology for predicting crack growth rates in high temperature materials by finding the simplest, physically justifiable material parameters required to characterize fracture in the presence of rate dependent cohesive zones.

These goals were reached before the end of our program. We were then led in a new direction by the advent of integrally woven ceramic matrix composite structures, which show outstanding promise in hot engine parts, including rocket motors and turbine engines. Delamination and other matrix cracks are still very likely to form in such 3D reinforced structures, but they will be bridged by fiber tows and therefore not fatal in a correct design. The key research question becomes understanding the bridging process for the delamination crack, including rate effects (creep and fatigue) at high temperatures. This was a natural extension of the work we had already completed on this contract. We therefore included in the scope of our research the following goal:

6. Lay out basic mechanics issues for rate dependent cohesive zones in textile composites, especially delamination cracks in 3D reinforced layered structures.

2. Status of Effort

This report covers the entire period of performance in our contract, from August, 1994, through September, 1997, with emphasis on work conducted in the final 20 months, which includes a 6 month no-cost extension. All work is now concluded.

At all stages, our research was highly leveraged by collaborations. The principal of these were with faculty, postdoctoral fellows, and students at the University of California, Santa Barbara. Other collaborations extended across the U.S. and to Australia. These collaborations continue.

3. Accomplishments and New Findings

A summary of our major accomplishments is as follows.

1. *Subcritical Cracking in Ceramic Matrix Composites (CMCs).*

We developed successful models to describe subcritical growth of matrix cracks in CMCs at high temperatures when the reinforcing fibers creep. Such crack growth is now recognized to be the primary mode of failure in many CMCs at high temperature. Experiments show that it dominates in SiC/SiC systems; and it is also likely to be important in oxide-oxide composites.

In work under another contract, we had studied the initiation of mode I tensile cracks (not delamination cracks) that tunnel down individual plies in brittle matrix laminates or woven textiles and then turn into plane cracks spreading across many plies en route to part failure.[1] Under this contract, we unified this modeling with our models of cracks bridged by creeping fibers.[2,3] In the absence of fiber creep, the plane strain phase of crack propagation often (and desirably) ends in crack arrest, because the plane strain crack grows into a lengthening bridging zone as the crack traverses plies. However, fiber creep relaxes the bridging and allows crack growth to resume, which leads to failure at undesirably low stresses. We developed comprehensive solutions to this mode of crack growth. Our predicted crack growth rates are in excellent agreement with trends seen in our own experiments (conducted under DoE funding) and experiments conducted at Pacific Northwest National Laboratory (Henager and Jones). We are very confident that we have the mechanics essentially right.

We have shown that the subcritical cracking is controlled by three parameters: the steady-state (ACK) matrix cracking stress for rate-independent (fast) cracking, σ_{ACK}; the characteristic bridging length scale, a_m; and a rate constant for the creep process in the fibers, β. The process of initiating cracks in cross-plied laminates involves as an additional parameter the ratio, η, of the fracture energies in the 0° and 90° plies. These parameters and the nontraditional fracture

---

[1] B. N. Cox and D. B. Marshall, "Crack Initiation in Fiber Reinforced Brittle Laminates" *J. Amer. Ceram. Soc.* **79**[5], 1181-8 (1996).

[2] B. N. Cox, D. B. Marshall, R. M. McMeeking, and M. R. Begley, "Matrix Cracking in Ceramic Matrix Composites with Creeping Fibers," in *IUTAM Symposium on Nonlinear Analysis of Fracture*, ed. J. R. Willis, Kluwer Series on Solid Mechanics and its Applications, series ed. G. M. Gladwell (Kluwer Academic, Dordrecht) in press.

[3] M. R. Begley, B. N. Cox, and R. M. McMeeking, "Time Dependent Crack Initiation and Growth in Ceramic Matrix Composites," in *Proc. International Gas Turbine Institute Conference*, ed. S. Cunningham, ASME, 1997.

concepts they represent are the basis for generating the simplest possible, physically correct model for predicting lifetime, conceptually separating the engineering problem of life prediction for a given material from the intricacies of the micromechanics of the underlying processes. We have developed comprehensive failure maps for the subcritical cracking, showing domains of stable and unstable cracking and transitions from cracking before fiber rupture to fiber rupture following crack initiation.

As part of our goal of finding simple representations of bridged crack phenomena, we developed complete analytical solutions for cracks bridged by creeping fibers in the small scale bridging limit.[4] This limiting case, which occupies one corner of the general failure map, can be expected to apply later in component life in the case that crack growth is accompanied by fiber creep rupture. It is also a common situation in experimental studies of crack growth, e.g., in notched specimens where the presence a large enough notch brings about small scale bridging conditions.

The fracture concepts represented by our four parameters and the failure maps will have general applicability to a wide range of subcritical growth problems in CMCs. For example, our model of the creeping fiber problem in the small-scale bridging limit is formally equivalent to the problem of fatigue crack growth in in-situ reinforced Si_3N_4. Likewise, our formulations for large-scale bridging will be pertinent to MMCs in which fatigue effects acting on fiber interfaces introduce rate dependent bridging.[5] And the fundamental concepts we have introduced will be applicable to diverse classes of CMCs in high temperature service, including laminates and textiles.

To conclude this part of our work, we have now developed a model for the two dimensional problem of how stress is transferred from fibers to matrix in the vicinity of a matrix crack, leading to a generalized constitutive model for the bridging effect of the fibers. The constitutive laws take account of loss of contact between the fibers and the matrix due to creep elongation of the fibers.[6] The modeling is an extension of the work presented by Hutchinson and Jensen.[7] We consider the case where the fiber is orthotropic and an arbitrary residual stress exists in both radial and axial directions. The friction between fiber and matrix is assumed to be uniform along a friction zone whose length varies with the residual radial stress and creep shrinkage. In contrast to earlier constitutive models we used to study single cracks, the mechanics in our new

[4] M. R. Begley, B. N. Cox, and R. M. McMeeking, "Creep Crack Growth with Small-Scale Bridging in Ceramic Matrix Composites," *Acta Mater.*, in press.

[5] B. N. Cox and L. R. F. Rose, "A Self-Consistent Approximation for Crack Bridging by Elastic/Perfectly Plastic Ligaments," *Mechanics of Materials* **22**, 249-63 (1996).

[6] C. Argento, "Mechanics of Creeping Fiber Debonding and Pullout in Bridged Cracks in Unidirectional Composites," to be submitted to *Acta Mater.*

[7] J.W. Hutchinson and S. Jensen, "Models of Fiber Debonding and Pullout in Brittle Composites with Friction", *Mech. Mat.*, **9**, 139-163 (1990).

solution are general enough to allow us to study crack-crack interactions, which are strongly influenced by the spreading zone of lost contact due to fiber creep.

One of the most interesting aspects of subcritical cracking in CMCs at high temperature is that multiple cracks give way in time to a single dominant crack. (Multiple cracking always persists to failure at room temperature.) Final experiments are being completed which illustrate better the transition temperature and the possible effect of applied stress intensity factor.[8] Our new constitutive model will allow us to understand the details of this transition (we already understand the essential mechanism - the overlap of non-contact zones caused by fiber creep), which we regard as central to determining life and predicting notch effects and ultimate strength.

2. *Bridged Cracks in Textile Composites.*

Some of the most interesting cohesive zones in all materials exist in textile composites. The length scales are extraordinary - characteristic zone lengths are often many cm. This implies exceptional notch insensitivity and fracture toughness. One particularly pertinent class of bridged cracks for high temperature applications is delamination cracks in layered structures for thermal barrier or load bearing applications. Such materials made from brittle matrix composites are especially vulnerable to delamination, which will inevitably be one of the primary failure modes. Many textile processes have been developed for suppressing delamination in polymer composites by introducing through-thickness reinforcement. The processes include weaving, braiding, stitching, or inserting short rods. The same methods are now being applied to CMCs.

Mode I, mode II, and mixed mode loading conditions can arise for bridged delamination cracks. Delamination that is primarily mode I can be driven, for instance, by opening bending moments applied to curved structures or thermal gradients in flat structures. Both of these conditions can be expected in hot structure applications, e.g. combustor liners, actively cooled rocket nozzle surfaces, hot structures in turbine engines, etc. Mode II or mixed mode delamination can be initiated where a layered structure terminates at an edge or cut-out.

We have now laid out most of the fundamental aspects of these delamination problems. We have put together some elementary models for mode II cracking[9] with experimental data and observations for End Notch Flexure (ENF) specimens to demonstrate how delamination cracks can be modeled successfully as bridged cracks. We have defined processes for evaluating

[8] D. R. Mumm, K. L. Rugg, and B. N. Cox, "High Temperature Transition to a Single Dominant Matrix Crack in Brittle Matrix Composites with Creeping Fibers," to be submitted to *Acta Mater* or *J. Am. Ceram. Soc.*

[9] R. Massabò and B. N. Cox, "Concepts for Bridged Mode II Delamination Cracks," submitted to *Mechanics of Materials.*

bridging parameters at room temperature, using data for stitched polymer composites.[10] Once again, there are fundamental length scales and material stresses associated with steady state cracking whose identification is very useful for understanding the scope of the problem. Significant differences exist in these length scales and stresses for polymer and ceramic composites, as one might expect: since the intrinsic (unbridged) delamination toughness of a CMC is 3 orders of magnitude less than that of a polymer composite, bridging must be much stiffer in the CMC to be effective.

We have also completed detailed models of the bridging of mode I cracks in curved panels[11] and for mode II cracks in shear loading,[12] showing how the details of the bridging law, which leads among other things to the critical stress for delamination, depends on the characteristics of the through-thickness reinforcement. Salient mechanisms include the flexural rigidity of the through-thickness reinforcement, debonding and sliding of the stitch, and rotation and ploughing of the stitch through the surrounding composite. Stitch failure generally occurs by rupture at some critical strain. We have completed a model of all these mechanisms which provides a micromechanical estimate of the bridging effect for general crack displacements.[13] It can treat small and large deflections of the through-thickness reinforcement appropriate to damage initiation and ultimate failure. The critical shear traction and the maximum angular rotation allowed before the pull-out of reinforcement can be determined analytically.

Our initial work now completed on bridged delamination cracks puts us in an ideal position to analyze the rate dependent mechanics of textile structures at high temperature. In one follow-on, we are now using our understanding of mechanisms and length scales to design CMC delamination fracture specimens. (This is non-trivial and could easily be done wrong, which would result in the waste of very expensive specimens and testing time.) We plan to test our specimens at high temperature in an internally funded program. We will look for creep and cyclic fatigue effects in the bridging zone, which we will model in this program by combining our new models for delaminations in textile laminates[9,10] with our models for rate depending bridging.[2,3,4,7] This represents a significant, new thrust in our research, yet is a natural outgrowth of our work to date.

---

[10] M. He and B. N. Cox, "Crack Bridging by Through-Thickness Reinforcement in Delaminating Curved Structures," submitted to *Composites*, 1996.

[11] B. N. Cox, R. Massabò, D. R. Mumm, A. Turrettini, and K. Kedward, "Delamination Fracture in the Presence of Through-Thickness Reinforcement," plenary paper in *Proc. 11th Int. Conf. Composite Materials*, Gold Coast, 1997, Australia, ed. M. Scott and I. Herszberg.

[12] B. N. Cox and M. He, "Constitutive Models for a Fiber Tow Bridging a Delamination Crack," to be submitted to *Composites.*

[13] C.-H. Kuo and B. N. Cox, "A Model for Through-Thickness Reinforcement in Laminates under General Crack Displacements," to be submitted to *Acta Mater.*

3. *Current Status of CMC Science Reviewed.*

Frank Zok and Brian Cox wrote an invited review article on developments in CMC science in the last two years, drawing on about 100 recent contributions to the literature.[14] We made the following summary remarks.

Ceramic matrix composites reinforced with continuous fibers are on the verge of insertion into hot engineering structures. Yet current research is only beginning to attack some of the most critical problems. Key developments in the last 24 months include the formulation of constitutive laws for continuum mechanics analyses; the discovery of stable, weak oxide-oxide interface systems; the analysis of how fiber creep limits life at high temperatures; confrontation of the problem of oxidation pesting at intermediate temperatures in SiC based systems; re-examination of the maxim that interfaces must be weak; and the advent of textile reinforcement as the solution to delamination problems.

Apart from the fact that making such a concerted effort to catch up with what is going on is marvelously instructive, the exercise left us very optimistic because of the number of significantly new ideas being pursued in processing and materials design; and also reassured that our own programs on CMC micromechanics and design and reliability issues are on the right track.

4. Personnel Supported

The following were directly supported:

Dr. Brian N. Cox, Manager, Design and Reliability Department, Rockwell Science Center.
Dr. David B. Marshall, Manager, Structural Ceramics Department, Rockwell Science Center.
Dr. Claudio Argento, Member of Technical Staff, Design and Reliability Department, Rockwell Science Center.
Dr. Daniel Mumm, Post-Doctoral Fellow, Structural Ceramics Department, Rockwell Science Center (left Rockwell before the end of the program).
Dr. Kevin Rugg, Post-Doctoral Fellow, Design and Reliability Department, Rockwell Science Center.
Dr. C.H. Kuo, Post-Doctoral Fellow, Design and Reliability Department, Rockwell Science Center

[14] B. N. Cox and F. Zok, "Advances in Ceramic Composites Reinforced by Continuous Fibers," *Current Opinion in Solid State and Materials Science*, **1**, 666-673 (1996).

The following students have worked or are still working towards Ph.D. degrees partly under the supervision of Brian Cox:

Matt Begley, Department of Mechanical and Environmental Engineering, UC Santa Barbara (Ph.D. granted; now on the faculty at the University of Connecticut).
Keith Yi, Materials Department, Stanford University.
Chad Landis, Departmental of Mechanical and Environmental Engineering, UC Santa Barbara.

The following researchers have joined in active collaborations:

Dr. L.R.F. Rose, AMRL, Melbourne, Australia.
Professor R.M. McMeeking, Department of Mechanical and Environmental Engineering, UC Santa Barbara.
Professor R.H. Dauskardt, Materials Department, Stanford University.
Professor Frank Zok, Materials Department, UC Santa Barbara.
Prof. Roberto Ballarini, Case Western Reserve University.
Dr. Haian Luo, Shanghai Jiao Tong University.

5. Publications under this contract

The following is a list of papers published or to be published under this contract. Preprints of papers 1 through 9 were mailed to Dr. Brian Sanders on June 17, 1997. A preprint of paper 10 and drafts of papers 13 and 16 are included as appendices to this report. Preprints of the remaining papers, 11, 12, 14, 15, and 17, will be forwarded as they are completed over the next few months.

1. B. N. Cox and L. R. F. Rose, "A Self-Consistent Approximation for Crack Bridging by Elastic/Perfectly Plastic Ligaments," *Mechanics of Materials* **22**, 249-63 (1996).

2. B. N. Cox, D. B. Marshall, R. M. McMeeking, and M. R. Begley, "Matrix Cracking in Ceramic Matrix Composites with Creeping Fibers," in *IUTAM Symposium on Nonlinear Analysis of Fracture*, ed. J. R. Willis, Kluwer Series on Solid Mechanics and its Applications, series ed. G. M. L. Gladwell (Kluwer Academic, Dordrecht, 1997) pp 353-65.

3. M. R. Begley, B. N. Cox, and R. M. McMeeking, "Creep Crack Growth with Small-Scale Bridging in Ceramic Matrix Composites," *Acta Mater.* **45**[7], 2897-2909 (1997).

4. M. He and B. N. Cox, "Crack Bridging by Through-Thickness Reinforcement in Delaminating Curved Structures," *Composites*, in press.

5. R. Massabò and B. N. Cox, "Concepts for Bridged Mode II Delamination Cracks," submitted to *Mechanics of Materials*.

6. B. N. Cox and F. Zok, "Advances in Ceramic Composites Reinforced by Continuous Fibers," *Current Opinion in Solid State and Materials Science*, **1**, 666-673 (1996).

7. M. R. Begley, B. N. Cox, and R. M. McMeeking, "Time Dependent Crack Initiation and Growth in Ceramic Matrix Composites," in *Proc. International Gas Turbine Institute Conference*, ed. S. Cunningham, ASME, 1997.

8. M. Y. He, B. N. Cox, and K. T. Kedward, "Modeling of Discrete Radial Reinforcement in Curved Polymer Matrix Composite Laminates," in *Proc. 11th Int. Conf. Composite Materials*, Gold Coast, Australia, 1997, ed. M. Scott (Woodhead Publishing, Melbourne, 1997).

9. B. N. Cox, R. Massabò, D. R. Mumm, A. Turrettini, and K. Kedward, "Delamination Fracture in the Presence of Through-Thickness Reinforcement," plenary paper in *Proc. 11th Int. Conf. Composite Materials*, Gold Coast, 1997, Australia, ed. M. Scott (Woodhead Publishing, Melbourne, 1997).

10. B. N. Cox and F. W. Zok, "Recent Advances in Fibrous Ceramic Composites," plenary paper in Brittle Matrix Composites V, Warsaw, October, 1997, ed. A. M. Brandt, V. C. Li, and I. H. Marshall.

11. C. Argento, "Mechanics of Creeping Fiber Debonding and Pullout in Bridged Cracks in Unidirectional Composites," to be submitted to *Acta Mater.*

12. P. Vandeurzen, C. Argento, and B. N. Cox, "Thermal conductivity of Textile Composites with through-Thickness Reinforcement," to be submitted to *J. Composite Sci. and Engng.*

13. B. N. Cox and M. He, "Constitutive Models for a Fiber Tow Bridging a Delamination Crack," to be submitted to *Composites.*

14. C.-H. Kuo and B. N. Cox, "A Model for Through-Thickness Reinforcement in Laminates under General Crack Displacements," to be submitted to *Acta Mater.*

15. D. R. Mumm, K. L. Rugg, and B. N. Cox, "High Temperature Transition to a Single Dominant Matrix Crack in Brittle Matrix Composites with Creeping Fibers," to be submitted to *Acta Mater* or *J. Am. Ceram. Soc.*

16. R. Massabò, D. R. Mumm, and B. N. Cox, "Characterizing Mode II Delamination Cracks in Stitched Composites," to be submitted to *Mechanics of Materials.*

17. H. Luo. R. Ballarini, and B. N. Cox, Fracture Stability in Structures Containing Bridged Cracks, paper in preparation (delayed by Dr. Luo's illness).

6. Interactions/Transitions

Presentations and other conference services by Brian Cox, including significant work funded by this contract:

Invited speaker in symposium on High Temperature Fracture, ASME Int. Mechanical Engineering Conference and Exposition, San Francisco, November, 1995.

Invited speaker, URI Workshop, Santa Barbara, January, 1996.

Session chair and invited speaker at the Annual Meeting of the American Ceramic Society, Indianapolis, April, 1996.

Plenary speaker at the Third International Conference on Composites Engineering, New Orleans, July, 1996.

Invited speaker for symposium on ceramic matrix composites, SES meeting, Phoenix, October, 1996.

Invited speaker in two symposia at ASME IMEC&E, Atlanta, November, 1996.

Departmental seminar, MAE Dept., UCLA, January, 1997.

Invited speaker, Symp. On Fatigue and Creep of Composite Materials (organized by Jim Larsen), TMS Fall Meeting, Indianapolis, September, 1997.

Invited speaker and session chair, 9th Int. Conf. on Fracture, Sydney, Australia, April, 1997.

Program Chair, Materials Division, ASME Summer Meeting, Northwestern University, July, 1997.

Plenary speaker, ICCM-11, Gold Coast, Australia, July, 1997.

Invited speaker, 5th Intl. Symp. on Brittle Matrix Composites, Warsaw, Poland, October, 1997.

Program Chair, Materials Division, ASME Int. Mech. Engng Cong. And Exhib., Dallas, November, 1997.

Keynote lecturer, Engineering Found. Conf. on Small Fatigue Cracks, Snowbird Resort, Utah, June, 1998.

Claudio Argento will deliver the following presentation:

Invited speaker, Fall Basic Sciences Meeting of the Amer. Ceram. Soc., San Francisco, October, 1997.

Throughout our contract, we interacted with Jim Larsen's group at WPAFB (including Dr. Reji John) on predicting fatigue crack growth rates in intermetallic matrix composites. Mr. Brian Rigling, a Ph.D. student, is developing models of fatigue cracks in metal matrix composites based on our bridged crack models.

We set up a contract using Rockwell IR&D funds to support Professor Frank Zok and a postdoctoral fellow, Dr. Xiao-Yan Gong, to transition models of CMC life into Boeing North American's Rocketdyne Division. We have encoded the simplified models we have developed in this program as well as simple versions of extensive models for room temperature behavior developed in the ARPA URI program on CMCs at UCSB into FEM

calculations for design engineers at Rocketdyne. The project has been a direct and successful test of the utility of our models. The first application has been to carbon/SiC turbopump rotors for rocket motors.

7. Inventions or patent disclosures

None.

8. Honours and awards

Brian Cox's status as an adjunct professor in the Department of Mechanical and Environmental Engineering, University of California, Santa Barbara, was extended through June, 1998.

Brian Cox was appointed to the editorial board of the journal *Fatigue and Fracture of Engineering Materials and Structures.*

In his service on the Executive Committee of the Materials Division of the American Society of Mechanical Engineers, Brian Cox was appointed program chair for the division at the summer and winter annual meetings.

Our paper "Time Dependent Crack Initiation and Growth in Ceramic Matrix Composites," by M. R. Begley, B. N. Cox, and R. M. McMeeking, was nominated for an award at the ASME *International Gas Turbine Institute Conference*, 1997.

Appendix - Preprints of Recent Papers

This appendix includes preprints of the following papers:

B. N. Cox and F. W. Zok, "Recent Advances in Fibrous Ceramic Composites," plenary paper in Brittle Matrix Composites V, Warsaw, October, 1997, ed. A. M. Brandt, V. C. Li, and I. H. Marshall.

B. N. Cox and M. He, "Constitutive Models for a Fiber Tow Bridging a Delamination Crack," to be submitted to *Composites.*

R. Massabò, D. R. Mumm, and B. N. Cox, "Characterizing Mode II Delamination Cracks in Stitched Composites," to be submitted to *Mechanics of Materials.*

RECENT ADVANCES IN FIBROUS CERAMIC COMPOSITES

Brian COX
Rockwell Science Center
Thousand Oaks, California, 91360, U.S.A.

and

Frank ZOK
Materials Department
University of California, Santa Barbara
Santa Barbara, California, 93106, U.S.A.

ABSTRACT

Recent developments in the science and engineering of ceramic matrix composites (CMCs) are reviewed. Important advances include the formulation of constitutive laws for continuum mechanics analyses; the discovery of stable weak oxide-oxide interface systems; the analysis of how fiber creep limits life at high temperatures; confrontation of the problem of oxidation pesting at intermediate temperatures in SiC based systems; re-examination of the maxim that interfaces must be weak; and the advent of textile reinforcement as the solution to delamination problems. These accomplishments are on the critical path to incorporating CMCs in hot engineering structures.

INTRODUCTION

From the early 1980's, when CMC research first enjoyed large scale funding and the attention of significant groups all over the world, work has concentrated on a simple paradigm of the ideal CMC. It must have a weak fiber/matrix interface to allow energy absorption during fracture by the deflection of cracks, in the complete absence of any dislocation based toughening. Freed of stress concentration when the matrix cracked, strong fibers would continue to bear high loads. This approach to protecting CMCs from intrinsic flaws, notches, and damage was pursued almost entirely in the context of unidirectionally reinforced CMCs, with aligned loads; and mostly in terms of room temperature phenomena. It is now very well understood [1,2].

However, structural applications almost never involve uniaxial stresses; and the long sought pay-off for CMCs will certainly come at high temperatures. But at last constitutive laws are being developed that are suitable for use in finite element calculations of non-unidirectional CMCs under complex loads. The serious difficulties of ensuring durability at high temperatures are being confronted; oxidation pesting of SiC fibers at intermediate temperatures, fiber creep at higher temperatures, and the chemical stability of interfaces are all hot topics. Textile reinforcement, especially with 3D architecture, has appeared as the solution to the unavoidable vulnerability of brittle matrix composites to delamination. And even the central axiom that CMCs cannot be tough unless the fiber/matrix interfaces are weak is being challenged.

CONSTITUTIVE LAWS FOR CONTINUUM CALCULATIONS

Major progress has been made in the last year or two in developing design and reliability codes suitable for field use from the wealth of micromechanical models in the CMC literature. Effort has focused on generating constitutive laws for insertion into finite element models, with the goal of reducing the treatment of nonlinearity in CMCs to standard continuum mechanics.

Nonlinearity in CMCs at room temperature involves matrix cracking, stochastic fiber fracture, damage localization, and fiber pullout. Two groups have presented exhaustive studies for unidirectional composites of the relation between micromechanical properties (including the interfacial friction stress, residual stresses, constituent elastic moduli, fiber radius, and fiber volume fraction) and the macroscopic stress-strain response under aligned loads prior to damage localization and ultimate failure [3-6]. Prior and well established models of matrix cracks bridged by sliding fibers are used as the physical basis for modeling. Micromechanical properties are deduced directly from experimental hysteresis loops, obviating any detailed tests of interface conditions, e.g., fiber pullout or pushout tests. One group couches its work in the language of micromechanics more familiar to the CMC community [3,4]; the other in the language of continuum damage mechanics, but with a thermodynamic potential function derived from the same micromechanics [5,6]. They offer equivalent treatments of nonlinearity up to localization, with some variations in point of view and in the level of micromechanical detail used in fitting data. Both sets of work are essential reading. More empirical (probably unnecessarily so) treatments of nonlinearity in unidirectional CMCs have also appeared [7].

Recent extensions of the continuum damage approach also deal with predicting the onset of damage localization, which is required to model ultimate failure and the notch sensitivity of strength [8]. Localization and subsequent fiber pullout involve distributions of flaw strengths and stress redistribution effects which are complex and not generally well known in a particular material. There is a commensurate increase in the number of material parameters to be determined by calibrating experiments. Applications to circumferentially reinforced rotors have been presented, but proof of the predictive power of localization models is not yet convincing.

Empirical approaches are most credible for multiaxial or off-axis loading, even in unidirectional CMCs, or for more complex fiber architectures [9,10].

This area of work represents the culmination of efforts to qualify CMCs as structural materials. Current activity focuses on dealing with rate dependent behaviour at high temperature, fatigue effects, and weakest link fracture statistics (volume effects).

TOUGHESS RELATED PROPERTIES

Tensile tests performed on specimens containing holes or notches have demonstrated that many CMCs are relatively notch-insensitive [11-15]. The net-section stress at fracture is typically 80-100% of the unnotched strength: considerably higher than the value calculated on the basis of the elastic stress concentration factor. Measurements of in-plane strains (using moiré interferometry [13]) and stresses (using SPATE [11,12]) have shown that *strain* concentrations are essentially unchanged by the inelastic deformation but *stress* concentrations are reduced dramatically. However, even in the most notch-insensitive materials, stress concentrations are not eliminated altogether, yet the net section strength is essentially equal to the unnotched strength. This suggests strength depends on volume, since the stressed volume ahead of a notch is small.

The degree of notch sensitivity is also influenced by the nature of the inelastic deformation occurring ahead of the notches (Figure 1). In some materials (e.g. Nicalon™/CAS), a damage zone of multiple matrix cracks forms ahead of the notch, which has an analogous effect to the plastic zone in metals (designated Class II behavior by Evans [16]). In others (e.g. C/C), nonlinearity arises from shear bands oriented parallel to the tensile direction (Class III behavior [16]). In more brittle CMCs, fracture occurs by the propagation of a dominant mode I crack, with fiber failure and pullout in the crack wake, but with minimal inelastic deformation elsewhere (Class I behavior [16]). Models of strength for Classes I and III have been developed, based on line-spring representations of the inelastic processes [17]. Models that take into account large scale sliding [18] indicate that the maximum fiber stress in the bridging zone is somewhat lower than that predicted from the line-spring models; the latter are thus expected to provide conservative predictions for the stresses at the onset of fiber failure.

Some censure is due to several authors over loose claims that a given material has been found to be "notch insensitive." This generally fallacious conclusion has been based on tests performed with relatively small notches: typically 1 – 5 mm. Moreover, there has been almost no discussion of the effects of notch shape (circular holes vs. sharp slits). For a sufficiently large, sharp notch, the strength must follow the Griffith relation and the material must be notch-sensitive. Researchers should identify the length scales associated with the bridging processes and hence the notch sizes and shapes for which notch sensitivity will occur.

FAILURE IN COMPRESSION

Some evidence exists that compressive strengths [19] fall below tensile strengths [20]. In CMCs with weak or porous matrices, observations show that compressive failure involves kink band formation within fiber bundles (plies or tows), similar to the prevalent failure

mechanisms in polymer matrix composites (laminates and textiles). In this case, compressive strength will be governed by the initial misalignment of segments of fiber bundles and the shear strength of the matrix. Compressive failure also involves interply and intraply delamination, which will probably be the principal mechanisms of failure in CMCs with nonporous, relatively strong matrices.

FATIGUE

Fatigue failure occurs in most CMCs. In CMCs based on oxide or SiC fibers, cyclic loading causes wear of fiber coatings, leading to a reduction in the interface sliding stress and a corresponding reduction in the fiber bundle strength [21,22] and possible loss of dimensional stability. Typically, fatigue thresholds remain $\geq 75\%$ of the ultimate tensile strength (UTS) and the retained strengths following fatigue loading are almost equal to the UTS. But the fatigue threshold can be reduced by notches and negative stress ratios [23].

While fatigue effects in CMCs with SiC or oxide fibers appear mainly related to interfacial degradation, with minimal fiber damage, carbon fibers can be entirely worn away by fatigue. Thus generally severe fatigue effects are found in CMCs based on carbon fibers.

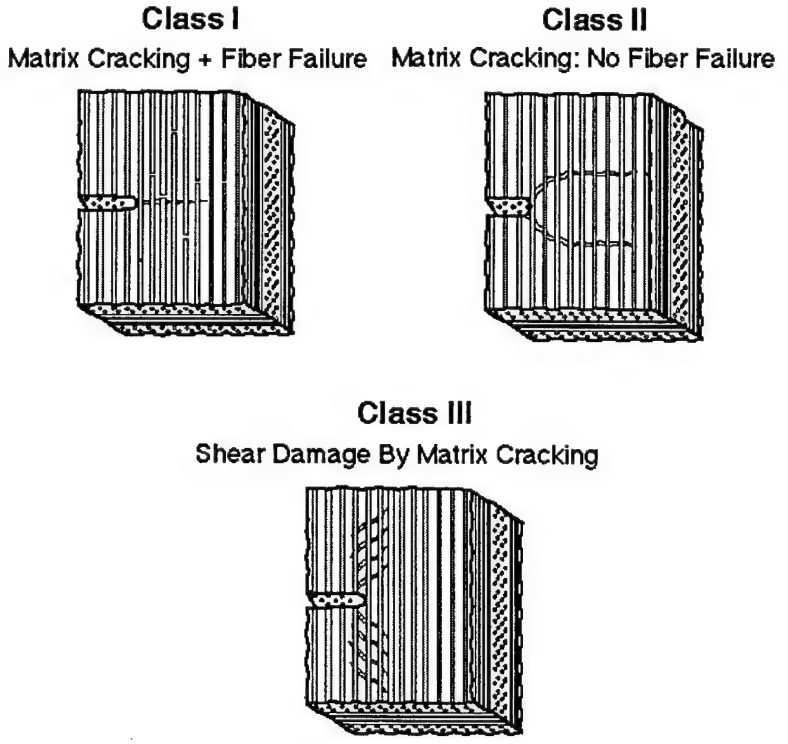

Figure 1. Schematics of three classes of cracking found in unidirectional or cross-plied CMCs. (Additional stress redistribution mechanisms exist in textile CMCs.)

DELAMINATION PROBLEMS

Whether toughness is achieved in a CMC by incorporating weak fiber/matrix interfaces or a porous or otherwise weak matrix around fiber bundles, strength under loads acting normal to the fiber direction will be seriously impaired. Thus while laminated CMCs exhibit encouraging in-plane toughness, they remain vulnerable to delamination. The delamination problem is one of the main reasons CMCs are not yet preferred for load bearing components in high performance applications such as turbine engines. The interaction of thermal gradients and delaminations imposes quite stringent design limits for realistic parameter values [24].

Delamination can be suppressed by through-thickness reinforcement, e.g., stitching, 3D weaving, or short rods. Very encouraging precedents exist in polymer composites [25,26]. The minimum volume fraction of through-thickness reinforcement required to suppress delamination is usually only a few percent or less [27,28]. Through-thickness reinforcement also transports heat across a delamination crack, reducing crack-induced thermal stresses [24].

FAILURE BY CREEP

In glass matrix composites, creep occurs predominantly in the matrix. In unidirectional glass matrix composites, high creep rates in the matrix under transverse loads cause considerable creep anisotropy. In asymmetrically laid-up laminates or in the presence of stress gradients, creep anisotropy within plies will compromise dimensional stability [29]. In CMCs designed for higher temperatures, which have non-glass matrices, the situation is often reversed. Polycrystalline fibers are fabricated with fine grains for strength, usually smaller than the grains in the matrix. It is therefore the fibers that creep first. Considerable progress has now been made towards understanding the important consequences. Under sustained loads, matrix cracks, which would be arrested and remain stable at room temperature, exhibit stable, time dependent growth as fiber creep degrades the shielding effects of bridging fibers [30-32]. Constitutive laws have been derived for bridging fibers that creep [33,34], the incubation of crack growth from prior matrix flaws has been modeled [35,36], and crack growth trends have been detailed [36], and failure modes mapped [37].

The creep properties of the fibers are obviously critical in setting design limits and for determining lifetime. Much is yet to be understood. For example, some early experiments have shown challengingly complex relationships between morphological changes and creep rates in Nicalon™ fibers [38-40]. Developing creep resistant fibers and establishing confidence in their performance remain central problems in the CMC field.

ENVIRONMENTAL VULNERABILITY

The problem of oxidation embrittlement continues to plague SiC-based CMCs. The embrittlement involves oxygen ingress through matrix cracks and the subsequent reaction of oxygen with both the fiber coatings and the fibers [41]. It occurs as a so-called pest phenomenon, being worst at temperatures (600 - 800°C) lower than those of intended service (1000°C). At higher temperatures, oxidation products near the external surfaces tend to seal cracks and inhibit further oxygen ingress.

NEW MATERIALS

One recent eye-catching advance in ceramic chemistry has been the advent of monazites and closely related structures, e.g. xenotimes, as interface coatings and matrices in all-oxide composites (Fig. 2). When prototypical $LaPO_4$ is deposited on Al_2O_3 fibers (with care to maintain accurate 1:1 La:P stoichiometry), a weak interface is formed which is extremely stable up to at least 1600°C [42,43].

Tough oxide-oxide CMCs with strong fiber/matrix interfaces have now also been demonstrated. Crack deflection characteristics likened to those seen in wood have been achieved without fiber/matrix debonding by bundling fibers in a porous matrix that offers easy splitting paths [44]. Weak matrices and fiber entanglement within fiber bundles must also favour splitting [20]. Precedents in polymer and carbon-carbon composites suggest that especially effective toughening mechanisms for strong interface CMCs exist in textile composites [45]: fiber bundles fail as units, but neighbouring bundles are protected from stress concentration by easy splitting between bundles; and 3D architectures bind failed fiber bundles together to large strains, giving exceptional values of work of fracture. Model brittle/brittle composites have been devised to demonstrate the benefits of interlocking 3D architectures [46].

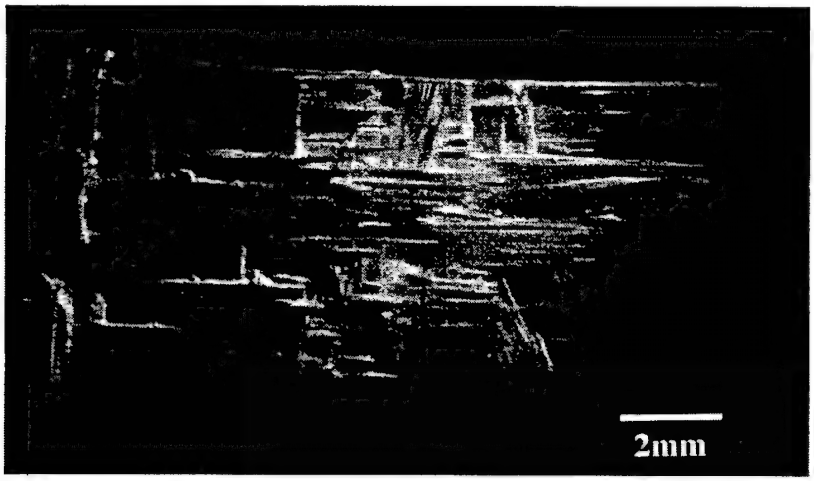

Figure 2. Fibrous energy tensile fracture in an oxide-oxide CMC made from woven fiber tows with no fiber coating (strong interfaces). (Courtesy B. D. Dalgleish, U. Ramamurty, and C. G. Levi.)

INTERFACE SCIENCE

The mechanics of fiber/matrix interfaces and their relation to bridged cracks and thence the constitutive properties of CMCs are mature areas of research (e.g.,[47]). One substantial and still fairly original recent effort has addressed the role of interface roughness. Roughness has been measured on several typical systems [48] and its effect on fiber pullout relations has been measured and modeled [49-51]. Quantitative predictions of roughness effects remain difficult, because the roughness is geometrically complex. In some cases, roughness appears

to cancel the effect of Poisson's contraction of a loaded fiber, validating the assumption of uniform interfacial friction stresses, which has been popular because of its simplicity [49]. But generally, determining the relation between interfacial conditions and fracture behaviour probably always requires calibrating fracture experiments [52]. It has been proposed that roughness effects can be controlled by incorporating a compliant fiber coating to accommodate mismatch strains caused by unseated asperities [53].

In SiC/glass composites, substantial rate effects in stress-strain curves have been measured [54]. The material is stronger and exhibits lower cracking densities at higher strain rates. These effects have been assigned tentatively to environmentally assisted matrix cracking (effective at low strain rates) and an increase in the interfacial friction stress with strain rate.

Acknowledgments. BNC was supported by AFOSR contract No. F49620-94-C0030, FWZ by the ARPA URI program, ONR contract No. N0014-92-J-1808. Drs. A. G. Evans, F. Leckie, D. B. Marshall, and P. E. D. Morgan kindly reviewed sections of the manuscript.

REFERENCES

1. Nair, S.V., Jakus, K., (eds), High temperature mechanical behaviour of ceramic composites, Butterworth-Heinemann, Boston, 1995

2. Lehman, R.L., El-Rahaiby, S.K., Wachtman, J.B., Jr., (eds), Handbook on continuous fiber-reinforced ceramic matrix composites, American Ceram Soc, Westerville, Ohio, 1995

3. Vagaggini, E., Domergue, J-M, Evans, A.G., Relationships between hysteresis measurements and the constituent properties of ceramic matrix composites: I, theory, J Am Ceram Soc., 1995, 78, 2709-20

4. Domergue, J-M, Vagaggini, E., Evans, A.G., Relationships between hysteresis measurements and the constituent properties of ceramic matrix composites: II, experimental studies on unidirectional materials, J Am Ceram Soc., 1995, 78, 2721-31

5. Burr, A., Hild, F., Leckie, F.A., Micro-mechanics and continuum damage mechanics, Arch Appl Mech, 1995, 65, 437-456

6. Burr, A., Hild, F., Leckie, F.A., Continuum description of damage in ceramic-matrix composites, Eur J Mech A/Solids, in press

7. Baste, S., El Bouazzaoui, R., An experimental investigation of stiffness reduction and cracks geometry in a unidirectional brittle matrix composite, J Comp Mater, 1996, 30, 282-308

8. Hild, F., Burr, A., Leckie, F.A., Fiber breakage and fiber pull-out of fiber-reinforced ceramic-matrix composites, Europ J Mechanics, 1995, A13, 731-749

9. Genin, G.M., Hutchinson, J.W., Composite laminates in plane stress: constitutive modeling and stress redistribution due to matrix cracking, J Amer Ceram Soc, 1997, in press.

10. Baste, S., El Bouazzaoui, R., Cracking orientation and induced anisotropy of a ceramic matrix composite under off-axis loading, J Mater Sci, 1996, 31, 1575-1584

11. Cady, C.M., Mackin, T.J., Evans, A.G., Silicon carbide/calcium aluminosilicate: a notch-insensitive ceramic-matrix composite, J Am Ceram Soc, 1995, 78, 77-82

12. Mackin, T.J., Purcell, T.E., He, M.Y., Evans, A.G., Notch sensitivity and stress redistribution in three ceramic-matrix composites, J Am Ceram Soc, 1995, 78, 1719-28

13. Mackin, T.J., Perry, K.E., Epstein, J.S., Cady, C., Evans, A.G., Strain fields and damage around notches in ceramic-matrix composites, J Am Ceram Soc, 1996, 79, 65-73

14. Shercliff, H.R., Beaumont, P.W.R, Vekinis, G., Direct observation of the fracture of CAS-glass/SiC composites: part II notched tension, J Mater Sci, 1994, 29, 4184-4190

15. Droillard, C., Lamon, J., Fracture toughness of 2-D woven SiC/SiC CVI-composites with multilayered interphases, J Am Ceram Soc, 1996, 79, 849-58

16. Evans, A.G., Zok, F.W., Review: the physics and mechanics of fibre-reinforced brittle matrix composites, J Mater Sci, 1994, 29, 3857-3896

17. He, M.Y., Wu, B., Suo, Z., Notch-sensitivity and shear bands in brittle matrix composites, Acta Metall Mater, 1994, 42, 3065-3070

18. Xia, Z.C., Hutchinson, J.W., Evans, A.G., Budiansky, B., On large scale sliding in fiber-reinforced composites, J Mech Phys Solids, 1994, 42, 1139-1158

19. Wang, M., Laird, C., Damage and fracture of a cross woven C/SiC composite subject to compression loading, J Mater Sci, 1996, 31, 2065-2069

20. Wang, M., Laird, C., Characterization of microstructure and tensile behavior of a cross-woven C-SiC Composite, Acta Mater, 1996, 44, 1371-1387

21. Evans, A.G., Zok, F.W., McMeeking, R.M., Fatigue of ceramic matrix composites, Acta Metall Mater,1995, 43, 859-875

22. Holmes, J.W., Sørensen Fatigue Behaviour of Continuous Fiber-Reinforced Ceramic Matrix Composites, High Temperature Mechanical Behaviour of Ceramic Composites, (ed.), Nair SV, Jakus K. Butterworth-Heinemann, Boston, 1995

23. Mall, S., Weidenaar, W.A., Tension-compression fatigue behaviour of fibre-reinforced ceramic matrix composite with circular hole, Composites, 1995, 26, 631-636

24. Hutchinson, J.W., Lu, T.J., Laminate delamination due to thermal gradients, Harvard University Report No. MECH-253, 1995

25. Dransfield, K., Baillie, C., Mai, Y-W, Improving the delamination resistance of CFRP by stitching - a review, Comp Sci Tech, 1994, 50, 305-317

26. Cox, B.N., Flanagan, G., Handbook of analytical methods for textile composites, Rockwell Science Center, Contractor Report to NASA Langley, to be published.

27. Lu, T.J., and Hutchinson, J.W., Role of fiber stitching in eliminating transverse fracture in cross-ply ceramic composites, J Am Ceram Soc, 1995, 78, 251-253

28. Cox, B.N., Massabò, R., Kedward, K.T., The suppression of delaminations in curved structures by stitching, Composites, 1996, in press

29. Weber CH, Löfvander JPA, Evans AG, Creep anisotropy of a continuous-fiber-reinforced silicon carbide/calcium aluminosilicate composite, J Am Ceram Soc, 1994, 77, 1745-52

30. Henager, C.H., Jr, Jones, R.H., Subcritical crack growth in CVI silicon carbide reinforced with Nicalon™ fibers: experiment and model, J Am Ceram Soc, 1994, 77, 2381-94

31. Jones, C.R., Henager, C.H., Jr, Jones, R.H., Crack bridging by SiC fibers during slow crack growth and the resultant fracture toughness of SiC/SiC_f composites, Scripta Metall Mater, 1995, 33, 2067-2072

32. Lamouroux, F., Vallés, J.L., Steen, M., Influence of damage on the creep behaviour of ceramic matrix composites, Comp Engng, 1995, 5, 1379-1386

33. Begley, M.R., Evans, A.G., McMeeking, R.M., Creep rupture in ceramic matrix composites with creeping fibers, J Mech Phys Solids, 1995, 43, 727-740

34. El-Azab, A., Ghoniem, N.M., Investigation of incubation time for sub-critical crack propagation in SiC-SiC composites, J Nucl Mater, 1995, 219, 101-109

35. Gwo ,T-J, Nair, S.V., Creep crack growth in fiber reinforced composites with rate dependent bridging - role of a viscous fiber matrix interface, Mech Mater 1996, in press

36. Begley, M.R., Cox, B.N., McMeeking, R.M., Time dependent crack growth in ceramic matrix composites with creeping fibers, Acta Metall Mater, 1995, 43, 3927-3936

37. Cox, B.N., Marshall, D.B., Crack initiation in fiber-reinforced brittle laminates, J Am Ceram Soc, 1996, 79, 1181-1188

38. Weber, C.H., Kim, K.T., Heredia, F.E., Evans, A.G., High temperature deformation and rupture in SiC-C composites, Mater Sci Engng, 1995, A196, 25-31

39. Bodet, R., Bourrat, X., Lamon, J., Naslain, R., Tensile creep behaviour of a silicon carbide-based fibre with a low oxygen content, J Mater Sci, 1995, 30, 661-667

40. Morscher, G.N., Tensile stress-rupture of SiC_f/SiC_m minicomposites with C and BN interphases at elevated temperatures in air, J Am Ceram Soc, submitted

41. Heredia, F.E., McNulty, J.C., Zok, F.W., Evans, A.G., Oxidation embrittlement probe for ceramic-matrix composites, J Am Ceram Soc, 1995, 78, 2097-2100

42. Morgan, P.E.D., Marshall, D.B., Ceramic composites of monazite and alumina, J Am Ceram Soc. 1995, 78, 1553-63

43. Morgan, P.E.D., Marshall, D.B., Housley, R.M., High-temperature stability of monazite-alumina composites, Mater Sci Engng, 1995, A195, 215-222

44. Tu, W-C, Lange, F.F., Evans, A.G., Concept for a damage-tolerant ceramic composite with "strong" interfaces, J Am Ceram Soc, 1995, 79, 417-424

45. Cox B.N., Modeling Three-Dimensional Composites, Advanced Technology for Design and Fabrication of Composite Materials and Structures (Torino, 1993), (ed) Sih G.C., Carpinteri, A., Surace, G. (Kluwer, Amsterdam, 1995) pp. 49-62

46. Cox, B.N., Lockup, chains, and the delocalization of damage, J Mater Sci, in press

47. Shin, D-W, Auh, K.H., Knowles, K.M., SiC fibre/borosilicate glass composite (part 2) - factors controlling the mechanical properties, J Ceram Soc Japan, 1995, 103, 409-417.

48. Parthasarathy, T.A., Barlage, D.R., Jero, P.D., Kerans, R.J., Effect of interfacial roughness parameters on the fiber pushout behavior of a model composite, J Am Ceram Soc, 1995, 78, 3232-36

49. Parthasarathy, T.A., Marshall, D.B., Kerans, R.J., Analysis of the effect of interfacial roughness on fiber debonding and sliding in brittle matrix composites, Acta Metall Mater, 1994, 42, 3773-3784

50. Huang, C.M., Zhu, D., Xu, Y., Mackin, T., Kriven, W.M., Interfacial properties of SiC monofilament reinforced β'-SiAlON composites, Mater Sci Engng, 1995, A201, 159-168

51. Peters, P.W.M., Martin, E., Quenisset, J.M., Slip and frictional shear stresses in ceramic matrix composites, J Comp Mater, 1995, 29, 550-572

52. Cox, B.N., Life prediction for bridged fatigue cracks, Life Prediction Methodology for Titanium Matrix Composites, ASTM STP 1253, ed. Johnson, W.S., Larsen, J.M., Cox, B.N., ASTM, Philadelphia, 1996

53. Kerans, R.J., The role of coating compliance and fiber/matrix interfacial topography on debonding in ceramic composites, Scripta Metall Mater 1995, 32, 505-509

54. Sørensen, B.F., Holmes, J.W., Effect of loading rate on the monotonic tensile behavior of a continuous-fiber-reinforced glass-ceramic matrix composite, J Am Ceram Soc, 1996, 79, 313-20

DRAFT ONLY

Characterizing mode II delamination cracks in stitched composites

by

Roberta Massabò[1a], Daniel R. Mumm[2], and Brian N. Cox[3]

[1] Department of Structural and Geotechnical Engineering, University of Genova, Via Montallegro 1, 16145 Genova, Italy.
[2] Division of Engineering and Applied Science, Harvard University, 40 Oxford Street, Cambridge MA 02138, U.S.A.
[3] Rockwell Science Center, 1049 Camino Dos Rios, Thousand Oaks CA 91360, U.S.A.

ABSTRACT

This paper deals with characterizing the bridging mechanisms developed across delamination cracks by through-thickness reinforcement, using stitched carbon/epoxy laminates under mode II loading as a prime example. End Notched Flexure (ENF) tests are performed which show that stitching can provide stable crack growth. The bridging law, which characterizes the bridging action of the stitches, is deduced from both crack profile measurements and load-deflection curves. Consistent results are obtained from the two methods. The inferred laws imply that delamination cracks will commonly grow in conditions that are neither accurately nor properly described by linear elastic fracture mechanics. Large scale bridging calculations are required, in which the essential material property is the bridging traction law. The level of detail in which the law must be determined can be inferred from the sensitivity of predicted crack growth to variations in the law. This reveals that only a few parameters suffice for reliability predictions of the fracture behavior in many applications. It is recommended that the required parametric traction law be deduced in engineering practice from load-deflection data from the standard ENF (or similar) test, with due regard to selecting the notch size and other specimen dimensions to ensure that crack growth is stable in the test.

1. INTRODUCTION

Bridging mechanisms contribute substantially to fracture toughness in many composites and self-reinforced materials. Continuous or discontinuous fibers, bars, particles, or aggregates bridge microcracks and macrocracks in ceramic, polymer, or cementitious matrix composites, and thus control their coalescence and growth (Cox and Marshall, 1994, Bao and Suo, 1992).

This paper deals with the bridging mechanisms developed by through-thickness reinforcement on delamination cracks in fiber-reinforced laminated composites. Through-

[a] Phone: +39 10 353 2956; Fax: +39 10 353 2534; e-mail: massabo@scostr.unige.it

thickness reinforcement is a recent technology developed to improve damage resistance. It is applied by various techniques, including stitching or weaving continuous fiber tows or implanting discontinuous fibrous or nonfibrous rods (Horton and McCarty, 1987; Smith and Wilson, 1985; Dow and Smith, 1989; Dransfield et al., 1994; Darbyshire, 1970; Bradshaw et al., 1973; Krasnov et al., 1987; Freitas et al., 1996; Cox et al., 1994).

Conventional fiber-reinforced laminates are highly sensitive to the presence of delamination flaws, which might be created by impact, stress concentrations near free edges or holes, or manufacturing errors. The growth of these flaws is controlled by the interlaminar fracture toughness, which is usually similar in magnitude to the matrix fracture toughness, as the flaws originate and propagate in the matrix rich regions between the plies (interply layers)[1]. Under loading conditions creating interlaminar stresses, the delamination flaws can propagate easily in the member and separate it into two unconnected halves, so leading the structural component to failure or substantially reducing its stiffness. This process is usually unstable.

Through-thickness reinforcement moderates the delamination process by shielding the tip of the delamination from the applied stress and reducing the crack driving force. Crack propagation can be rendered stable, which is critical to damage tolerant design; while ultimate strength can be increased and notch and impact sensitivity reduced.

To realize these benefits in structural design, the shielding or bridging effect must be quantified. It is the aim of this paper to provide a simple engineering approach to quantifying bridging in laminates containing through-thickness reinforcement, with stitching taken as the prime example.

The quantification must extend beyond the ideas of Linear Elastic Fracture Mechanics (LEFM), which does not in general describe crack growth in stitched laminates correctly. Crack growth in stitched laminates cannot be characterized by a single fracture parameter, such as fracture toughness; the toughness increment supplied by the through-thickness reinforcement is not a material constant, but depends on crack length, geometrical ratios, and loading conditions. In other words, cracks bridged by stitches grow under large scale bridging conditions (defined here as the absence of the LEFM relation between the applied load and the net crack tip stress intensity factor), for which a bridged crack model is required.

In a bridged crack model, the bridging action of the reinforcement is represented as a distribution of tractions acting along the fracture surfaces and opposing their relative

[1] In fiber reinforced laminates, the interlaminar fracture toughness can be improved by in-plane fibers crossing the crack at shallow angles if the delamination meanders from the interply layer into the plies themselves. However, this effect is modest in polymer matrix laminates and sensitive to processing details.

displacement. The tractions are related to the crack displacement by a bridging law which embodies the mechanism of load transfer from the reinforcement to the surrounding material. To know the bridging law is to be able to predict delamination cracking. The essential questions are therefore: in what detail must the bridging law be known; and what experiments suffice to determine it to the required level of detail?

The answer depends on what needs to be predicted. Certain characteristics of the bridging law will determine delamination crack propagation in a structure in the absence of stitch failure, while other characteristics will determine ultimate strength. Both crack propagation, which can result in significant loss of stiffness, and ultimate strength may be of engineering interest, separately or together.

This paper examines methods for determining bridging laws for mode II delamination cracks in stitched polymer laminates. Fracture experiments using End Notched Flexure specimens are analyzed via a formulation of the bridged crack problem proposed by Massabò and Cox (1996). The bridging traction law is deduced from crack profile measurements and load-versus-deflection data, emphasizing the question of how well the experiments can determine the traction law and conversely the extent to which variations in the law bear on crack propagation and structural behavior. By this analysis, strong conclusions can be inferred about how many (or few!) characteristics of the bridging law are relevant to fracture and what constitutes a sufficient test or set of tests for quantifying the delamination resistance of a given stitched laminate in general applications.

The paper does not deal with the details of damage mechanisms associated with the bridging stitches, nor with micromechanical models of the resulting tractions. Such information is superfluous in the prediction of delamination in a given composite; it is only necessary to know the traction law itself, as determined by a standard and simple test, and not how the law relates to the properties and geometry of the constituents of the stitches and laminate and details of the fiber architecture. Indeed, micromechanical models can be severely misleading if they are used to predict service behaviour, because they inevitably involve simplifications and idealizations which may be inappropriate in a particular laminate, no matter how consistently they appear in prior cases. However, micromechanical models of mechanisms are essential to the development of optimal reinforcement, i.e., to the materials design problem. Observations and models of stitches in shear appropriate to materials design will be presented elsewhere.

On the other hand, insight into mechanisms and micromechanics can be helpful in deducing the maximum information about a bridging law from fracture data. Optimal interpretation of data is a balance between taking advantage of insight by specifying the

general form of the bridging law a priori and erring by overconstraining the law. Deciding the right degree of constraint is a subjective matter, not amenable to algorithm but rather depending on the judgment of the decision maker. The quality of his judgment rises with his understanding of mechanisms.

All of these considerations are addressed below for the mode II delamination problem. Section 2 is devoted to the theoretical analysis of delamination crack growth in ENF specimens reinforced through the thickness. The materials investigated and the experimental tests performed are described in Section 3. The inverse problems for the determination of the bridging law from fracture data **is are** presented in Section 4. Implications for engineering reliability methods are discussed in Section 5.

2. THEORETICAL MODELING OF THE END NOTCHED FLEXURE SPECIMEN (ENF)

The End Notched Flexure (ENF) specimen is a long and thin three-point bending beam with a mid-surface delamination starting from one end. The specimen typically consists of laminated plies laid up symmetrically about the mid-plane. Figure 1 shows an ENF specimen of length $2L$, depth $2h$, and width d, with a delamination of length a, subject to a concentrated load P. The specimen is reinforced in the through-thickness direction along its entire length apart from a region of length a_0 which represents a machined notch or an insert placed at the specimen mid-surface before processing the material. The bridged portion of the delamination, of length a-a_0, represents a sharp pre-crack which is usually introduced to give the delamination tip the natural crack tip morphology. The same schematic describes an unstitched laminate if the reinforcement is absent, in which case $a = a_0$ since a sharp notch and an unbridged segment of crack are mathematically equivalent.

If the ENF specimen is long and thin, i.e. $a>>h$ and $L>>a$, and the upper and lower arms of the specimen in the delaminated region are free to bend with the same curvature (i.e., free sliding is ensured along the surfaces of the notch), the ENF test represents a mode II fracture problem. Then, if the ENF specimen is wide, i.e. $d>>h$, and the lay-up of the laminate is such that a plane of elastic symmetry normal to the axis y exists, plane strain conditions can be assumed parallel to the plane x-z. The specimen can be modeled as a two-dimensional, anisotropic plate in cylindrical bending.

The schematic of the plate is shown in Fig. 2.a. The bridging action developed by the through-thickness reinforcement is represented by a continuous distribution of shear tractions, τ_b, which oppose the crack sliding displacement. They depend on the crack

sliding through a bridging law, $\tau_b(w)$, (the parameter w is defined so that the total crack sliding displacement is $2w$). No other mechanisms, other than those described by the bridging tractions, are assumed to oppose the relative sliding between the crack faces. The validity of the proposed approach and its range of applicability are discussed in Appendix A.

The problem of Fig. 2.a is studied as the superposition of the two problems shown in Fig. 2.b and 2.c, which can be analyzed by adapting the first-order shear deformation theory proposed for an anisotropic bending plate by Whitney and Pagano (1970). Figure 2.b describes an intact three-point bending plate subject to the applied load, P. For a homogeneous, specially orthotropic laminate (i.e., a laminate in which the axes of orthotropy coincide with the specimen axes), the mid-span deflection, $\delta_{(b)}$, for this uncracked plate is

$$\delta_{(b)} = \frac{PL^3}{Eh^3 d}\left[\frac{1}{4} + \frac{3}{10}\left(\frac{h}{L}\right)^2 \frac{E}{G_{xz}}\right]. \tag{1}$$

where G_{xz} is the shear modulus in the plane x-z and $E=E_x/(1-\nu_{xy}\nu_{yx})$, with E_x the axial Young's modulus, ν_{xy} and ν_{yx} Poisson's ratios in the plane x-y.

The problem of Fig.2.c describes the fracture process in the ENF specimen. The uniform shear tractions applied along the faces of the delamination, τ, are equal in magnitude but opposite in sign to the shear stresses generated by the external load P at the mid-plane of the intact plate of Fig. 2.b. For an orthotropic homogeneous laminate

$$\tau = \frac{3}{8}\frac{P}{hd}. \tag{2}$$

(Chatterjiee, 1991). Two dominant toughening mechanisms control the growth of the delamination in Fig. 2.c. The first is the toughness peculiar to the unreinforced laminate, which is assumed to be brittle and characterized by the mode II interlaminar fracture energy, $\mathcal{G}_{IIC}$ (a material property). The second is the toughness due to the through-thickness reinforcements, which shield the crack tip stress field, so reducing the driving force for crack propagation. The latter contribution is not a material property, since it depends on crack length and geometrical ratios, but it can be calculated once the bridging law, $\tau_b(w)$, is known. Two different approaches for determining $\mathcal{G}_{IIC}$ and $\tau_b(w)$ from ENF tests will be proposed in Section 4.

Two limiting crack configurations characterize the various possible fracture histories in the schematic of Fig. 2.c (or in the ENF specimen). The first is referred to as the ACK limit, in reference to the seminal work of Aveston, Cooper, and Kelly (1971) on mode I matrix cracks in fibrous composites. The second is the small scale bridging limit, where

Linear Elastic Fracture Mechanics (LEFM) prevails. The analytical definition of the two limits has been given by Massabò and Cox (1996).

The essential concepts introduced by the two limiting configurations will be summarized in the following. Moreover, the basic relationships which govern the problem in large scale bridging conditions will be recalled in order to be used in the inverse formulation proposed in Section 4.

2.1 The Mode II ACK Limit

The mode II ACK limit is a stable configuration characterized by a long delamination crack which is entirely bridged by intact ligaments. The limit will be reached in a long enough specimen if the through-thickness reinforcements do not fail in the crack wake during crack growth and the bridging law, $\tau_b(w)$, is an increasing function of the crack sliding, at least over an interval of w.

In the ACK limit the applied shear tractions, τ, are equilibrated along most of the crack wake by equal and opposing bridging tractions, τ_b. The critical applied shear stress for crack propagation approaches a constant value, τ_{ACK}, which is independent of crack length and specimen dimensions. It is defined through Griffith's energy criterion by equating the intrinsic **interlaminar** fracture energy, $\mathcal{G}_{IIC}$, and the strain energy release rate of the member, $\mathcal{G}_{II}$,

$$\mathcal{G}_{IIC} = 2\left[\tau_{ACK} w_{ACK} - \int_0^{w_{ACK}} \tau_b(w)\, dw\right] \tag{3}$$

where w_{ACK} is such that $\tau_{ACK}=\tau_b(w_{ACK})$ **(see Fig. 16)**. If the bridging law has the form $\tau_b(w)= \tau_b(0)+\beta w^{\alpha}$ (which will prove especially pertinent for stitched laminates), the ACK shear stress reduces to

$$\tau_{ACK} = \tau(0) + \left[\mathcal{G}_{IIC}\beta^{\frac{1}{\alpha}}\frac{1+\alpha}{2\alpha}\right]^{\frac{\alpha}{1+\alpha}}. \tag{4}$$

(Massabò and Cox, 1996). The ACK limit configuration is approached when the crack has propagated beyond any notch a distance which is typically several times the length, l_{ACK}, a material-structure parameter given by

$$l_{ACK} = \sqrt{a_{IIm} h} \tag{5.a}$$

$$a_{IIm} = \frac{1}{A}\left(\frac{1+\alpha}{2\alpha}\mathcal{G}_{IIC}\right)^{\frac{1-\alpha}{1+\alpha}}\beta^{\frac{-2}{1+\alpha}} \tag{5.b}$$

where a_{IIm} is a material constant and $\overline{A}$ is an elastic constant depending on the lay-up of the laminate (Massabò and Cox, 1996). For the special case of a homogeneous, specially orthotropic laminate, $\overline{A}=4/E$. If the bridging law is linear ($\alpha=1$), a_{IIm} becomes

$$a_{IIm} = \frac{E}{4\beta} \quad . \tag{5.c}$$

2.2 The Small Scale Bridging Limit

If the bridging ligaments fail during crack propagation, as the sliding displacement at the root of the notch reaches the critical value, w_0, the unbridged segment of the crack will start to extend. In a long enough specimen, the size of the bridged zone will eventually assume a constant value, l_{SSB}, and become much smaller than the crack length, a. In this *small scale bridging configuration* the composite fracture energy is a material constant and the sum of two contributions: the intrinsic interlaminar fracture energy, $\mathcal{G}_{IIC}$, and the energy supplied by the bridging mechanisms, $\mathcal{G}_b$. The latter is just twice the area under the bridging curve (Rose, 1987; Budiansky et al. 1986).

The critical shear stress for crack propagation in this limit, $\tau_{SSB}(a)$, is defined through LEFM by neglecting the actual dimensions of the bridged zone. Griffith's energy criterion, which equates the strain energy release rate of the member, $\mathcal{G}_{II}$, and the composite fracture energy,

$$\mathcal{G}_{II} = \mathcal{G}_{IIC} + \mathcal{G}_b = \mathcal{G}_{IIC} + 2\int_0^{w_0} \tau_b(w)\mathrm{d}w, \tag{6}$$

and solutions from plate theory, lead to

$$\tau_{SSB}(a) = \frac{1}{a}\sqrt{\frac{h(\mathcal{G}_{IIC} + \mathcal{G}_b)}{\overline{A}}} \tag{7}$$

(Massabò and Cox, 1996). If either $\tau_b(0)\neq 0$ or $\mathcal{G}_{IIC} >> \mathcal{G}_b$ (e.g., $\mathcal{G}_{IIC} > 1.5\mathcal{G}_b$ for a linear bridging law), the constant length of the bridged zone in this limit, l_{SSB}, is approximated by

$$l_{SSB} \sim \sqrt{a_{IIs} h} \tag{8.a}$$

$$a_{IIs} = 4\frac{w_0}{\tau_{b0}\overline{A}}\left(\sqrt{1+\frac{\mathcal{G}_{IIC}}{\mathcal{G}_b}} - \sqrt{\frac{\mathcal{G}_{IIC}}{\mathcal{G}_b}}\right)^2 \quad . \tag{8.b}$$

with τ_{b0} the maximum value of the bridging tractions (Fig. 16). When $\tau_b(0) = 0$ and $\mathcal{G}_{IIC}/\mathcal{G}_b \rightarrow 0$, l_{SSB} will become much larger than $(a_{IIs}h)^{1/2}$, rising in proportion to $\mathcal{G}_b/\mathcal{G}_{IIC}$, but still scaling with $h^{1/2}$.

In the limit $\mathcal{G}_{IIC} \rightarrow 0$ and for a homogeneous specially orthotropic laminate, the material length scale a_{IIs} reduces to

$$\lim_{\mathcal{G}_{IIC}\rightarrow 0} a_{IIs} = \frac{w_0 E}{\tau_{b0}} \tag{9}$$

which is an upper bound estimate for a_{IIs} and, in the particular case of a linear bridging law, $\tau_b(w)=\tau_{b0}(1-w/w_0)$, defines the mode II characteristic length

$$l_{IIch} = \frac{\mathcal{G}_b E}{\tau_{b0}^2} \tag{10}$$

analogous to the well known mode I characteristic length **noticed** by Cottrell (1963) and Hillerborg (1983) for the description of material brittleness.

It will be shown in Section 2.3 that in laminates characterized by $\mathcal{G}_{IIC}=0$ the material-structure parameter $(l_{IIch}h)^{1/2}$ controls the dependence of the ultimate shear strength on the length of flaws.

2.3 Crack Propagation in Large Scale Bridging Conditions

Crack growth in large-scale bridging conditions is studied through the bridged crack model formulated by Massabò and Cox (1996). The model substantially differs from another previously proposed model (Jain and Mai, 1994) as it does not put any restriction on the shape of the bridging law and permits analysis of crack growth in general bridging conditions (e.g., when the unbridged crack is propagating in the specimen).

The model examines two different regions of the laminate (Fig. 2.c). In the delaminated region, $0 \leq x \leq a$, the plate is represented as the assemblage of two disbonded sublaminates, placed above and below the mid-plane. Due to the antisymmetry of the problem, constitutive and equilibrium equations are derived and solved explicitly for only one of them, solutions for the other following immediately by a simple symmetry operation. In the bonded region, $a \leq x \leq 2L$, the entire thickness of the laminate plate is examined. The solution for the whole plate is then assembled by imposing continuity between the bonded region and the two sublaminates of the delaminated region at $x = a$.

All of the assumption of the first order shear deformation theory for bending plates in small deformations (Whitney and Pagano, 1970) hold in the present model. The in-plane displacements (x component) vary linearly through the thickness, $u(z)=u^0+\varphi z$, with u^0 the displacement on the mid-plane of the laminate or sublaminate under consideration and φ the bending rotation. The transverse displacements, v, (z component) are constant through the thickness. The stress field is described by the stress resultants over a unit width:

normal force, N, bending moment, M, and shear force, Q. The through-thickness interlaminar stress, σ_z, is neglected.

With partial differentiation denoted by a comma and the subscripts d and i indicating variables in the delaminated and bonded regions, respectively, the constitutive equations for the two regions are

$$\begin{cases} N_d = A_d u^0_{d,x} + B_d \varphi_{d,x} \\ M_d = B_d u^0_{d,x} + D_d \varphi_{d,x} \quad \text{if } 0 \le x \le a \\ Q_d = K_d (v_{d,x} + \varphi_d) \end{cases} \qquad \begin{cases} N_i = A_i u^0_{i,x} \\ M_i = D_i \varphi_{i,x} \quad \text{if } a \le x \le 2L \\ Q_i = K_i (v_{i,x} + \varphi_i) \end{cases} \tag{11}$$

and the equilibrium equations

$$\begin{cases} N_{d,x} = \tau - \tau_b(w)\chi \\ M_{d,x} = -0.5h(\tau - \tau_b(w)\chi) + Q_d \quad \text{if } 0 \le x \le a \\ Q_{d,x} = 0 \end{cases} \qquad \begin{cases} N_{i,x} = 0 \\ M_{i,x} = Q_i \quad \text{if } a \le x \le 2L \\ Q_{i,x} = 0 \end{cases} \tag{12}$$

where w is the crack sliding displacement,

$$w = u^0_d - \varphi_d h/2, \tag{13}$$

and χ is zero for $x \le a_0$ and unity for $x \ge a_0$; A_d, D_d, and K_d are the axial, bending, and shear stiffnesses of the upper sublaminate, calculated over a unit width, and B_d is the axial-bending coupling stiffness; A_i, D_i, and K_i are the stiffness components of the laminate in the bonded region (see Massabò and Cox, 1996, for general expressions). In the case of a homogeneous specially orthotropic laminate, the stiffness terms for the delaminated region are $A_d=Eh$, $D_d=Eh^3/12$, $K_d=5G_{xz}h/6$, and $B_d=0$. The stiffness terms for the bonded region are obtained from these by substituting $2h$ for h.

Equations (11) and (12) and the related boundary and continuity conditions for stress resultants and generalized displacements define a nonlinear boundary-value problem in terms of the displacement variables. The boundary conditions consist of: $(N_d, M_d, v_d)=0$ at $x=0$; $(M_i, u^0_i, v_i)=0$ at $x=2L$; (N_d, M_d, Q_d) and (u^0_d, φ_d, v_d) at $x=a_0^-$ equal to (N_d, M_d, Q_d) and (u^0_d, φ_d, v_d) at $x=a_0^+$; $(v_d, \varphi_d)=(v_i, \varphi_i)$, $u^0_i = u^0_d - \varphi_d h/2 = 0$, $N_i=0$, $Q_i=2Q_d$ and $M_i=2M_d+N_d h$ at $x=a$. The last equalities follow from the antisymmetry of the problem and equilibrium conditions at $x=a$.

Stress resultants and generalized displacements are calculated for fixed delamination and notch lengths, a and a_0, and applied shear stress, τ, through the numerical procedure proposed in (Massabò and Cox, 1996). The evolutionary process of crack growth in the ENF specimen is then studied by calculating the critical shear stress for crack propagation, $\tau_{cr}(a)$, corresponding to a known length of the delamination.

When the crack is at the onset of propagation the energy balance, $\mathcal{G}_{II}= \mathcal{G}_{IIC}$, must hold. The strain energy release rate, $\mathcal{G}_{II}$, is defined through application of the J-Integral (Rice, 1968):

$$\mathcal{G}_{II} = +2\tau w_{cmsd} - 2\int_0^{w_{notch}} \tau_b(w)\mathrm{d}w \tag{14}$$

where w_{cmsd} is the crack mouth sliding displacement (at x=0) and w_{notch} is the sliding displacement at the root of the notch (at $x=a_0$) (Massabò and Cox, 1996).

During crack growth the failure of the reinforcements can take place at the root of the notch ($x=a_0$) when the sliding displacement equals the critical value, $w(a_0)=w_0$. With further crack growth, the unbridged crack starts to propagate and the new length at each step of loading, a_r, is found by maintaining the condition $w(a_r)=w_0$. After the first failure of the reinforcement, the length of the bridged zone will progressively decrease during crack growth approaching the minimum, l_{SSB}, of Eq. (8.a) when the small scale bridging configuration is reached.

Figure 3 shows the critical load for crack propagation, τ_{cr}, as a function of crack length for a laminate whose through-thickness reinforcements never fail and for three different bridging laws, viz., linear, quadratic, and square root. The shear stress is normalized by τ_{ACK} of Eq. (4) and the crack length by the characteristic length $l_{ACK}=(a_{IIm}h)^{½}$ of Eq. (5.a). Laminates with different notch lengths, a_0, are examined. The lower curves refer to unreinforced laminates.

All of the curves share the asymptote $\tau_{cr}=\tau_{ACK}$ and the ACK limit is well approximated after the crack has propagated over a distance of approximately 6-8 times the characteristic length l_{ACK}. Crack growth is always stable for large notches, i.e. all those for which $\tau_{cr}(a_0)<\tau_{ACK}$. The minimum notch length for stability follows from Eqs. (4) and (7), and is given in the particular case of a linear bridging law, $\tau_b(w)=\tau_b(0)+\beta w$, by

$$\frac{a_0}{\sqrt{a_{IIm}h}} = 1 - \frac{\tau_b(0)}{\tau_{ACK}}. \tag{15}$$

Figure 4 shows histories of the critical stress for one of the cases from Fig. 3, namely a linear bridging law with a normalized notch of length $a_0/\sqrt{a_{IIm}h}=1.0$, when the through-thickness reinforcements have various finite ultimate strengths, τ_{b0}. If the ultimate strength is high enough, i.e. $\tau_{b0}/\tau_{ACK}\geq 2$ for the notch size under consideration, the ACK limit is reached without failure of the reinforcement. For lower strengths, a period of stable growth is succeeded by failure of the reinforcements and unstable, catastrophic cracking. The ultimate strength of the reinforcements required for noncatastrophic cracking (towards the ACK limit) rises linearly with increasing notch

size, a_0, for large notches in a laminate of fixed depth (not as $a_0^{1/2}$, as it would in an infinite or very thick specimen). For small notches, whether cracking is noncatastrophic or catastrophic depends on the relative magnitudes of τ_{ACK} and τ_{b0}; or, equivalently, of the length scales a_{IIs} and a_{IIm} (Massabò and Cox, 1996).

The role of the length scale, $(l_{IIch}h)^{1/2}$, in notch sensitivity is illustrated in Fig. 5, which shows how the ultimate shear strength of the laminate, τ_{ult}, depends on notch size for several bridging laws when the intrinsic delamination toughness, $\mathcal{G}_{IIC}$, is zero. This will be a useful approximation in discussing the failure of stitches whenever $\mathcal{G}_{IIC} << \mathcal{G}_b$, which is often the case in stitched polymer matrix laminates. The ultimate shear strength has been evaluated for a specimen of effectively infinite length. The notch size is normalized by $(l_{IIch}h)^{1/2}$. When $a_0/(l_{IIch}h)^{1/2} > 1$, all curves converge, approaching the curve obtained for a Griffith crack in a material with toughness equal to that supplied by the bridging ligaments, $\mathcal{G}_b$ (dashed curve). Only when $a_0/(l_{IIch}h)^{1/2} < 1$ is there significant dispersion among the curves and even then it is modest. For vanishing notch size, the composite strength is limited by τ_{b0}, the ligament strength. Thus $(l_{IIch}h)^{1/2}$ and τ_{b0} alone are sufficient to define the ultimate notched strength to a fair approximation (Cottrell, 1963, Bao and Suo, 1992).

When $\mathcal{G}_{IIC} \neq 0$ and $\mathcal{G}_{IIC} \sim \mathcal{G}_b$ or $\mathcal{G}_{IIC} >> \mathcal{G}_b$, which may be the case in a composite with a tough matrix, solutions from Fig. 5 are not applicable and the ultimate notched strength will also depend quite strongly on $\mathcal{G}_{IIC}/\mathcal{G}_b$ and on the size of any initial bridged delamination crack (or matrix flaw). See Massabò and Cox (1996) for details.

The concepts outlined in this section are of course not peculiar to mode II cracks or to delamination specimens. Length scales and nondimensional parameters similar to those defined here control mode I fracture and apply to infinite specimens (Bao and Suo, 1992, Cox and Marshall, 1994). However, one important distinction of thin plates is that the lengths l_{ACK} and l_{SSB} are not material constants, as they are in infinite specimens, but material-structure parameters, involving the plate thickness, h.

3. ENF TESTS OF STITCHED AND UNSTITCHED LAMINATES

3.1. Materials

The materials investigated were stitched carbon/epoxy laminates.[2] Individual laminae consisted of so-called "uniweave" carbon fabric,[3] which is a plain woven ply

[2] These materials were fabricated under NASA's Advanced Composite Technology program for the investigation reported by Dickinson (1993).
[3] Textile Technologies Inc., Hatboro, Pennsylvania.

containing a preponderance of AS4 carbon fibers in warp yarns woven together with a small weight percent (2%) of E-glass fibers in weft yarns. Thus each uniweave ply is close in mechanical properties to a unidirectional ply of carbon fibers, the glass fibers serving mainly to hold the carbon fibers in place during processing. The uniweave layers were stacked in a repeating [45°/0°/-45°/90°] pattern to form symmetric 48-ply fiber preforms with quasi-isotropic in-plane properties.

The composites were fabricated by first stitching dry preforms. The stitches were inserted in parallel rows using a modified lock stitch,[4] shown schematically in Fig. 6. Different stitching patterns were used with 0.32-0.64 rows of stitching per mm (4-8 rows per inch) and 0.32-0.64 stitches per mm in each row. The bobbin thread was a 3640 denier S2-glass fiber tow (nominally 1250 yard/lb), the needle thread a 200 denier two-end-twisted Kevlar fiber tow. The through-thickness part of the reinforcement consisted of doubled 3640 denier glass tows, which may be represented effectively as a single 7280 denier tow, since they were always observed to act in unison in experiments. The stitch (doubled tow) is approximately cylindrical in the composite, with an internal fiber volume fraction of 0.51 and a cross-sectional area of 0.64 mm^2 (Turrettini, 1996).

After stitching, the composites were consolidated by resin transfer moulding using E905L epoxy resin.[5] The panel thickness was controlled to approximately 6.9 mm by a shim plate in the RTM mould, which resulted in a nominal in-plane fiber volume fraction of 0.60. Actual panel thickness ranged from 6.7 - 7.2 mm. Further details of the processing, which are not germane to the bridging problem, can be found in (Dickinson, 1993).

The specimens used in this work were remnants from Dickinson's earlier work. The remnants were machined into long rectangular strips, typically 24 mm wide and 120 - 200 mm long. In the tests reported here, the rows of stitches were oriented along the length of the specimen. In each specimen, a notch of length 10 - 40 mm and height typically 1 mm was cut along the mid-plane from one end using a diamond saw. A pre-crack of length ~ 10 mm was then created by pressing a razor blade into the notch root.

3.2 Experiments

Delamination cracks were grown in both stitched and unstitched composites using the End Notched Flexure (ENF) test configuration (Fig. 1). Testing was conducted under displacement control on a screw-driven mechanical test frame,[6] with a displacement rate

[4] Stitching done by Ketema, Textile Products Division.
[5] British Petroleum.
[6] Instron 1125 Mechanical Testing System, Instron Inc., XX, Massachusetts.

of 0.05 mm/min. The center point displacement was determined using a linear variable differential transformer (LVDT). This displacement and the load were recorded continuously by a LabVIEW-based data acquisition system.[7]

Representative load-displacement curves for unstitched and stitched composites are shown in Figs. 7.a and 7.b. For the unstitched composite, the load increases almost linearly to its peak value, at which point unstable crack growth fractures the specimen to the center loading point. For the stitched composite, the load increases linearly to the point at which stable crack growth initiates, beyond which it continues to increase monotonically but with a lower slope because the specimen compliance increases with delamination crack growth. A fall of about 35% in the flexural stiffness of the specimen is observed during the growth of the crack. In the case shown in Fig. 7.b, all stitches remained intact in the wake of the crack.

In general, the character of delamination crack growth in stitched specimens will depend on the stitching specifications, **the interlaminar fracture energy** and the specimen geometry (Massabò and Cox, 1996). The case of stable crack growth shown in Figure 7.b is just one possibility for this or any other stitched laminate. Its special virtue for this paper is that it permits detailed observations of the effect of the bridging stitches on delamination propagation.

3.3 Differential Image Analysis

To determine the bridging law, $\tau_b(w)$, from crack displacement profiles, the crack displacements must be measured to within a few percent of the maximum displacement at the notch root or crack mouth (Cox and Marshall, 1991.a), i.e., in the present problem to within a small fraction of 1 μm. This challenging requirement may be satisfied by differential image analysis of micrographs of quite modest magnification (X30). The same technique provides excellent detail of the extent of crack propagation and crack morphology. In particular, it permits accurate identification of the location of the crack tip, which is essential to fracture mechanics analyses. In prior work, various methods including photomicrography, x-radiography, and ultrasonic C-scanning failed to measure the crack length accurately (Sharma and Sankar, 1995).

Differential image analysis requires quality images of the specimen surface contrast taken during various stages of a test procedure, for instance before and after an increment in specimen loading. Displacements are measured by determining the relative change in position of surface contrast features. The useful contrast features included fiber bundles, matrix pockets, scratches, and other naturally occurring features, as well as lines scribed

[7] LabVIEW Graphical Programming Software, National Instruments, Austin, Texas.

onto the specimen surface. The image analysis was performed by manual stereoscopy, rather than by an automated system. Manual stereoscopy is just as accurate as computer based systems; and the operator can detect many qualitative characteristics an automated system would overlook. In manual stereoscopy, in-plane displacements are perceived as changes in height and a crack appears as a sharp ledge viewed from above. Manual stereoscopy takes advantage of the exceptional sensitivity of the human visual system to changes in apparent depth. Quantitative measurements are obtained through comparison of the perceived surface profile with a calibrated traveling spot (Williams et al., 1980; Cox et al., 1986; James et al. 1990).

In this work, the area of interest often spanned more than 40 mm, the length of a delamination crack. At a magnification of X30, the field of view is much less than this and the area of interest had therefore to be recorded as a collage of three images. Further, as the crack grew, the specimen deflected significantly, complicating the capture of high quality images for differential analysis. It was quite critical to maintain uniform focus conditions between images taken before and after loading. In spite of these experimental challenges, stereoscopic analysis worked very well. Crack opening and sliding displacements were measured with an error of at most 0.3 μm.

Stereoscopy reveals many details about the delamination process. Near the notch root, the damage consists of a band of small cracks and plastic shear deformation approximately equal in width to the height of the notch. Away from the notch root, the width of the band diminishes, until over a domain of 5 - 10 mm behind the crack tip, it consists of a single crack. At other locations (between the tip zone and the notch zone), up to four parallel cracks may be discerned over brief intervals. However, even where four cracks are observed other than in the notch damage zone, they are confined to a single [45°/0°/-45°/90°] four-ply stack at the center of the beam (total width ~ 0.5 mm or half the notch height).

Both crack sliding and opening displacements are evident. Pursuing the view that the entire damage band can be modeled as a single fracture event, the displacements were summed, where multiple cracks existed, to yield the net displacement, sliding or opening, over the whole damage band. These summed displacements are analyzed in detail below. Thus the analysis of the bridging traction law refers to the constitutive behavior of the entire delamination band, whether it consists of single or multiple cracks.

Figure 8 shows the total crack opening and sliding displacements measured along the delamination crack in the specimen of Fig. 7.b at one point in its growth. The zone of detectable sliding displacement extends some 20 mm from the notch. Its extremity indicates the position of the crack tip. The opening displacement becomes undetectable

by stereoscopy at a point about 2.5 mm behind the crack tip, where the sliding displacement is still ~ 5 μm. Since the measurement error is ~ 0.3 μm, the sliding displacement therefore ranges from zero to at least 15 times the opening displacement over this tip zone. Thus the crack tip conditions are purely mode II.

At a much finer scale, perhaps ~ 1 μm, one might expect to find that the furthest advance of damage consists of arrays of ogive microcracks, whose shapes and orientation are just such as to create pure mode I conditions at each of their tips when the far field stress is pure shear. Such microcracks have been seen in shear-loaded, constrained layers of various brittle materials, including ceramics and epoxy resins (Fleck, 1991; Xia and Hutchinson, 1994; Cox et al., 1994). In the ENF specimens, they are likely to be confined to a domain of ~10 μm at the furthest advance of damage. Beyond this zone, the magnitude of the sliding displacement will be so great that the putative microcracks must give way to more severe states of damage, in which the microcracked resin will form a fine layer of rubble within the observed single dominant crack. The relevant scale for modeling the crack tip in Fig. 8 is ~ 1 mm, two orders of magnitude greater than the zone of ogive micro cracking. At this greater scale, the stress fields must be almost entirely shear (where macroscopic opening displacements are not observable) and the delamination can be modeled as a mode II crack.

In the further crack wake, the opening displacement rises to an approximately constant value. This behavior is reminiscent of crack opening due to surface roughness in mixed mode fatigue crack tests in alloys. The plateau in the opening displacement corresponds in alloys to the size of mismatched asperities. In the stitched laminates, the opening is due to the propping effect of the bridging stitches when they bend plastically within the crack. Propping may be represented as opening tractions acting on the fracture surfaces, which will generate a mode I crack tip stress field. However, since the opening tractions act some distance behind the crack tip in a thin specimen, their effect on the crack tip stress fields will be relatively small. This is confirmed by the observation that the opening displacement vanishes near the crack tip. The opening tractions can therefore be neglected in analyzing the fracture behaviour of this specimen.

The measurement error in the data of Fig. 8 is considerably less than the fluctuations they exhibit, which reflect material inhomogeneity. The opening displacement shows minima at intervals of approximately 3 mm, which is similar to the stitch spacing, suggesting that the crack opening is reduced locally by discrete stitches. However, it is not possible to be certain by examining the images of the specimen surfaces that the minima coincide with the locations of stitches, which are some distance below the observed surface. The sliding displacements are smoother over most of the crack length.

Since the stitches are much stiffer normal to the delamination plane (i.e., in the stitch fiber direction), they should indeed cause smaller local effects in the sliding displacements than in the opening displacements. Fluctuations in the sliding displacements, such as they are, tend to occur where the delamination damage band contains multiple cracks.

Further crack sliding displacement profiles were determined at several loads for the stitched composites tested. Profiles for the specimen of Fig. 7.b, in which the crack grew stably to the specimen midpoint, are shown in Fig. 9.

4. THE BRIDGING LAW FROM FRACTURE TESTS

The crack sliding displacement profiles and the load-deflection curve shown in Figs. 9 and 7.b, which were obtained from an ENF test on a stitched laminate, can be used to define the bridging law characterizing the mechanism developed by the stitches within a bridged-crack model.

The specimen being analyzed had dimensions $2L$=120 mm, $2h$=7.2 mm and d=24.07 mm, with a notch length, a_0=20 mm, and a starter matrix crack length, a-a_0≅10 mm. It was stitched by glass fiber tows on a square array of side 3.2 mm. The total stitch area fraction was c_s=0.062. The specimen satisfies to a good approximation all of the restrictions necessary for the application of bending theory for laminated plates and the superposition scheme of Fig. 2 (see Appendix A and Section 2). Application of homogenization rules (Hashin, 1979) and lamination theory (Christensen, 1979), for the definition of the homogenized elastic constants of each fiber-reinforced lamina and the stiffness properties of the laminate, respectively, shows that the material can be approximated as being homogeneous and specially orthotropic, with a shear modulus G_{xz} ≈ 1/17E, E=E_x/(1-ν_{xy}^2) and ν_{xy}=0.3. The shear stress, τ, applied along the faces of the delamination in the problem of Fig. 2.c, is then given by Eq. (2).

4.1 The Bridging Law from Crack Profile Measurements

In the forward boundary value problem posed by Eqs. (11) and (12) and related boundary conditions, the bridging law, $\tau_b(w)$, is known and the crack sliding displacement, $w(x)$, given by Eq. (13), is to be calculated for fixed delamination and notch lengths, a and a_0, and applied shear stress, τ. In the inverse problem proposed here, the crack sliding displacement is known at a set of m points along the delamination for a given value of the applied shear stress, τ, and the bridging law, $\tau_b(w)$, is sought. A numerical solution of the inverse problem, based on a discretization, is detailed in Appendix B.

The first studies dealing with the problem of determining the bridging law from measurements of the entire crack profile were performed by Rödel et al. (1990) and Du et al. (1989) on an alumina ceramic and a concrete, respectively. Later studies are due to Cox and Marshall (1991a), Fett et al. (1994) and Guo et al. (1993). In all cases the bridging tractions represented bridging mechanisms acting along mode I cracks and supplied either by aggregates, coarse grains, or fibers. The inverse model proposed here is inspired by the formulation of Cox and Marshall (1991a). They developed a numerical procedure based on the fracture mechanics integral equation relating bridging tractions and crack opening displacement for a mode I fracture process in large scale bridging conditions.

Two different formulations of the inverse problem are proposed in Appendix B.1 and B.2. In the formulation of Appendix B.1, the bridging tractions are sought as a function, $\phi_b(x)$, of position along the crack, x. The bridging law, $\tau_b(w)$, can then be defined by interpolating the deduced $\phi_b(x)$ over the crack sliding displacements, $w(x)$. In the formulation of Appendix B.2, the bridging law, $\tau_b(w)$, is sought directly without the intermediate step of deducing $\phi_b(x)$.

The inverse problem is solved through a linear least square fit, according to which the norm of the residuals between the experimental data, which are the crack sliding displacements at m points along the crack, and the theoretical predictions must be minimized. This straightforward procedure is complicated by the inevitable presence of noise, including not only experimental error in the measurements, but also computer round-off errors and errors inherent to the model, e.g., the approximation of describing the localized actions of discrete stitches by a continuous distribution of tractions. Further, the minimization problem is ill-conditioned and highly degenerate. The instability of the solution is evident in large oscillations in the calculated bridging tractions.

Analysis of synthetic crack sliding displacement profiles, i.e., profiles calculated theoretically for some known bridging laws with Gaussian noise added to simulate typical experimental errors, was used to define two different procedures that treat instability effectively.

The first procedure is based on a Linear Regularization Method (Twomey, 1977, Tikhonov, 1963), which combines the problem of minimization with a constraint on the degree of smoothness required in the solution. The method can be applied when either $\phi_b(x)$ or $\tau_b(w)$ is sought (Appendixes B.1 and B.2). The constraint function for smoothness is weighted by a Lagrange multiplier, λ, whose value defines a progressive transition from the solution giving the best agreement between the data and the prediction ($\lambda=0$) and that giving the smoothest bridging tractions ($\lambda\rightarrow\infty$). If a good model exists for

noise in the data and the goodness-of-fit has been assessed, then the optimal choice for λ is that for which the root mean square deviation of the model from the data equals the a priori assigned deviance in the measurements (see Eq. (B.9)).

The second procedure, which can be coupled or not to the previous one, is based on the utilization of more than one profile in the minimization problem. Crack profiles acquired during the same test at different values of the applied load and corresponding to different crack lengths can be analyzed together as shown in Appendix B.2.2. This method has two advantages. First, it increases the number of data points near the tip of the crack, a region which is very sensitive to errors in the data. Second, it includes in the same analysis a much greater range of crack sliding displacements. The noise tolerance of the model is thus substantially improved (see Cox and Marshall (1991a) for examples). Simultaneous analysis of several data sets is applicable only when the bridging tractions are sought as a function of the crack sliding, $\tau_b(w)$, since the function $\phi_b(x)$ in not unique for different crack lengths or for different applied loads.

All of the above approaches were assessed in treating the noise in the experimental data of Fig. 9. In the fitting procedures, the axial Young's modulus of the laminate was taken to be $E = E_x/(1-\nu_{xy}^2) = 49$ GPa, a value deduced from the linear elastic branch of the load deflection curve for the same specimen (Fig. 7.b), whence the axial and bending stiffnesses of the laminate are $A_i = 2Eh = 353$ KN/mm and $D_i = 2/3Eh^3 = 1530$ KNmm.

In the first calculations the bridging tractions were sought as a function of position along the crack, by applying the constrained minimization problem, Eq. (B.12), separately to each of the three crack profiles of Fig. 9. The results of the investigation are not reported here. In fact, even if they gave some insight into the bridging mechanisms acting along the crack, the noise in the data was such to prevent a reliable definition of the bridging law.

The problems found in the first calculations were overcome by seeking the bridging tractions directly as a function of w, using the three crack profiles of Fig. 9 simultaneously through Eq. (B.23). In accordance with Eq. (B.14) the unknown continuous distribution $\tau_b(w)$ was expanded in Legendre polynomials to order 8. Using such a high order of polynomials avoids any a priori constraint on the shape of the bridging law. The sum of the squares of the second derivatives of the bridging tractions at the m experimental points was used in Eq. (B.23) as a measure of deviation from smoothness. Figures 10.a and 10.b depict the calculated bridging tractions, $\tau_b(w)$, found on varying the Lagrange multiplier, λ. The curve for λ=0 defines the unconstrained solution which is highly unstable. On increasing the value of λ the oscillations in the solution are reduced and for λ higher than $1 \cdot 10^{-15}$ small oscillations localize at the

smallest and highest values of w (Fig. 10.b). As already shown by Cox and Marshall (1991a), the estimate of $\tau_b(w)$ at small w could be improved only if a very high density of data points were present near the tip of the crack and the data were almost noiseless. The oscillations at the highest w arise from the presence of the notch, which increases the noise in that region. Values of λ higher than $\lambda=1\cdot10^{-12}$ define the smoothest solution, which is linear (solid line in Fig. 10b) because of the assignment k=2 Eq. (B.22).

All of the bridging traction curves of Fig. 10 give very good predictions of the crack sliding displacements for the three applied loads examined, the residuals between the data and the predictions being of the same order of magnitude. They define the estimated error in the data, Eq. (B.9). This result indicates that the information content of the experimental crack profiles is limited by noise to the extent that the data contain only enough information to reveal the general shape of the function being sought but not its details. In fact, a perfectly smooth solution exists which satisfies the fundamental equation (B.23) within the estimated error: the bridging law can therefore be considered as linear to within the sensitivity of the experiment, with its slope given by the average slope of the various curves in Fig. 10.b.

Since no detailed information regarding the shape of the bridging law can be obtained from the inversion, a different and expeditious technique has been tried based on the use of lower order basis functions for the traction law in the unconstrained problem (λ=0). The curves shown in Fig. 11 depict the bridging tractions deduced from the simultaneous analysis of the three crack profiles of Fig. 9, by assuming polynomials of different orders as basis functions and setting λ=0 in Eq. (B.23). It can be seen that reducing the order of the function has the same influence on the solution as increasing the value of the Lagrange multiplier in the constrained problem. In both cases the stability of the solution is improved and the curve in Fig. 10 for $\lambda=1\cdot10^{-12}$ coincides with the solid curve corresponding to a first order polynomial of Fig. 11. Again, all of the curves give similar residuals between the data and the predictions.

The bridging tractions shown in Fig. 12 have been obtained by expanding the bridging law in low order polynomials with the added constraint that they pass through the origin (i.e., $\tau_b(0)=0$). These predictions give obviously inferior agreement with the data and the solutions prove to be more unstable. Figures 11 and 12 together show that the offset from the origin of the traction law, $\tau_b(w)$, is necessary if the law is represented by a single straight line or low order polynomial. Further remarks on the possible behaviour of $\tau_b(w)$ at small w appear in Section 4.4. From the above calculations, the linear bridging law, $\tau_b(w)= 12.7+102w$ MPa, is deduced to be representative of the bridging mechanisms developed by intact stitches in this particular composite over the

range of w examined ($0.\leq w\leq 0.15$ mm). The sliding displacement profiles computed for this law are compared with the experimental data in Fig. 13.

Mode II interlaminar fracture energy

Once the bridging law has been determined, an approximate evaluation of the mode II interlaminar fracture energy, $\mathcal{G}_{IIC}$, can be obtained from the critical load measured experimentally for a particular crack length, P_{cr}, or equivalently τ_{cr} (Eq. 2), through the condition $\mathcal{G}_{II}=\mathcal{G}_{IIC}$, with $\mathcal{G}_{II}$ the strain energy release rate given by Eq. (14). Analysis of the two longer cracks of Fig. 9, of lengths a=39.8 mm and a=53.6 mm, with critical shear stresses, τ_{cr}=10.4 MPa and τ_{cr}=13.8 MPa, leads to $\mathcal{G}_{IIC}\cong 0.25$ KJ/m^2 and $\mathcal{G}_{IIC}\cong 0.37$ KJ/m^2, respectively. These values are approximately 1/15th of the energy dissipated by the bridging mechanism for the same loads, which is defined by the second term on the right hand side of Eq. (14). The variance in the values found for $\mathcal{G}_{IIC}$ will be discussed in the next section.

Structural behavior

In order to validate the results of the inverse problem, the deduced linear bridging law and intrinsic fracture energies were used in the forward problem to calculate the load-deflection curve of the ENF specimen. The evolution of crack growth was computed up to a maximum crack length, a=53.6 mm, corresponding to the measured crack length at P=3.2KN (see Fig. 9). The shear modulus was assumed equal to $G_{xz}=1/17E$=2.88 GPa, the ratio 1/17 resulting from standard laminate analysis for the lay-up in question.

In Fig. 14 the experimental load vs. mid-span deflection curve (thin lines) is compared with the theoretical curves (solid lines). The elastic response expected of an uncracked specimen and given by $\delta_{(b)}$ of Eq. (1) has been subtracted from the actual mid-span deflection to highlight the nonlinear behavior. The three curves of Fig. 14 describe the response of the specimen shown in Fig. 2.c.

The knees in the curves indicate the onset of stable crack propagation. Their position is controlled primarily by $\mathcal{G}_{IIC}$. The flexural stiffness of the specimen when the crack is growing is controlled mainly by the bridging law (which amounts for the linear law to control by the intercept and slope, $\tau_b(0)$ and β). The slope of the curve is satisfactorily reproduced by the model for both values found for $\mathcal{G}_{IIC}$. On the other hand, $\mathcal{G}_{IIC}$ affects the values of the critical load and the deflection corresponding to a given crack length, which both decrease on decreasing $\mathcal{G}_{IIC}$. The theoretically predicted response of the specimen proves to be slightly stiffer than the actual response and the theoretical deflection at the maximum crack length is somewhat lower than the experimental value. The

discrepancies are small – for example that in the secant stiffness, including the component computed for the uncracked specimen in the superposition problem, is never greater than ??% – but they are beyond the errors expected. They could be explained by the existence of nonlinear phenomena which the crack profile data will not incorporate (and which would therefore not be represented in the law deduced from profile data), such as diffuse damage in the bulk of the laminate or viscous behavior of the resin. Further experiments are needed to resolve these questions.

4.2 The Bridging Law from the Load-Deflection Curve

The macrostructural response of composite members depends on how the bridging mechanisms control the fracture process. Conversely, the bridging law can be inferred from the structural response, e.g. by a parametric fit of experimental load vs. load-point displacement data. This approach requires only the execution of experimental tests which are easy to perform in any laboratory, such as three point bending tests or compact tension tests. It has been applied to concrete and fiber-reinforced concrete by Wittmann et al. (1987, 1988), Guinea et al. (1994), Uchida et al. (1995), and Nanakorn et al. (1996), and to coarse-grained alumina by Fett (1995).

The measured set of load vs. mid-span deflection data shown in Fig. 7.b contain information about all of the parameters which control the flexural behavior of the laminate: the elastic constants of the material, the interlaminar fracture energy, and the bridging law of the reinforcement. A nonlinear minimization problem can be defined and the best fitting parameters, $\mathcal{G}_{IIC}$, E, and $\tau_b(w)$, evaluated by seeking the minimum of the norm of the residuals between the data points and the theoretical predictions. The stiffness modulus E characterizes the elastic behavior of the homogeneous orthotropic laminate by itself, since it defines the axial, bending, and shear stiffnesses (the ratio G_{xz}/E being assumed known for the given lay-up from laminate theory).

The analysis of load-deflection data was restricted to linear bridging laws, $\tau_b(w)=\tau_b(0)+\beta w$. The load-deflection curve, in fact, cannot give any detailed information about the shape of the bridging law, since it arises from the combination of many local phenomena. The same macrostructural response, for instance, can be computed for different combinations of $\tau_b(w)$ and $\mathcal{G}_{IIC}$, and the latter can be set equal to zero if the bridging tractions are chosen in order to represent all the toughening mechanisms of the whole composite (Carpinteri and Massabò, 1996). This observation along with the results of the local analysis of Section 5.1, suggest the above bound to the range of $\tau_b(w)$ examined.

The estimation of the parameters of best fit, $\tau_b(0)$, β, $\mathcal{G}_{IIC}$ and E was performed through an algorithm based on the Levenberg-Marquardt Method (Marquardt, 1963) and the uncertainties in the fitted parameters were calculated by a Monte Carlo simulation of synthetic data sets. The synthetic data sets were generated by adding Gaussian noise to the load-deflection curve of best fit. The standard deviation of the noise was set equal to the estimated error in the data, given by the root mean square deviation of the model from the data. The values of the fitted parameters and their uncertainties are $\tau_b(0)=11\pm0.6$ MPa, $\beta=110\pm11$ MPa/mm, $\mathcal{G}_{IIC}=0.2\pm0.03$ KJ/m^2, and $E=49\pm0.1$ GPa. These values are quite close to those deduced from crack sliding displacement profiles (Section 4.1).

Figure 15 compares the load-deflection curve of best fit (solid line) with the experimental curve (thin line). Again, the elastic response expected of an uncracked specimen has been subtracted from the actual mid-span deflection. As expected, the model faithfully reproduces the experimental results. However, the fitted parameters do not lead to accurate predictions of the crack lengths corresponding to the data points. Over the dashed part of the theoretical curve shown in Fig. 15, the predicted crack length exceeds a=53.6 mm, the maximum value measured experimentally. The relative indeterminacy of the crack length and the modest effect this has on the parameters deduced for the bridging law in analyzing load-deflection data is discussed further in Section 4.4.

4.3 Bridging Law from Other Measurements

Bridging traction laws can also be measured by direct methods. In prior work, small, notched cuboidal specimens containing just one stitch were cut out of a panel of the same stitched laminate analyzed here (Turrettini, 1996). The small specimens were loaded in large, stiff grips and tested in shear under displacement control. The bridging law expected of the stitches in a laminate can be deduced from the load-displacement curve of such tests when allowance is made for the stitching area density. The resulting laws show an approximately linear increase with much the same slope as the bridging laws deduced here (Cox et al., 1997). Some differences are found for small values of w, but the direct tests are vitiated in that regime by compliance in the test jig and the specimen, the displacements having been measured in the far field rather than across the fracture plane. For values of w near ultimate failure, which are two or three times the maximum crack sliding displacement reached in the present ENF tests, the direct tests also reveal mechanisms of further damage, including debonding and pulling down of the stitch from the outer surface of the laminate toward the fracture plane, which lead to softening in the traction law.

The maximum bridging traction deduced from the ultimate load at failure of the stitch is approximately $\tau_{b0} \approx 55$ MPa and the corresponding critical sliding displacement, w_0, is in the range $0.4 \leq w_0 \leq 0.6$ mm, the limits indicating variance from specimen to specimen. The fracture energy supplied by the stitches, $\mathcal{G}_b$, which represents twice the area beneath the bridging curve, $\tau_b(w)$, was deduced from the tests to be $\mathcal{G}_b \approx 30$ KJ/m^2. These three parameters could also be inferred from ENF tests on the stitched laminate, provided the stitches fail during crack growth.

4.4 Sensitivity of the Fracture Process and Limits to Information

The value of $\mathcal{G}_{IIC}$ and the traction law $\tau_b(w)$ deduced from the fracture tests, using either crack profiles or load-deflection data, incorporate the effects of all delamination toughening mechanisms and are therefore in principle sufficient information to predict the fracture behaviour of the stitched laminate. However, in practice one must further consider how perfectly $\mathcal{G}_{IIC}$ and $\tau_b(w)$ have been determined and the implied margins for error in subsequent predictions.

In many applications, shear stresses comparable to the ultimate stress required for stitch failure will not be expected, but delamination crack propagation in the presence of intact stitches will still be a concern. For through-thickness shear loads of ~ 10-20 MPa, which are typical of design limits near cut-outs in airframes, for example, the relevant domain of the traction law, $\tau_b(w)$, is covered by the data of the ENF tests of Figs 7 and 8. The quality of the information about $\mathcal{G}_{IIC}$ and $\tau_b(w)$ is therefore to be understood by analyzing the accuracy of the procedures presented here for deducing them from crack profiles and load-deflection data.

In fact, $\mathcal{G}_{IIC}$ is not precisely determined and correspondingly $\tau_b(w)$ is indeterminate at low values of w ($w < 25$ μm, Figs. 10 and 11). This indeterminacy is rooted in the nature of the bridged crack problem. Consider, in particular, the hypothetical bridging laws sketched in Fig. 16, one defined by the path ABC and the other by the path OBC. The difference in both the complementary energy of the ligament (the term in square brackets in Eq. (3)) and the contribution to the work of fracture due to the ligament (the term $\mathcal{G}_b$ in Eq. (6)) for these two laws is just twice the shaded area Δ(OAB). The ACK limit stress, τ_{ACK}, is determined by the condition of Eq. (3), that the complementary energy must equal half the intrinsic critical strain energy release rate, $\mathcal{G}_{IIC}$. Thus τ_{ACK} will be the same for the two laws provided the law ABC is coupled with some $\mathcal{G}_{IIC}$ while the law OBC is coupled with the greater quantity, $\mathcal{G}_{IIC} + 2\,\Delta$(OAB). Similarly the critical stress in small scale bridging, τ_{SSB}, will be the same for these two pairings.

Fracture energy associated with the traction law, $\tau_b(w)$, at small w and with $\mathcal{G}_{IIC}$ is always interchangeable provided the fracture phenomena in question involve crack displacements that are substantially larger over the preponderance of the crack than the displacements over which $\tau_b(w)$ is being modified (see also Cox and Marshall, 1994, and Carpinteri and Massabò, 1996). Therefore, indeterminacy of $\mathcal{G}_{IIC}$ and $\tau_b(w)$ for $w < 10$ μm is to be expected when analyzing the load-displacement data of Fig. 7, since displacements are ~100 μm over most of the crack (Figs. 8 and 9). Further, only the most precise measurements at small w, very near the crack tip, will be able to resolve $\mathcal{G}_{IIC}$ and $\tau_b(w)$ for small w in analyzing crack sliding profile data. In Fig. 9, few data exist near the crack tip; most lie in the further crack wake, where they are determined mainly by the balance between far-field stresses and bridging tractions at larger w.

This indeterminacy is of little consequence for predicting delamination in stitched laminates. Just as $\mathcal{G}_{IIC}$ and $\tau_b(w)$ for small w cannot be determined from fracture data, so conversely the fracture process and predictions of fracture are insensitive to the interchange of energy assigned to $\mathcal{G}_{IIC}$ and $\tau_b(w)$ for small w. It is sufficient that $\mathcal{G}_{IIC}$ and $\tau_b(w)$ for small w be determined consistently from a single analysis.

For this very reason, a fracture test such as the ENF test probably provides the best data for determining the bridging parameters of stitching. As far as the test is representative of the loading conditions expected in a structure in service, the degree to which it is sensitive or insensitive to details of the bridging model will be a faithful reflection of the influence of the stitches as bridging entities in the structure.

Indeterminacy between $\mathcal{G}_{IIC}$ and $\tau_b(w)$ for small w might in principle be removed by measuring $\mathcal{G}_{IIC}$ independently in an unstitched laminate. However, $\mathcal{G}_{IIC}$ in a stitched laminate might not be the same as the fracture toughness of an equivalent unstitched laminate. The stitching process introduces damage into the laminate, especially the distortion of in-plane fibers; and the stitches must interfere with the mechanics of propagation at the delamination crack tip, even before they pass into the crack wake where they might supply bridging tractions. Distorted in-plane fibers and stitches deflect the delamination, introduce local residual stress fields, and create resin pockets, among other effects. The net effect on the apparent intrinsic toughness, i.e., that toughness not ascribed to bridging, is very difficult to quantify.

A second characteristic of the fracture that may not be well determined without direct measurement is the length of the delamination crack. When the bridging parameters, $\mathcal{G}_{IIC}$ and $\tau_b(w)$, are inferred from load-deflection data, the crack length predicted at applied loads for which it had been measured turned out to be in significant error (see previous section). The reason for this lies once again in the mechanics of bridged cracks in large

scale bridging. When the crack length is large compared to the ACK limit length scale, l_{ACK}, the applied load becomes independent of the crack length. Further, the specimen compliance (or the load-point displacement) in this limit varies much more weakly than it would for a crack in an unstitched specimen. While the cracks in the load-deflection fracture experiments of Fig. 7 were not yet in the ACK limit, they were nevertheless somewhat larger than l_{ACK} and the indeterminacy of the ACK limit will have begun to be felt. Thus, the information contained in load-deflection data about the crack length is imprecise; in other words, if the crack length is specified ad hoc at different values during the fitting procedure, the inferred bridging parameters will not change very much. Conversely, when fracture predictions are made using the inferred parameters, the crack length may not be accurately predicted. Once again, this may be of little consequence for failure prediction. In many applications, it is enough to assure that the structural compliance will remain within design limits and it is not necessary to know or desirable to need to know the exact length of a delamination crack.

5. PREDICTIONS FOR ONE STITCHED LAMINATE

The bridging parameters $\mathcal{G}_{IIC}$ and $\tau_b(w)$ having been determined, instructive calculations can be made of the range of delamination behaviour expected for such a stitched laminate. In the calculations in this section, the bridging law is assumed to be a linear extrapolation of that inferred from the crack profile data up to the failure of the stitches at τ_{b0}. Thus the laminate was assigned the characteristics E=49 GPa, G_{xz}=2.88 GPa, $\mathcal{G}_b$ = 30 KJ/m^2, τ_{b0} = 55 MPa, $\mathcal{G}_{IIC}$=0.37 KJ/m^2, and $\tau_b(w)$= 12.7+102w MPa. The qualitative behaviour illustrated would be much the same for bridging laws that were nonlinear at high values of w.

5.1 Stitched and Unstitched Specimens in Flexure

The influence of stitching on the flexural behavior of the laminate can be highlighted by comparing the theoretical response of the stitched ENF specimen with the response the same specimen would show in the absence of bridging tractions, i.e., $\tau_b(w) = 0$. The load-deflection curves are shown in Fig. 17 (solid curves) along with the experimental curve obtained for the stitched specimen and already shown in Fig. 7.b (thin curve). The specimen without stitching shows linear elastic behavior up to the ultimate load at which the crack starts to propagate (P $\approx$ 1 KN). A snap-back instability indicates that the ensuing crack propagation is unstable. The unstable branch of the curve can be revealed in an experiment only if the loading process is controlled by a monotonically increasing

function of the time, such as the crack length. This branch will be virtual in a test performed under deflection control (see for instance Fig. 7.a).

This curve does not necessarily describe the response of the laminate used in this investigation in the absence of stitching, whose interlaminar fracture energy may not be equal to $\mathcal{G}_{IIC}$=0.37 KJ/m^2 (see Section 4), and the data for the unstitched laminate indeed indicate otherwise. Assuming that the unstitched laminate is perfectly brittle, plate theory analysis of the load-deflection curve of Fig. 7a yields $\mathcal{G}_{IIC} \approx 1.3$ KJ/m^2 (Eq. A.1). The elastic constant E for the unstitched laminate can also be deduced from Fig. 7.a and is found to be $E \approx 53$ GPa. As expected E is higher than for the stitched specimen (E=49 GPa), whose in-plane properties are degraded by the stitching process (e.g., Dickinson, 1993). The dashed curve of Fig. 17 depicts the behavior of an unstitched laminate with this higher fracture toughness. Even though the loading capacity of the specimen is increased, the fracture process remains unstable.

Figure 17 highlights the beneficial effects provided by the stitching, which not only increases the loading capacity of the specimen, but also changes the failure from an unstable and catastrophic process to a stable one.

5.2 Crack Propagation and Failure for More General Flexure Cases

The breadth of possibilities for fracture and failure during flexure can be understood more generally by reference to the material/structure parameters which characterize the two limiting solutions of the fracture problem: the ACK limit and the small scale bridging limit (Section 2).

The bridging law satisfies one condition for existence of the ACK limit, since it is an increasing function of the crack sliding displacement. For the given bridging law, the ACK limit has the following characteristics: the ACK shear stress, τ_{ACK} = 18.8 MPa (Eq. (4)); the material length scale, $a_{IIm} \cong 120$ mm (Eq. (5.b)); and the noncatastrophic length scale, $l_{ACK} = (a_{IIm}h)^{1/2} \cong 20$ mm.

The small scale bridging limit has the characteristics: ultimate strength of the ligaments, τ_{b0} = 55 MPa; ratio between the energy supplied by the stitches and the intrinsic interlaminar fracture energy, $\mathcal{G}_b/\mathcal{G}_{IIC} \cong 30/0.37 = 80$; and mode II characteristic length scale, l_{IIch} = 485 mm (Eq. (10)). Since $\mathcal{G}_b/\mathcal{G}_{IIC}$ is so large, the length of the bridging zone in small scale bridging, l_{SSB}, can be approximated within a factor near unity by $l_{SSB} = (l_{IIch}h)^{1/2} \cong 40$ mm (Section 2). Moreover, Figure 5, obtained for $\mathcal{G}_{IIC} = 0$, can be used to describe the notch sensitivity of ultimate shear strength.

The various length scales controlling the fracture process in the stitched laminate are much higher than the stitch spacing ($\approx$ 3 mm). This confirms the validity of the modeling

step of replacing discrete stitches by a continuous distribution of shear tractions. The delamination must span many stitches before the effects of bridging are significant.

Unnotched laminates

The ACK shear stress is about one third of the ultimate shear strength of the ligaments (τ_{ACK}/τ_{b0}=0.34). Therefore the ACK limit will be approached in an unnotched ENF specimen, provided the length of the crack, and therefore the half length of the specimen, is greater than 40 mm (i.e., $L > 2\cdot(a_{IIm}h)^{1/2}$, Fig. 3). Once the applied load reaches τ_{ACK}, a delamination crack fully bridged by intact stitches will propagate right across the member. A higher applied load will then be necessary to fail the stitches. For an unnotched laminate, the ACK shear stress represents a design limit, because it defines a conservative bound for the applied shear stress required for noncatastrophic delamination cracking (Fig. 3). The delamination cracking stress is not reduced by the pre-existence of a delamination crack provided it remains fully bridged by undamaged stitches. The ACK shear stress can then be used to tailor the minimum stitch density required to avoid delamination.

Notched laminates

The presence of a notch or a region of the laminate where the stitches have failed can substantially modify delamination behavior. The stress concentration at the tip of the notch can be high enough to fail the stitches, initiating catastrophic delamination failure (i.e. the first crack will separate the specimen in two). The limit length of the notch dividing the regimes of noncatastrophic and catastrophic failure can be obtained from Fig. 5 by identifying the ordinate with τ_{ACK}/τ_{b0}. Thus for the subject case, where τ_{ACK}/τ_{b0} = 0.34 and the traction law is intermediate between the linear and rectangular cases of Fig. 5, the limit notch length is given by $a_0/(l_{IIch}h)^{1/2} \approx 1.0$ or $a_0 \approx 40$ mm. The shape of the bridging law affects the limit value by less than 10%.

Another limit length of the notch is that which defines the stability of the initial propagation of the crack. Initial crack growth will be stable if $\tau_{cr}(a_0) < \tau_{ACK}$ or, from Eq. (15), $a_0 > 7$ mm.

Thus stable crack growth can be observed in a specimen of the subject material if and only if $7 < a_0 < 40$ mm. The ENF specimens that exhibited stable crack growth in this investigation fall in this range (e.g., Fig. 7.b). On the other hand, the ACK limit will be reached only if $L\text{-}a_0 \geq 100$ mm **(see Fig. 3).** For typical laminate depths this length would be too large to avoid the flexural failure of the laminate. Delamination cracks in ENF specimens of typical size, e.g., $L \approx 60$ mm (Fig. 7.b), will propagate stably in large scale

bridging conditions at critical stresses still 10% below the ACK limit (although 3-4 times the critical stress for an unbridged crack). Accurate analysis of the fracture process thus requires full solution of the bridged crack problem and asymptotic solutions will be inadequate.

If the notch length is higher than the limit value defined for noncatastrophic failure, the stitches will start to fail at the root of the notch during crack growth. The crack will then propagate unstably toward the small scale bridging limit. However, the critical stress will be within 20% of τ_{SSB} only when the crack length is greater than $2 \cdot l_{SSB}$, or 80 mm (see Section 2 and Fig. 5). The length of the bridging zone will progressively decrease during the unstable propagation, tending to the lower bound given by l_{SSB} when the small scale bridging limit is achieved.

Thus a specimen of half length greater than 160 mm would be required to approximate small scale bridging conditions. This will not be the case in specimens of common dimensions and full solution of the bridged crack problem rather than asymptotic solutions (i.e., in this regime, linear elastic fracture mechanics) is again required.

Large Scale Bridging Solutions for Crack Growth

Figure 18 compares accurate solutions of the large scale bridging problem with the ACK and small scale bridging limits for a laminate characterized by a general linear bridging law, $\tau_b(w) = \tau_b(0) + \beta w$, that is consistent with the specific values listed at the beginning of this section ($\tau_b(0) = 2(\mathcal{G}_{IIC}\,\beta)^{1/2}$ and $\mathcal{G}_b/\mathcal{G}_{IIC} = 80$). The different solid curves refer to different notch lengths. The diagram also demonstrates the transition from noncatastrophic to catastrophic failure on varying the length of the notch. Three different regimes of fracture are recognized: a) unstable delamination crack growth with intact stitches in the crack wake for notch lengths lower than $0.33 \cdot (a_{IIm} h)^{1/2}$ (or 7 mm for the case study); b) stable delamination crack growth in laminates whose notch lengths are in the range $0.33 < a_0/(a_{IIm} h)^{1/2} < 2.3$ (or $7 < a_0 < 46$ mm), with the ACK limit approached in long enough specimens; and c) stable delamination crack growth followed by stitch failure beginning at the notch root and further unstable crack growth to ultimate failure in laminates whose notch lengths satisfy $a_0 > 2.3 \cdot (a_{IIm} h)^{1/2}$ (or 46 mm). The small scale bridging solution of the problem, obtained through application of linear elastic fracture mechanics and represented in Fig. 18 by the dotted curve, will be reached in the last case (to within 10% in the critical stress) only after the crack has propagated over a length $\approx 10 \cdot (a_{IIm} h)^{1/2}$ (or 200 mm). For the subject case, the length of the bridged zone in this limit is l_{SSB}=38 mm.

7. CONCLUSIONS

Mode II delamination cracks in typical stitched laminates propagate under large scale bridging conditions to lengths greater than those likely to be considered admissible in an engineering structure. Therefore, engineering structural behavior cannot be analyzed in terms of small scale bridging concepts, including the critical mode II strain energy release rate, $\mathcal{G}_{SSB}=\mathcal{G}_{IIC}+\mathcal{G}_b$. It must instead be computed via a bridged crack calculation, in which the essential material characteristic is the bridging traction law, $\tau_b(w)$.

A viable approach to determining $\tau_b(w)$ sufficiently well to make engineering reliability predictions appears to be the analysis of load-deflection data in ENF tests. The traction law deduced from load-deflection data is confirmed by the analysis of crack sliding displacement profiles and by direct measurements on miniature specimens. The virtue of using load-deflection data is that they directly represent the performance of the laminate as an engineering structure in mode II applications. Moreover, these data can be obtained through tests, such as the End Notched Flexure test, which are already standard engineering procedures. The notch size and other specimen dimensions should be selected to ensure that crack growth is stable in the test and that crack sliding displacements comparable to those expected in service are achieved.

Mode II delamination propagation, when the through-thickness reinforcement does not fail, is sensitive to at most three parameters, which can be chosen conveniently to be: the value of the traction law at zero displacement, $\tau_b(0)$, the slope of the traction law, and the intrinsic delamination resistance, $\mathcal{G}_{IIC}$.

ACKNOWLEDGMENTS

The authors are very grateful to Dr. Larry Dickinson for supplying stitched laminate specimens and to Dr. Fred Morris for stereoscopic analysis of images. BNC was supported by AFOSR Contract No. F49620-94-C-0030 and RM by Rockwell Independent Research and Development funds and funding from the Italian Department for the University and for Scientific and Technological Research.

REFERENCES

Aveston, J., Cooper, G.A., and Kelly, A. (1971) , Single and multiple fracture, in *The properties of fiber composites*, Conf. Proc., National Physical Laboratory, IPC Science and Technology Press Ltd., 15.

Bao, G. and Suo, Z., (1992), Remarks of crack-bridging concepts, *Appl. Mech. Rev.*, **24**, 355-366.

Bao, G. , Ho, S., Suo, Z. and Fan, B. (1992), The role of material orthotropy in fracture specimens for composites, *Int. Journal Solids Structures*, **29**(9), 1105-1162.

Bradshaw, F. J., Dorey, G., and Sidey, G. R. (1973), Impact Resistance of Carbon Fiber Reinforced Plastics, *Royal Aircraft Establishment Technical Report 72240*, Farnborough, England.

Budiansky, B., Hutchinson, J.W., Evans, A.G., (1986), Matrix fracture in fiber reinforced ceramics, *J. Mech. Phys. Solids,* **34**(2), 167-189.

Carpinteri, A., and Massabò, R. (1996) Bridged versus cohesive crack in the flexural behavior of brittle matrix composites, *Int. Journal of Fracture,* **81** (1996), 125-145.

Carlsson, L.A. and Gillespie, J.W., (1989), Mode-II interlaminar fracture of composites, in *Application of Fracture Mechanics to Composite Materials*, ed. K. Friedrich, Elsevier Science Publisher, Amsterdam, The Netherlands..

Chatterjiee, S.N. (1991), Analysis of test specimen for interlaminar mode II fracture toughness, part 1. elastic laminates, *J. of Composite Materials*, **25**, 470-493.

Christensen, R.M., (1979) *Mechanics of composite materials*, John Wiley & Sons Inc., new York, USA.

Cottrell, A.H., (1963), Mechanics of Fracture, *Tewksbury Symposium of Fracture,* University of Melbourne, Australia, 1-27.

Cox, B.N., Morris, W.L. James, M.R (1986), High Sensitivity, High Spatial Resolution Strain Measurements in Alloys and Composites, in *Proceedings of Nondestructive Testing and Evaluation of Advanced Materials and Composites*, Colorado Springs, CO, 25-39.

Cox, B.N., and Marshall, D.B. (1991a), The determination of crack bridging forces, *Int. Journal of Fracture* **49**, 159-176.

Cox, B.N., and Marshall, D.B. (1991b), Stable and Unstable Solutions for Bridged Cracks in Various specimens, *Acta Metall. Mater.* **39**, 579-89.

Cox, B.N., and Marshall, D.B. (1994), Concepts for bridged cracks in fracture and fatigue, *Acta Metall. Mater.*, **42**(2), 341-363.

Cox, B. N., Dadkhah, M. S., Morris, W. L., and Flintoff, J. G. (1994), Failure mechanisms of 3D woven composites in tension, compression, and bending, *Acta Metall. Mater.*, **42**(12), 3967-3984.

Cox, B. N., R. Massabò, D. R. Mumm, A. Turrettini, and K. Kedward, (1997), Delamination Fracture in the Presence of Through-Thickness Reinforcement, in Proc. 11th

Int. Conf. Composite Materials, Gold Coast, 1997, Australia, ed. M. L. Scott Woodhead Publishing, Melbourne, ????-????.

Darbyshire, H. F. (1970), Bendix Aerospace-Electronics Company Report BDX-613-144.

Dickinson, L. (1993), Effects of Stitching Parameters on Mechanical Properties and Damage Tolerance of Stitched/RTM Composites, *Fourth NASA/DoD Conference on Advanced Composites Technology*, Salt Lake City, Utah, 1993, ed. J. G. Davis, J. E. Gardner, and M. B. Dow, NASA, 1993.

Dow, M. B., and Smith, D. L. (1989), Damage Tolerant Composite Materials Produced by Stitching Carbon Fabrics, *Int. SAMPE Technical Conf. Series*, **21**, 595-605.

Dransfield, K., Baillie, C., and Mai, Y.-W. (1994), Improving the Delamination Resistance of CFRP by Stitching - a Review, *Composite Science and Technology*, **50**, 305-17.

Du, J., Hawkins, N.M. and Kobayashi, A.S. (1989), A hybrid analysis of fracture process zone in concrete, in Fracture of Concrete and Rock. Recent Developments, S.P. Shah, S.E. Swartz and B. Barr, eds., Elsevier Applied Science, Cambridged, UK.

Fett, T., Munz, D., Yu, C-T. and Kobayashi, A.S. (1994), Determination of bridging stresses in reinforced Al_2O_3, *J. of Am. Ceram. Soc.*, **77**(12), 3267-69.

Fett, T. (1995), Determination of bridging stresses and R-curves from load-displacement curves, *Engineering Fracture Mechanics*, **52**(5), 803-810.

Fleck, N. A. (1991), Brittle Fracture due to an Array of Microcracks, *Proc. Roy. Soc. London* **A432**, 55-76.

Freitas, G., Fusco, T., Campbell, T., Harris, J., and Rosenberg, S. (1996), Z-Fiber Technology and Products for Enhancing Composite Design, AGARD Conference.

Guinea, G.V., Planas, J., Elices, M. (1994), A general bilinear fit for the softening curve of concrete, *Materials and Structures*, **27**, 99-105.

Guo, Z.K., Kobayashi, A.S. and Hawkins, N.M. (1993), Further studies on fracture process zone for mode I concrete fracture, *Engineering Fracture Mechanics*, **46**(6), 1041-1049.

Hashin, Z. (1979) Analysis of properties of fiber composites with anisotropic constituents, J. Appl. Mech., **46**, 543-550.

He, M.Y. and Evans, A.G. (1992), Finite element analysis of beam specimens used to measure the delamination resistance of composites, *J. Composites Tech. & Research*, **14**(4), 235-240.

Hillerborg, A. (1983), Analysis of a single crack, in *Fracture Mechanics of Concrete*, ed. F.H. Wittmann, 223-249, Elsevier Science, Amsterdam.

Horton, R. E., and McCarty, J. E. (1987), Damage Tolerance of Composites, in *Engineered Materials Handbook, Vol. 1: Composites*, ASM International, Metals Park, Ohio.

Jain, L.K., Mai, Y-W. (1994), Analysis of stitched laminated ENF specimens for interlaminar mode-II fracture toughness, *Int. Journal of Fracture* **68**(3), 219-244.

James, M.R., Morris, W.L. and Cox, B.N., A High Accuracy Automated Strain Field Mapper, *Experimental Mechanics*, **30**, 60-67.

Krasnov, V. I., Kuznetsov, V. A., and Maksakov, A. Yu. (1987), Automated Method of Transverse Reinforcement of Composites by Short Fibers, *Mekhanika Kompozitnykh Materialov*, **3**, 449-504.

Marquardt, D.W. (1963), *J. of the Society for Industrial and Applied Mathematics*, **11**, 431-441.

Massabò, R., and Cox, B. N. (1996), Concepts for Bridged Mode II Delamination Cracks, submitted for publication.

Nanakorn, P. and Horii, H. (1996), Back analysis of tension-softening relationship of concrete, *J. Materials, Conc. Struct., Pavements*, JSCE, 265-275.

Rice, J.R., (1968), A path independent Integral and the approximate analysis of strain concentration by notches and cracks, *Journal of Applied Mechanics*, **35**, 379-386.

Rödel, J., Kelly, J.F. and Lawn, B.R. (1990), In situ measurements of bridged crack interfaces in the scanning electron microscope, *J. of Am. Ceram. Soc.*, **73**(11), 3313-18.

Rose, L.R.F., (1987), Crack reinforcement by distributed springs, *J. Mech. Phys. Solids*, **34**, 383-405.

Sharma, S.K., and Sankar, B.V. (1995), Effects of through-the-thickness stitching on impact and interlaminar fracture properties of textile graphite/epoxy laminates, *Nasa Contractor report* 195042, Nasa Langley, Virginia.

Smith, P. J., and Wilson, R. D. (1985), Damage Tolerant Composite Wing Panels for Transport Aircraft, Boeing Commercial Airplane Company, NASA Contractor Report 3951.

Tikhonov, (1963), Solution of incorrectly formulated problems and the regularization method, *Soviet Mathematics (Crovidence)*, **4**, 1035-1038.

Turrettini, A. (1996), An Investigation of the Mode I and Mode II Stitch Bridging Laws in Stitched Polymer Composites, Masters Thesis, Department of Mechanical and Environmental Engineering, University of California, Santa Barbara, 1996.

Twomey, S. (1977), *Introduction to the mathematics of inversion in remote sensing and indirect measurements*, Elsevier, Amsterdam, The Netherlands.

Xia, Z. C., and Hutchinson, J. G. (1994), Mode II Fracture Toughness of a Brittle Adhesive Layer, *Int. J. Solids Structures* **31**, 1133-48.

Uchida Y., Kurihara, N., Rokugo, K. and Koyanagi, W. (1995), Determination of tension softening diagrams of various kinds of concrete by means of numerical analysis, in proc. II Int. Conference *on Fracture Mechanics of Concrete Structures*, FRAMCOS 2, Zurich, Switzerland; F.H. Wittman, ed., Aedificatio Publisher, vol. I, 17-30.

Whitney, J.M., and Pagano, N.J., (1970), Shear deformation in heterogeneous anisotropic plates, *Journal of Applied Mechanics,* **37**, 1031-1036.

Williams, D.R., Davidson, D.L. and Lankford, J. (1980), **TITLE TITLE TITLE**, *Experimental Mechanics,* **20**, 134-139.

Wittmann, F.H., Rokugo, K., Bruhwiler, E., Mihashi, H. and Simoni, P. (1988), Fracture energy and strain-softening of concrete as determined by means of compact tension specimens, *Materials and Structures*, 21, 21-32.

Wittmann, F.H., Roelfstra, P.E., Mihashi, H., Huang, Y.Y., Zhang, X.H. and Nomura, N. (1987), Influence of age of concrete as determined by means of compact tension specimens, *Materials and Structures*, 20, 103-110.

APPENDIX A. SIZING OF THE ENF SPECIMEN

In this Appendix it will be shown that, provided the geometrical ratios of the ENF specimen and the stacking sequence of the plies satisfy certain restrictions, the ENF test can be depicted as a mode II delamination problem and the bridged crack model recalled in Section 2, based on a first order shear deformation theory for bending plates, is applicable.

Failure by delamination and minimum depth of the specimen

Many experimental ENF tests, including those of the present research, have shown that both stitched and non-stitched laminates in the ENF configuration fail by delamination provided the depth, h, exceeds a minimum value which corresponds to simultaneous failure by delamination and flexure (Sharma and Sankar, 1995). Flexural failure (caused by in-plane tension or compression) occurs at the attainment of the ultimate strength on the inner or outer surfaces of the beam. The minimum depth is easily defined for unstitched laminates as a function of material and geometrical properties (Carlsson and Gillespie, 1989). In stitched laminates it is to be calculated by a bridged crack model. It will be higher, since the maximum load the specimen can sustain during delamination is increased by the bridging mechanisms. For the plate model used in this

paper to be valid, the depth of the ENF specimen must also be large enough to satisfy the small-deformation requirement (Carlsson and Gillespie, 1989).

Influence of the concentrated loads

Finite element calculations on unstitched ENF specimens have shown that compressive stresses normal to the delamination surfaces act only in the vicinity of the beam support in a region centered about the load line. The region's length depends on the orthotropy of the material in the plane x-z and is typically less than $4h$. The region under compression will be thus avoided by choosing $a \geq 2h$. At the specimen mid-span the applied load, P, creates a compressive stress field which covers a region whose length is again less than $4h$. These compressive stresses can arrest the propagation of the crack. Therefore meaningful results will be obtained by limiting the delamination length to $a \leq L\text{-}2h$ (He and Evans, 1992, Carlsson and Gillespie, 1989).

In the region of the crack which is under compression, some frictional forces may arise which oppose the relative crack displacement unless free sliding of the crack surfaces is ensured by proper measures. The energy dissipated in this mechanism adds to the energy absorbed in creating new fracture surfaces and to the energy dissipated by the bridging mechanism of the through-thickness reinforcement. Nevertheless, finite element and beam theory calculations (He and Evans, 1992, Carlsson and Gillespie, 1989) have shown that the reduction in strain energy release rate of unstitched ENF specimens due to this mechanism (modeled as Coulomb friction) is very small for typical ENF geometries, being linearly proportional to the coefficient of friction, μ, and to the ratio h/a (e.g., $\mathcal{G}_{II}(\mu)/\mathcal{G}_{II}(\mu=0) \approx 93 - 99\%$ for $\mu \approx 0.25 - 0.5$ and $h/a = 0.1$). The fractional reduction will be much lower in stitched laminates.

Mode II delamination crack growth

The ENF test represents a mode II crack problem provided the lengths of the beam, L, and the crack, a, are much longer than the depth, h, and the upper and lower arms of the beam in the delaminated region are free to bend with the same curvature. This result has been proved by means of finite element analyses on unstitched laminates by Carlsson and Gillespie (1989) and He and Evans (1992). They verified the absence of interlaminar normal stresses along the centerline ahead of the crack tip and the absence of mode I crack openings.

The actual conditions of delamination cracks in stitched ENF specimens have been investigated in Section 3 by means of experimental observations of crack profiles in polymer matrix laminates. The results of the investigation show that delamination cracks

in stitched ENF specimens can be considered as being mode II cracks. Moreover, the basic bridging mechanism supplied by the stitches proves to be that of opposing the relative sliding between the crack faces. This mechanism can then be represented as a distribution of shear tractions, $\tau_b(w)$, directly applied along the faces of the delamination.

Theoretical analysis based on plate theory

The validity of plate theory for analysis of typical polymer matrix laminates in the ENF configuration can be studied by comparing the results of the approach proposed in Section 2 to those of rigorous elasticity methods. He and Evans (1992) carried out finite element analyses of specially orthotropic laminates in the ENF configuration (non-stitched), and proposed a fitting formula for the strain energy release rate in the case of plane-stress in the plane x-z. The formula can be extended to problems in a state of plane strain (Bao et al, 1992). It summarizes the strain energy release rate computed by the finite element method, $\mathcal{G}_{II(FE)}$, as a function of that of plate theory,

$$\mathcal{G}_{II(PL)} = \frac{9}{16}\frac{P^2a^2}{Eh^3d^2}, \tag{A.1}$$

and of two parameters, ρ and λ, which characterize the orthotropy of the laminate in the plane x-z. It is worth noting that $\mathcal{G}_{II(PL)}$ is independent of the in-plane orthotropy of the laminate.

Figure A.1.a shows the normalized strain energy release rate, $\mathcal{G}_{II(FE)}/\mathcal{G}_{II(PL)}$, as a function of the ratio a/h for a specially orthotropic material with the same properties of the carbon-epoxy laminate described in Section 3, namely ρ=3 and λ= 0.14. The strain energy release rate of an isotropic material, $\rho=\lambda=1$, is also shown in Fig. A.1.a. Figure A.1.b shows a comparison between the critical loads for crack propagation, P_{cr}, obtained by assuming $\mathcal{G}_{II}=\mathcal{G}_{IIC}$ from plate theory and finite element calculations. Figure A.1 highlights the influence of the material orthotropy on the behavior of the ENF specimen. The range of applicability of the bending theory in a typical non-stitched polymer matrix laminate is substantially reduced with respect to that of an isotropic material, and it is only for high values of the ratio a/h that the bending theory and the finite element solutions show a good agreement. For example, a discrepancy lower than 5% in the critical load for crack propagation is ensured only for $a/h>10$. However, this condition is commonly satisfied in ENF tests, since the notch alone usually exceeds $10h$. Inferences from calculations for unstitched laminates are extended here to stitched laminates.

APPENDIX B. THE INVERSE PROBLEM

B.1. Determination of the Bridging Stresses $\phi_b(x)$ from Crack Profile Measurements

Data of the problem are: the vector of the sliding displacements, $\tilde{\mathbf{w}}=\{\tilde{w}_1,\ldots,\tilde{w}_m\}^T$, measured at m points along the delamination in the ENF specimen of Fig. 1, $\tilde{\mathbf{x}}=\{\tilde{x}_1,\ldots,\tilde{x}_m\}^T$; the lengths of delamination and notch, a and a_0; the value of the applied load, P (or equivalently the shear stress, τ); and the elastic constants of the laminate. Unknown quantities are the bridging stresses, $\phi_b(x)$, defined as a function of the variable for position along the crack, x, which represent the bridging mechanisms supplied by the stitches.

The problem is solved through discretization. The continuous bridging stresses, $\phi_b(x)$, are represented by a set of n-1 cubic splines, $\{\phi_k(x),\ k=1,n-1\}$

$$\phi_k(x)=\sum_{l=0}^{3}\alpha_{lk}f_{lk}(x) \qquad x_k\le x\le x_{k+1} \tag{B.1}$$

where $\mathbf{x}=\{x_1,\ldots..,x_n\}^T$ is a grid of n points along the bridged crack, with $x_1=a_0$ and $x_n=a$, and $f_{lk}(x)=(x-x_k)^l$. The bridging stresses at $\mathbf{x}$, $\underline{\phi}=\{\phi_1,\ldots..,\phi_n\}^T$, take on the form

$$\underline{\phi}=\mathbf{Q}\,\underline{\alpha} \tag{B.2}$$

with $\underline{\alpha}$ the $4(n-1)$ vector of the parameters α_{lk}, and $\mathbf{Q}$ a $n\times4(n-1)$ matrix whose coefficients are known once the discrete grid is fixed (Cox and Marshall, 1991b). The vector, $\mathbf{w}$, of the theoretical crack sliding displacements at the m experimental points, $\tilde{\mathbf{x}}$, is calculated through the following equation

$$\mathbf{w}=\mathbf{D}\,\alpha+\mathbf{w}_L=\mathbf{A}\,\phi+\mathbf{w}_L \tag{B.3}$$

with

$$\mathbf{A}=\mathbf{D}\,\mathbf{Q}^{-1}. \tag{B.4}$$

representing the $(m\times n)$ design matrix of the inverse problem. The vector $\mathbf{w}_L$ in Eq. (B.3) defines the theoretical crack sliding displacement in $\tilde{\mathbf{x}}$ due to the applied shear stresses, τ, and $\mathbf{D}$ is a $m\times4(n-1)$ matrix whose generic coefficient D_{ij} represents the crack sliding displacement at $\tilde{x}_i$ due to the bridging stresses $f_{lk}(x)=(x-x_k)^l$ acting in the range $x_k\le x\le x_{k+1}$, with $k=j/4+1$ and $l=j-4k+3$. The matrix $\mathbf{D}$ and the vector $\mathbf{w}_L$ are calculated through Eq. (13) and solutions of the boundary value problem represented by Eqs. (11) and (12). By assuming the bridging stresses as a function of x and substituting Eq. (B.1), the problem becomes linear and the superposition principle can be applied. The equilibrium Eqs. (12) modify in

$$\begin{cases} N_{d,x} = \tau - \sum_{k=1}^{n-1}\sum_{l=0}^{3} \alpha_{lk}(x-x_k)^l \chi_k \\ M_{d,x} = -0.5h(\tau - \sum_{k=1}^{n-1}\sum_{l=0}^{3} \alpha_{lk}(x-x_k)^l \chi_k) + Q_d, & \text{if } 0 \le x \le a \\ Q_{d,x} = 0 \end{cases} \tag{B.5}$$

$$\begin{cases} N_{i,x} = 0 \\ M_{i,x} = Q_i, & \text{if } a \le x \le 2L \\ Q_{i,x} = 0 \end{cases}$$

where $\chi_k=1$ if $x_k \le x < x_{k+1}$ and $\chi_k=0$ everywhere else. The boundary conditions are those defined in Section 2, along with continuity conditions for stress resultants and displacements at $x = x_k$ (k=1,...,n).

If n=m and the grid of points $\mathbf{x}$ coincides with the experimental points $\tilde{\mathbf{x}}$, the bridging stresses ϕ are obtained by imposing the condition $\mathbf{w}=\tilde{\mathbf{w}}$, through direct inversion of Eq. (B.3)

$$\phi = \mathbf{A}^{-1}(\tilde{\mathbf{w}} - \mathbf{w}_L) \quad , \quad \text{if } n=m. \tag{B.6}$$

If $m>n$ or $\mathbf{x} \neq \tilde{\mathbf{x}}$, a general linear least square fit can be performed through the minimization of a functional S over the n unknown parameters ϕ_j, j=1,...,n. S is chosen as the norm of the residuals between the data points and the theoretical predictions:

$$S = \sum_{j=1}^{m} (\tilde{w}_j - w_j)^2 . \tag{B.7}$$

This yields to the normal equation

$$\phi = (\mathbf{A}^T\mathbf{A})^{-1}\mathbf{A}^T(\tilde{\mathbf{w}} - \mathbf{w}_L) \quad , \quad \text{if } m>n \tag{B.8}$$

which reduces to (B.6) for n=m (for the validity of this statement in the presence of errors see Twomey, 1977).

Equation (B.8) defines the maximum likelihood estimation of the fitted parameters in the case of measurement errors on $\tilde{\mathbf{w}}$ which are statistically independent, normally distributed, and with constant standard deviation, σ_m. If the uncertainties in the data are not known a priori but the model can be assumed to be correct, σ_m can be defined as the root mean square deviation of the model from the data

$$\sigma_m^2 = \frac{1}{m-n}\sum_{j=1}^{m} (\tilde{w}_j - w_j)^2 \tag{B.9}$$

where the terms on the right hand side are calculated making use of the fitted bridging stresses, $\underline{\phi}$, through Eq. (B.3). This quantity gives an indication of the measurement error.

Equations (B.6) and (B.8) prove to be extremely sensitive to computer roundoff errors and to errors in the measurements. The solution is unstable, and the fitted bridging stresses, $\underline{\phi}$, tend to have very large magnitudes that cancel out almost precisely when the fitted crack sliding displacement is evaluated. This is explained by the near-singularity of the matrices **A** and $\mathbf{A}^T\mathbf{A}$, which have very small eigenvalues and, after the inversion, can greatly magnify small errors in the data.

To treat this difficulty a Linear Regularization Method is used (Twomey, 1977, Tikhonov, 1963). The basic idea is that the data points, $\tilde{\mathbf{w}}$, are actually defined within error bars or error zones, so that a set of $\phi_b(x)$, probably infinite, can be calculated which can generate crack sliding displacements, **w**, falling within the error bars. To select one of the possible $\phi_b(x)$ an additional and arbitrary constraint is imposed, e.g., that of a smooth solution. The norm of the k^{th} derivatives of the bridging tractions at a set of r points along the crack is assumed as a measure of the deviation from smoothness. In this case the problem requires the minimization of the functional S'

$$S' = \sum_{i=1}^{r} \left| \frac{d^k \phi(\bar{x}_i)}{dx^k} \right|^2 . \tag{B.10}$$

where $\bar{\mathbf{x}} = \{\bar{x}_1, \ldots, \bar{x}_r\}^T$ defines the grid of r points along the bridged portion of the crack. Taking advantage of the method of Lagrange undetermined multipliers, the solution is then obtained by finding an unconstrained extremum of a new functional S'' given by

$$S'' = \sum_{j=1}^{m} (\tilde{w}_j - w_j)^2 + \lambda \sum_{i=1}^{r} \left| \frac{d^k \phi(\bar{x}_i)}{dx^k} \right|^2 \tag{B.11}$$

where λ is the Lagrange multiplier ($\lambda \geq 0$). The normal equation of the least square fit, Eq. (B.8), becomes

$$\phi = (\mathbf{A}^T\mathbf{A} + \lambda\mathbf{H})^{-1}\mathbf{A}^T(\tilde{\mathbf{w}} - \mathbf{w}_L) \tag{B.12}$$

where

$$\mathbf{H} = \mathbf{B}^T\mathbf{B} \tag{B.13}$$

is a $n \times n$ matrix depending on the $r \times n$ matrix **B** which defines the k^{th} derivatives of the unknown bridging stresses with respect to x calculated at $\bar{\mathbf{x}}$, $\underline{\phi}_b^k(\bar{\mathbf{x}}) = \mathbf{B}\,\underline{\phi}$.

Once the vector $\underline{\phi}$ has been found, the coefficients α_{lk} of the spline functions are calculated through Eq. (B.2) and the bridging stresses, $\phi_b(x)$, are defined as a function of position along the crack according to Eq. (B.1). On varying λ a progressive transition between two limiting solutions is found. For $\lambda = 0$, Eq. (B.12) ≡ Eq. (B.8) provides the best

agreement between the data and the prediction, but the bridging stresses $\phi_b(x)$ can be wildly oscillating. On increasing λ the solution becomes smoother and the shape of $\phi_b(x)$ is controlled by the degree k of the derivatives in Eq. (B.11), e.g. linear for k=2. If the experimental errors in the measured displacements are known a priori, the optimal choice for λ is that which yields σ_m of Eq. (B.9) equal to σ_u, the experimental error. Otherwise, the preferred degree of smoothness must be determined subjectively, based on insight into the expected form of the result and with care not to admit as physically significant fluctuations which may be an artefact of noise (underconstraint).

The bridging law, $\tau_b(w)$, is then defined by interpolating the calculated $\phi_b(x)$ over the fitted crack sliding displacements.

B.2.1 Determination of the Bridging Stresses $\tau_b(w)$ from Measurements of a Single Crack Profile

The data of the problem are the same of the previous case, but now the bridging stresses are sought as a function of the crack sliding displacement, $\tau_b(w)$. The continuous bridging stresses are represented by a convenient set of basis functions

$$\tau_b(w) = \sum_{k=1}^{o} \gamma_k g_k(w) \tag{B.14}$$

where a viable choice for the $g_k(w)$ is orthogonal polynomials, e.g. Legendre polynomials. The bridging stresses, $\underline{\tau}_b=\{\tau_{b1},.....,\tau_{bm}\}^T$, at the m experimental points, $\tilde{\mathbf{x}}$, are given by

$$\underline{\tau}_b = \mathbf{G}\,\underline{\gamma} \tag{B.15}$$

where $\underline{\gamma}$ is the vector of the coefficients γ_k, k=1,....o, and $\mathbf{G}$ is a $m\times o$ matrix which depends on the crack sliding displacements in $\tilde{\mathbf{x}}$. The generic component of the vector $\underline{\tau}_b$ takes the form

$$\tau_{bj} = \sum_{k=1}^{o} \gamma_k g_k(w(\tilde{x}_j)), \qquad j=1,....,m. \tag{B.16}$$

From Eq. (B.3) and the assumptions n=m and $\mathbf{x}=\tilde{\mathbf{x}}$, the vector of the theoretical crack sliding displacements at the m points $\tilde{\mathbf{x}}$, $\mathbf{w}=\{w_1,.....,w_m\}^T$, is given by

$$\mathbf{w} = \mathbf{A}\,\mathbf{G}\underline{\gamma} + \mathbf{w}_L \tag{B.17}$$

where $\mathbf{A}$ has been previously defined in Eq. (B.4).

To define the vector $\underline{\gamma}$ and consequently the bridging tractions, $\tau_b(w)$, the procedure shown in Appendix B.1 is applied. Three different cases are outlined:

1) if o=m a direct inversion of Eq. (B.17) under the condition $\mathbf{w}=\tilde{\mathbf{w}}$ leads to

$$\underline{\gamma} = (\mathbf{AG})^{-1}(\tilde{\mathbf{w}} - \mathbf{w}_L) \tag{B.18}$$

2) if $m>o$ a least square fitting of the data points gives

$$\underline{\gamma} = [(\mathbf{AG})^T(\mathbf{AG})]^{-1}(\mathbf{AG})^T(\tilde{\mathbf{w}} - \mathbf{w}_L) \tag{B.19}$$

3) if $m>o$ and the data are noisy a linear regularization method gives

$$\underline{\gamma} = [(\mathbf{AG})^T(\mathbf{AG}) + \lambda\mathbf{H}]^{-1}(\mathbf{AG})^T(\tilde{\mathbf{w}} - \mathbf{w}_L) \tag{B.20}$$

where

$$\mathbf{H} = \mathbf{R}^T\mathbf{R} \tag{B.21}$$

is a $o\times o$ matrix and $\mathbf{R}$ is a $m\times o$ matrix which defines the k^{th} derivatives of the bridging stresses, $\tau_b(w)$, with respect to w calculated at $\mathbf{w}$, $\underline{\tau}_b^k(\mathbf{w})=\mathbf{R}\underline{\gamma}$.

All of the Eqs. (B.18), (B.19) and (B.20) contain the matrix $\mathbf{G}$ which depends on the crack opening displacement $w(x)$ (see Eqs. B.14 and B.15). The problem is thus nonlinear and must be solved iteratively. A tentative definition of $\mathbf{G}$ is obtained at the first iteration, $i=1$, by assuming the vector of the theoretical crack sliding displacements, $\mathbf{w}^{i=1}$, equal to the noisy data, $\tilde{\mathbf{w}}$. Eqs. (B.20) and (B.17) lead to the new profile of best fit, $\mathbf{w}^{i=2}$. The calculation is repeated until convergence is reached in the $\mathbf{w}^i$ and $\mathbf{w}^{i+1}$. Finally, the bridging law is defined by Eq. (B.14).

B.2.2 Determination of the Bridging Stresses $\tau_b(w)$ from Measurements of Several Crack Profiles

The formulation shown in Appendix B.2.1 can be generalized to analyze data acquired at different values of the applied shear stress, τ. The different crack profiles, $\tilde{\mathbf{w}}^{(l)}$, with $l=1,...,n_L$, n_L being the number of profiles examined, correspond to different and known crack lengths, $a^{(l)}$. In this case the problem is solved by minimizing the functional S''

$$S''=\sum_{l=1}^{n_L}\sum_{j=1}^{m}(\tilde{w}_j^{(l)} - w_j^{(l)})^2 + \lambda\int\left(\frac{d^k\tau(w)}{dw^k}\right)^2 dw\,. \tag{B.22}$$

This leads to the final system of equations

$$\underline{\gamma}=\left[\sum_{l=1}^{n_L}(\mathbf{A}^{(l)}\mathbf{G}^{(l)})^T(\mathbf{A}^{(l)}\mathbf{G}^{(l)}) + \lambda\sum_{l=1}^{n_L}\mathbf{H}^{(l)}\right]^{-1}\sum_{l=1}^{n_L}(\mathbf{A}^{(l)}\mathbf{G}^{(l)})^T(\tilde{\mathbf{w}}^{(l)} - \mathbf{w}_L^{(l)}) \tag{B.23}$$

where $\mathbf{A}^{(l)}$, $\mathbf{G}^{(l)}$ and $\mathbf{H}^{(l)}$ relate to the lth profile (from Eqs. (B.4), (B.15) and (B.21)). If the parameter λ is set equal to zero, Eq. (B.23) defines the unconstrained minimization problem for the simultaneous analysis of several crack profiles (from Eq. (B.19)).

FIGURE CAPTIONS

Figure 1: The End Notched Flexure (ENF) test and coordinate system.

Figure 2: (a) Schematic of the delaminated plate loaded in shear. The superposition of problems (a) and (b), which represents an intact plate, creates the ENF test of (c).

Figure 3: Normalized shear cracking stress as a function of the normalized crack length for a laminate with intact through-thickness reinforcement: power law bridging (from Massabò and Cox, 1996).

Figure 4: Transition from stable to unstable crack growth for decreasing values of the ligament strength in a laminate plate with a normalized notch of length $a_0/(a_{IIm}h)^{1/2}=1.0$. Linear bridging law (from Massabò and Cox, 1996).

Figure 5: Ultimate notched strength for bridging laws of different shapes in a material with a vanishing intrinsic interlaminar fracture toughness (from Massabò and Cox, 1996).

Figure 6: Schematic of modified lock stitching.

Figure 7: (a) Load versus mid-span deflection curve for an ENF specimen with no stitches. (b) Load versus mid-span deflection curve for a stitched ENF specimen.

Figure 8: Total opening and sliding displacements for a delamination crack in the ENF specimen of Fig. 7.b.

Figure 9: Total sliding displacements for three different values of the applied load in the ENF specimen of Fig. 7.b.

Figure 10: Bridging laws obtained from crack profile data on varying the Lagrange multiplier in the constrained minimization problem (Legendre polynomials to order 8).

Figure 11: Bridging laws obtained from crack profile data. Unconstrained minimization problem (Legendre polynomials to order 4).

Figure 12: Bridging laws obtained from crack profile data. Unconstrained minimization problem (Legendre polynomials to order 4 and $\tau_b(0)=0$).

Figure 13: Theoretical and experimental crack sliding profiles for the specimen of Fig. 7.b.

Figure 14: Theoretical and experimental load-deflection curves for the specimen of Fig. 7.b. The elastic response expected of an uncracked specimen has been subtracted from the actual mid-span deflection (bridging law from crack profile data).

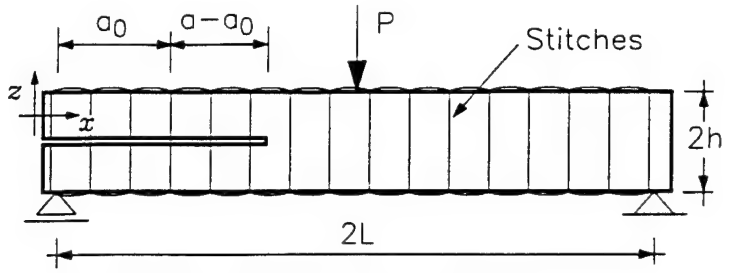

End–Notched Flexure specimen
L >> h a >> h

Figure 1

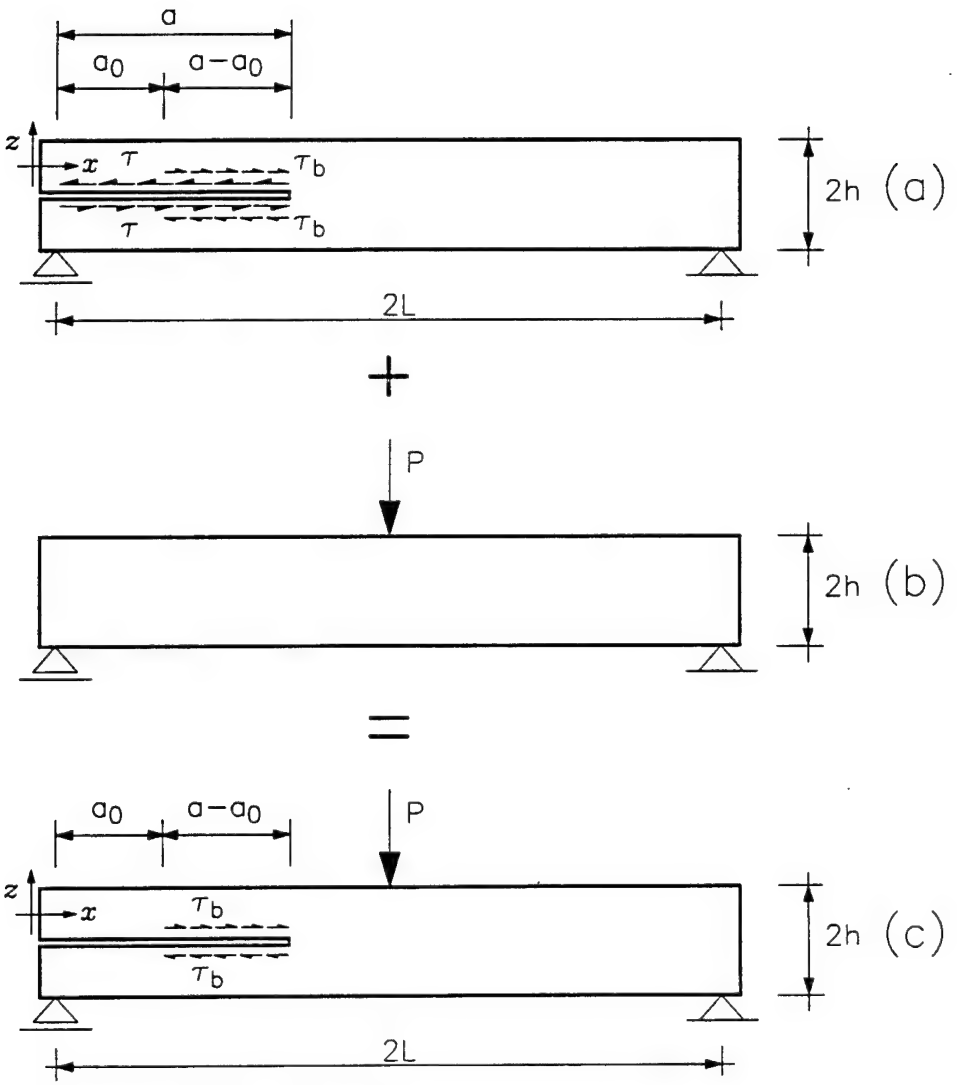

Stitched ENF specimen
L >> h a >> h

Figure 2

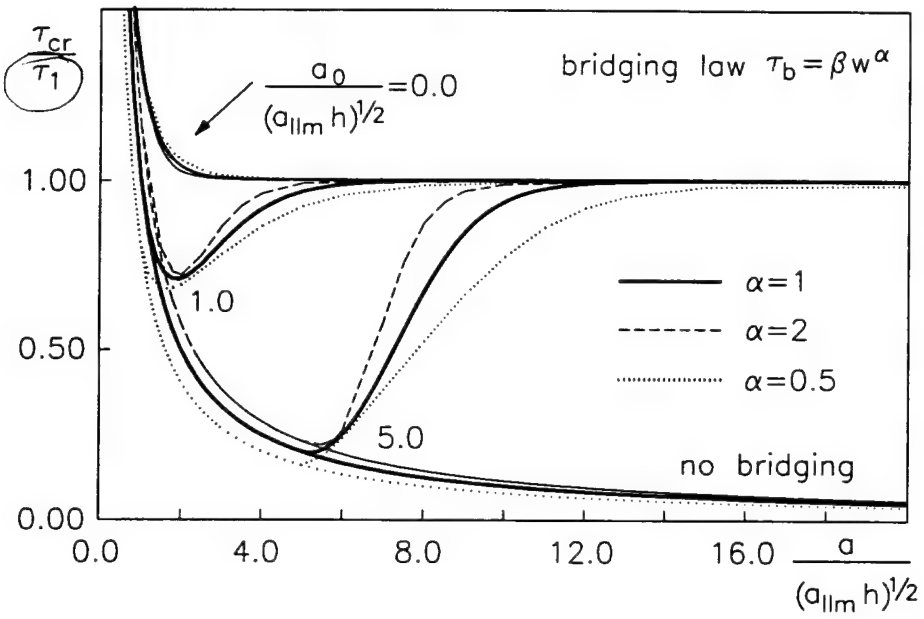

Figure 3

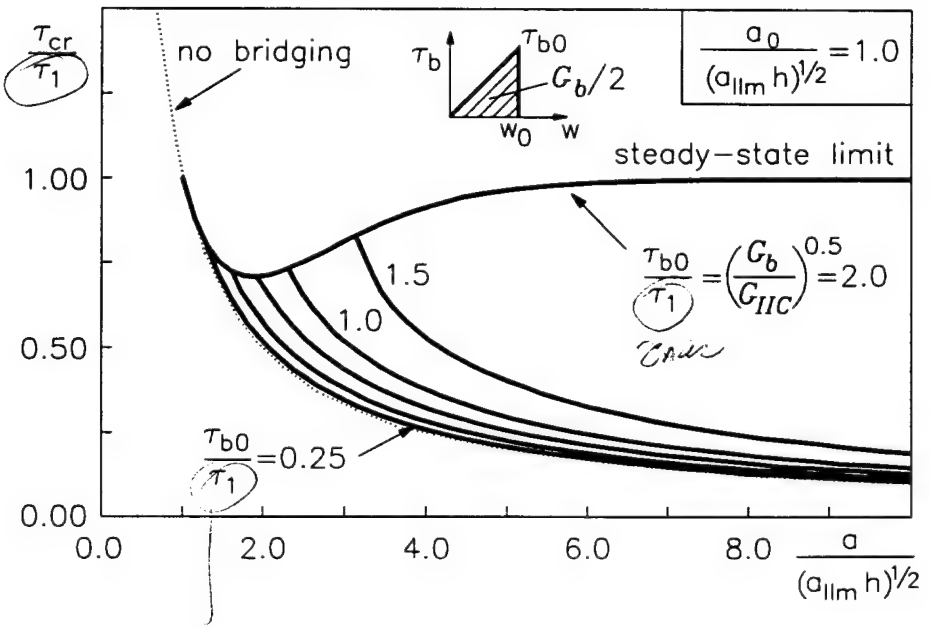

Figure 4

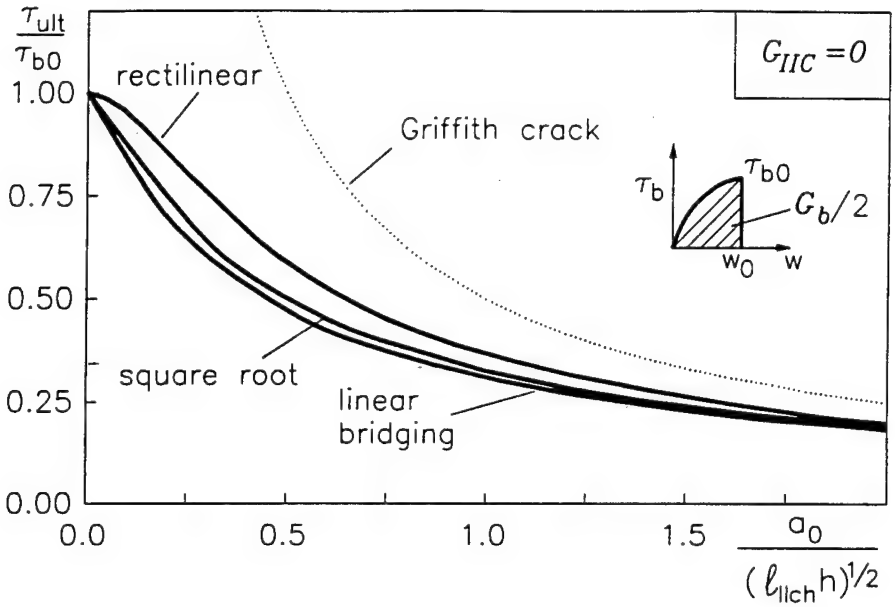

Figure 5

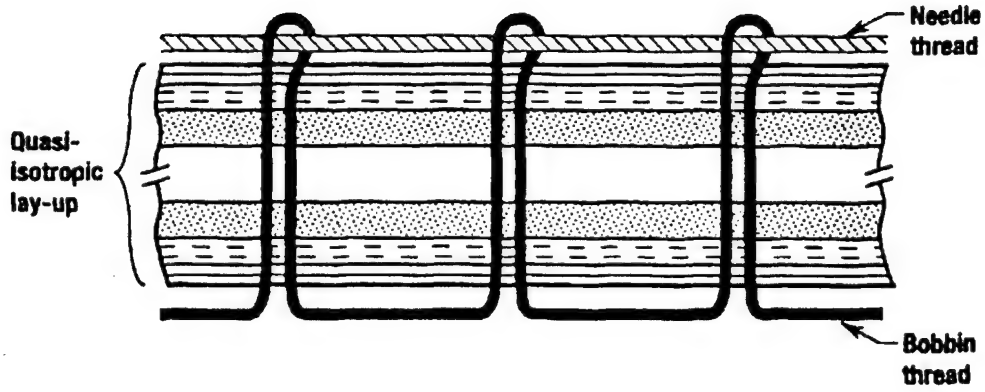

Figure 6

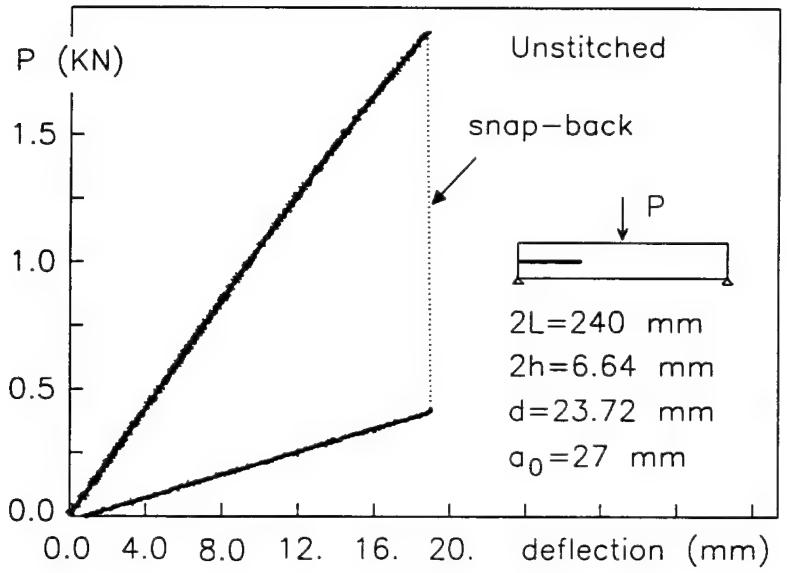
P (KN)
Unstitched
snap–back
P
1.5
1.0
0.5
0.0
2L=240 mm
2h=6.64 mm
d=23.72 mm
a_0=27 mm
0.0 4.0 8.0 12. 16. 20. deflection (mm)

(a)

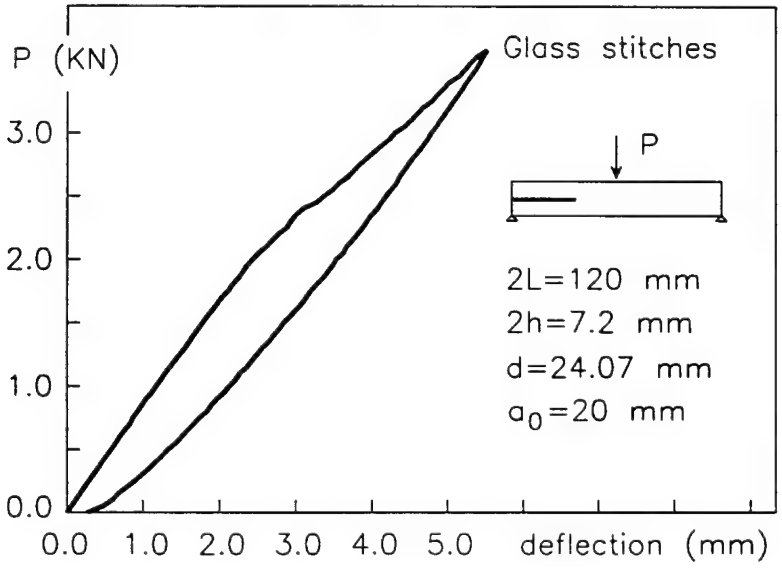
P (KN)
Glass stitches
P
3.0
2.0
1.0
0.0
2L=120 mm
2h=7.2 mm
d=24.07 mm
a_0=20 mm
0.0 1.0 2.0 3.0 4.0 5.0 deflection (mm)

(b)

Figure 7

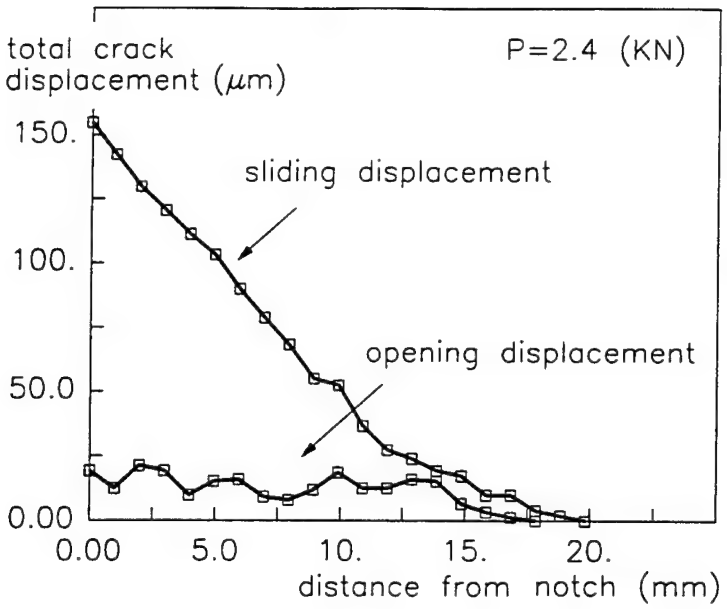

Figure 8

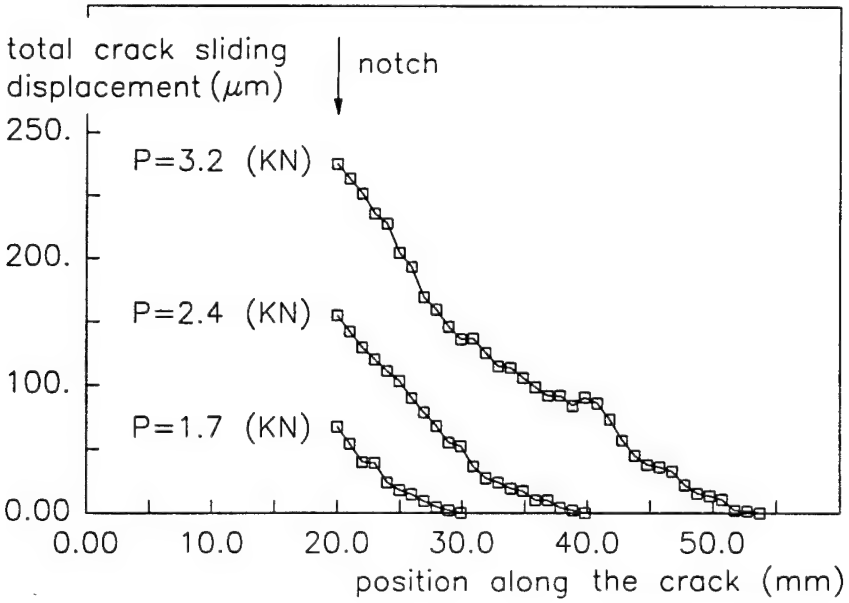

Figure 9

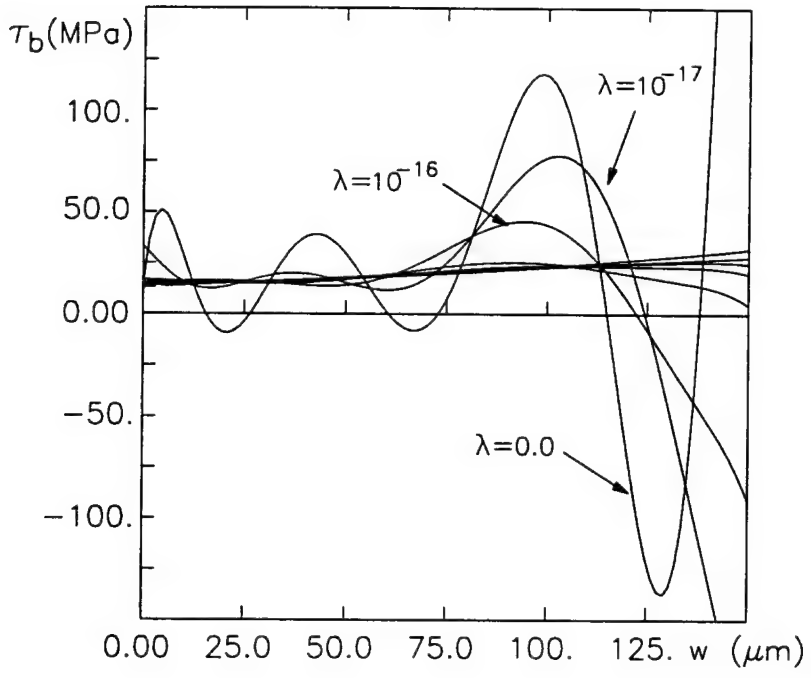
τ_b(MPa)
100.
50.0
0.00
−50.
−100.
λ=10⁻¹⁷
λ=10⁻¹⁶
λ=0.0
0.00 25.0 50.0 75.0 100. 125. w (μm)

(a)

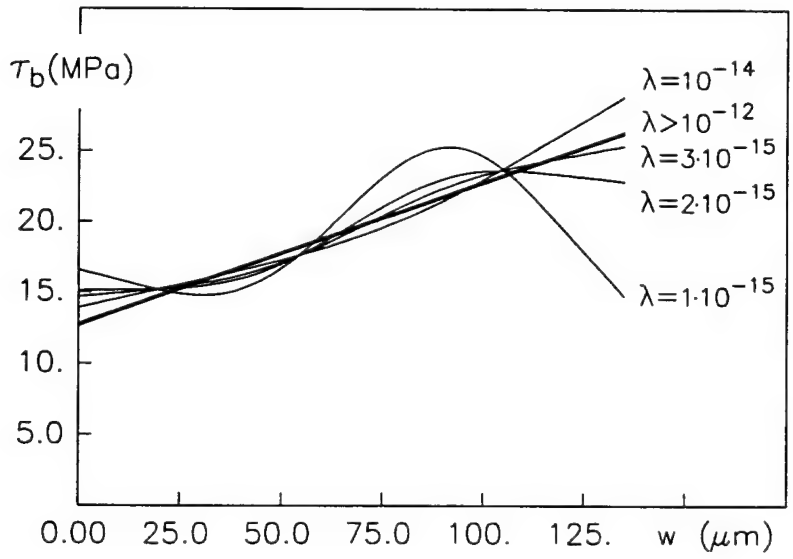
τ_b(MPa)
25.
20.
15.
10.
5.0
λ=10⁻¹⁴
λ>10⁻¹²
λ=3·10⁻¹⁵
λ=2·10⁻¹⁵
λ=1·10⁻¹⁵
0.00 25.0 50.0 75.0 100. 125. w (μm)

(b)

Figure 10

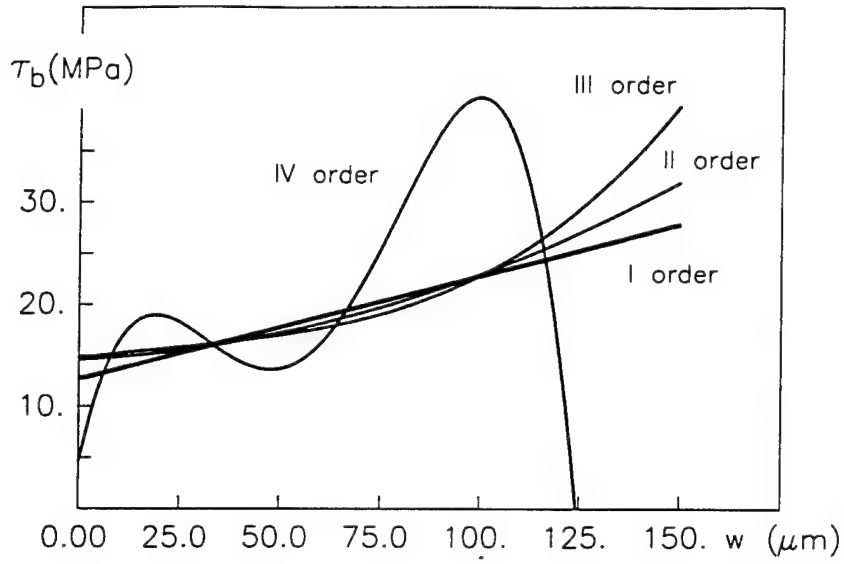

Figure 11

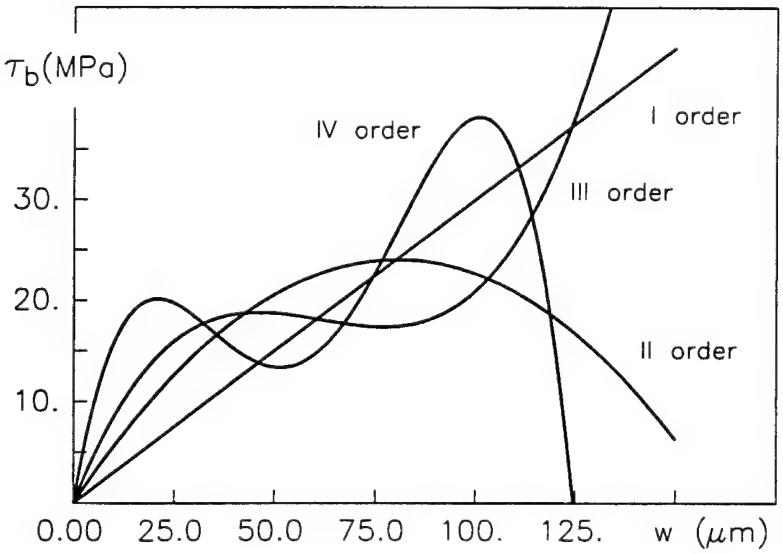

Figure 12

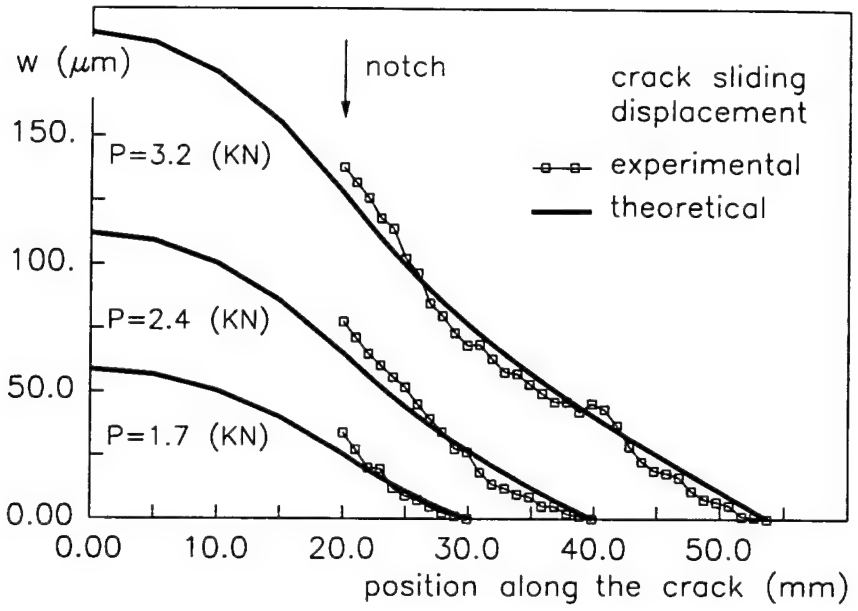

Figure 13

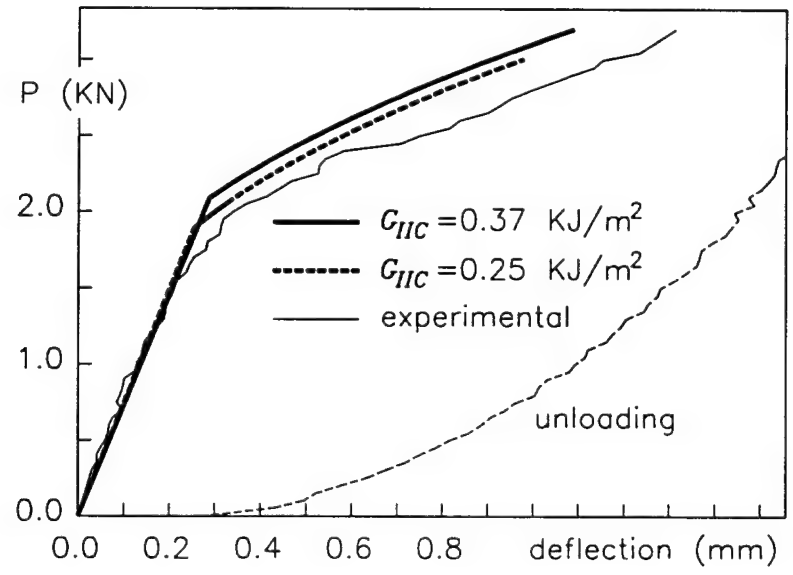

Figure 14

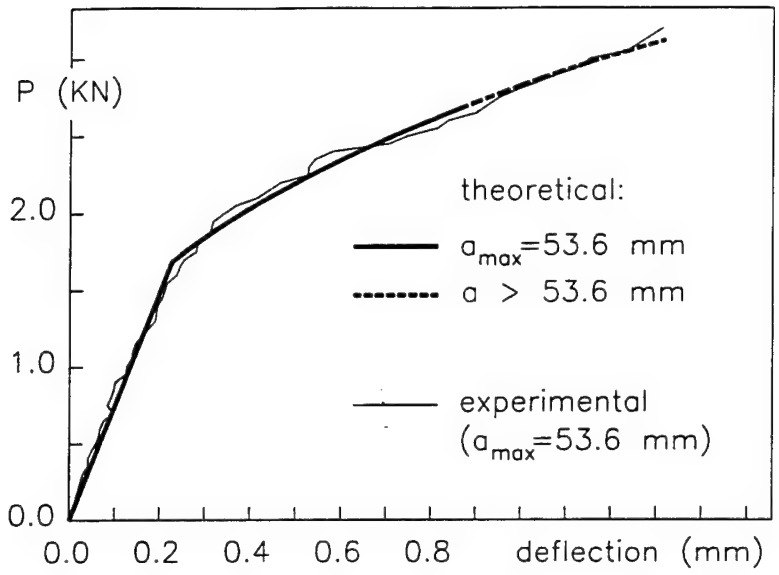

Figure 15

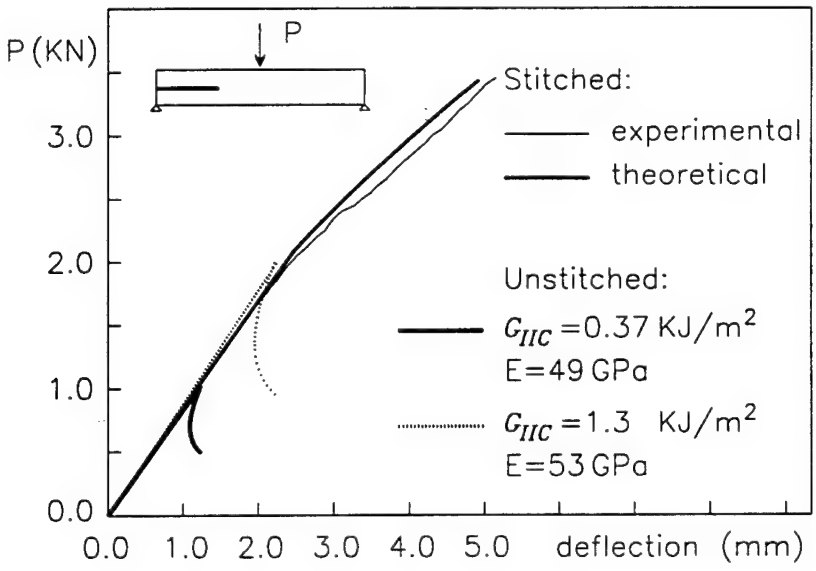

Figure 16

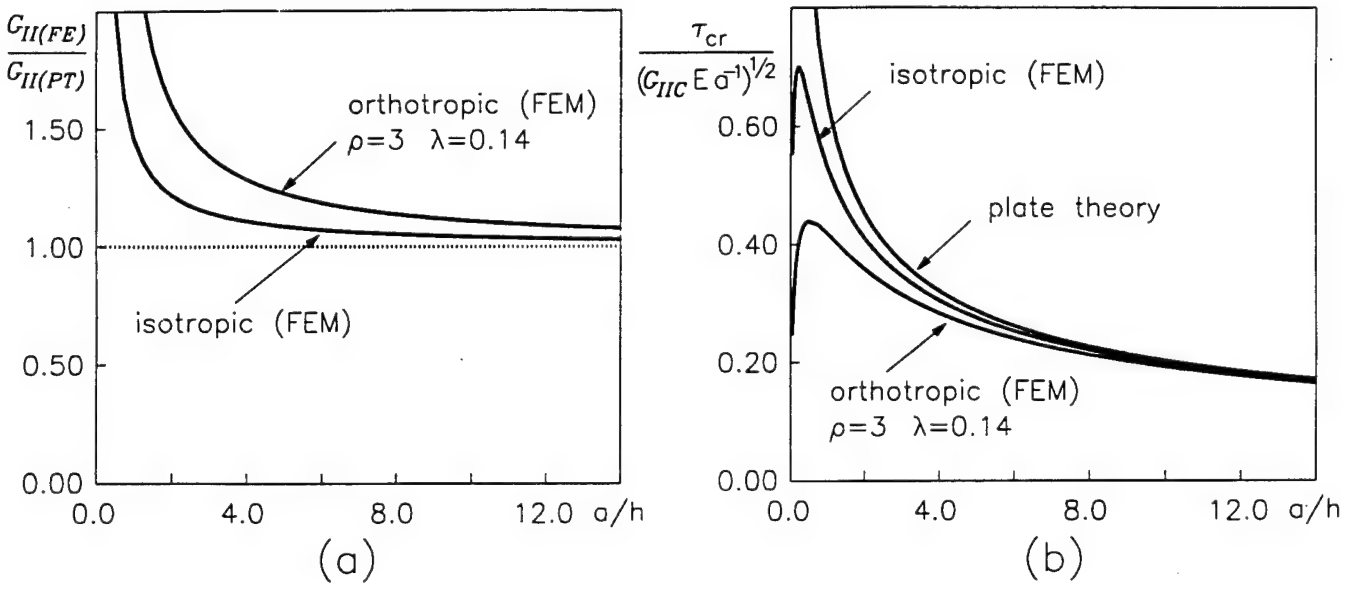
$G_{II(FE)}/G_{II(PT)}$
1.50
1.00
0.50
0.00
orthotropic (FEM)
ρ=3 λ=0.14
isotropic (FEM)
0.0
4.0
8.0
12.0 a/h
(a)
$\tau_{cr}/(G_{IIC}\,E\,a^{-1})^{1/2}$
0.60
0.40
0.20
0.00
isotropic (FEM)
plate theory
orthotropic (FEM)
ρ=3 λ=0.14
0.0
4.0
8.0
12.0 a/h
(b)

Figure A.1

PP 96-...

DRAFT ONLY

Rockwell

Materials Science, Rockwell Science Center

Constitutive Models for a Fiber Tow Bridging a Delamination Crack

B. N. Cox
Rockwell Science Center
1049 Camino Dos Rios
Thousand Oaks CA 91360

and

M. He
Materials Department
University of California, Santa Barbara
Santa Barbara CA 93106

to be submitted to *Acta Materialia*

ABSTRACT

A class of simple models is introduced for a fibrous tow, stitch, or rod that bridges a delamination crack in a laminate. The models are introduced for mode II delamination cracks but are intended for general mixed mode cracks. Modeling is guided by prior observations and measurements on laminates reinforced through the thickness by stitches and short rods. Salient phenomena include shear deformation of the bridging tow, its debonding from and sliding relative to the surrounding laminate, and its sideways displacement through the laminate. The tow is represented as a beam that can bend, shear, and extend axially. Its axial displacement relative to the laminate is resisted over its debonded periphery by friction. The forces associated with its sideways displacement are estimated by regarding it as a cylindrical punch being driven through a plastic medium (the laminate). Thus the mechanics of the whole problem are reduced to a set of one dimensional equations. With realistic values assigned to undetermined parameters, experimental data are reproduced over the whole range of displacements up to ultimate failure of the bridging tow. The effects of tow orientation and length (whether a short rod or continuous stitch) can be assessed. The model allows optimal design of through-thickness reinforcement in a wide variety of structures.

1. INTRODUCTION

Delamination cracks in laminates can be arrested effectively by though-thickness reinforcement, which can take the form of stitches, short rods, or woven interlock tows [1-11]. The through-thickness reinforcement acts by bridging the delamination crack, opposing its opening or sliding displacement. Many structures are now being fabricated and tested with partial reliance on this bridging effect, including skins designed to resist delamination failure, particularly after impact, joints reinforced to safeguard against pull-off, and laminates reinforced selectively around holes and cutouts (Fig. 1).

While many significant successes have been chronicled in developing through-thickness reinforcement, progress has been almost entirely empirical. Through-thickness reinforcement cannot yet be designed by analysis to meet specified requirements; designs are arrived at by a combination of guesswork and extrapolation from test data from previous attempts.

In the case of crack bridging effects, the material information required for intelligent design can be summarized quite simply. It is the relationship between the tractions acting in the bridging tow where it crosses the fracture plane and the opening and sliding displacements of the bridged crack (Fig. 2). Some attempts have already been made to estimate this relationship for stitches, short rods, and interlock tows in weaves, but without proper attention to the damage mechanisms occurring within and around the bridging tow [12-17]. For mode I delaminations and bridging tows that are normal to the delamination plane, simple micromechanical arguments give credible (although as yet unverified) estimates or bounds [15,16]. But whenever mode II crack displacements arise or when the bridging tow is not oriented in its undamaged state normal to the delamination plane, the damage mechanisms are known to be complex and poorly described by existing models [18-22].

Detailed observations of damage events in bridging tows have now been reported for both stitches and short rods in shear [18-22]. They will be summarized here. With these observations providing guidance, new models will be proposed for the bridging characteristics of a generic

bridging tow (stitch, short fibrous rod, or woven interlock tow). The response at small displacements is modeled by finite element calculations. For larger displacements, up to and beyond failure of the bridging tow, a very simple representation of the deforming bridging tow is formulated with reference to experiment for justification, leading to an analytical equation for its mechanical equilibrium which requires minimal numerical work for solution. Trends in behavior are thus highlighted. The model is formulated for stitches or short rods that are initially perpendicular to the delamination fracture plane. Straightforward generalization to the technologically important case of initially inclined stitches or rods will be presented elsewhere.

2. OBSERVED DAMAGE MECHANISMS

Observations of damage during shear delamination cracking of end notch flexure, cantilever beam, and lap joint specimens have been reported in [18-21] and during tests of small cuboidal specimens containing a single stitch under controlled shear displacement in [22]. Different mechanisms operate at different values of the sliding displacement discontinuity or total crack sliding displacement, $2u$, defined by Fig. 2. From [18-22], the salient mechanisms in the deformation of bridging stitches or short rods under shear loading are as follows.

Ahead of the delamination crack tip in a typical stitched laminate, stitches are not visibly deformed or damaged [19]. No microcracking or debonding is observed. The stitch debonds from the surrounding laminate when the delamination crack reaches it, in some cases before [21] and in others after [22] the stitch has been circumscribed by the delamination crack. The debond cracks involve no fiber/matrix separation, but consist of matrix cracks that separate the stitch as a whole from the surrounding composite. Debond cracks are most pronounced on the side of the stitch where local tensile stress would be expected. In stitches in the immediate wake of the delamination crack tip, where $2u \sim 10$ μm, polarized light microscopy reveals a well demarked zone of crazing [21]. The crazing is confined mainly within the stitch, extending over its whole diameter and approximately two stitch diameters away from the delamination plane on either side. Thus the stitch accommodates the crack sliding displacement by internal plastic shear, presumed to be mediated by arrays of microcracks and crazing similar to those seen in other

shear tests of polymer composites [9]. Stitches subject to greater crack sliding displacement ($2u$ ~ 100 μm) are debonded around their entire circumference from the laminate over slip zones that eventually extend to the surface of the laminate. Beginning at displacements $2u$ ~ 100 μm, significant plasticity is seen in the laminate; and eventually ($2u$ > 0.6 mm), splitting cracks and spalling are seen. At these higher sliding displacements, the stitch itself is also split by numerous axial matrix cracks, separating it into strands which slide along one another to accommodate bending (Fig. 3).

An overview of typical strain and stress levels and associated mechanisms during loading of a stitch in shear up to and beyond ultimate failure is shown in Fig. 4 (eclectic idealization of data from [19], [22], and [23]). At crack sliding displacements $2u$ < 0.2 mm, the shear stress in the stitch at the fracture plane (left ordinate) is just a few hundred MPa. For similar polymer composite plies under pure deviatoric shear, matrix microcracking leads to large strains at stresses above approximately 75 MPa, with hardening to ~ 100 MPa as the shear strain approaches 10% [9,24]. Thus, for the stitch to support loads much above 100 MPa, it must bend near the fracture plane so that significant load is carried by the fibers in tension. But the degree of bending need not be very great to achieve equivalent shear stresses on the fracture plane of ~ 200 MPa, since the fibers have very high axial stiffness. Thus plasticity and some stitch realignment will account for the total loads found below displacements $2u$ < 0.2 mm. For $2u$ > 0.2 mm, sliding displacements and total load increase to ultimate failure when the shear traction in the stitch on the fracture plane is ~ 1 GPa. Such a high load can only be sustained if the fibers in the stitch have rotated on the fracture plane through quite large angles. Post-mortem failure shows that such rotations have occurred but only near the fracture plane, where the stitch has dragged through the laminate and assumed a locus approximating a hyperbolic tangent. But the total crack sliding displacement at peak load is much larger than could be expected if the stitch stretched only in this region. Much of the crack displacement is evidently permitted by axial sliding of the stitch: in specimens tested to stitch failure, pronounced dimples are left on the outer laminate surfaces where the stitch has been pulled down towards the fracture plane. After peak load, there is a dramatic drop in load followed by some relatively small but enduring pullout forces.

Because stitch debonding and plasticity within the stitch occur very close to the delamination crack tip, there is no appreciable interval of crack sliding displacement where deformation is purely elastic. The stiffness of the bridging system expected for an elastic, undamaged stitch and laminate in the presence of a delamination crack is relatively high - of the same order as the shear modulus of the composite. On the scale of Fig. 4, the line representing such an elastic response will be almost coincident with the ordinate. The first significant departure from the ordinate should herald the onset of stitch debonding and stitch plasticity, as shown in Fig. 4.

3. MODEL FORMULATION

3.1 Model for Small Displacements

The transition of the response of the stitch and laminate to shear loading from elastic to plastic is examined by finite element calculations. The calculations ignore the effect of rotation of the stitch near the fracture plane and are therefore only pertinent to small crack sliding displacements. The small displacement model deals with the regime where the bridging tractions are determined predominantly by the properties of the matrix rather than those of the stitching fibers, since the stitching fibers are orthogonal to the shear tractions resolved on the fracture plane.

3.2 Model for Large Displacements

The problem of the deflecting stitch for large displacements will be idealized by the following assumptions, with reference to the nomenclature shown in Fig. 5.

1. Most of the bridging shear tractions in the stitch on the fracture plane at large displacements arise from axial tension in the fibers in the stitch, which must therefore rotate out of its initially perpendicular alignment to the fracture plane. Thus this model is applicable to loads that are much larger than those that can be borne by the strength of the stitch in shear (~ 70

MPa). The condition of the stitch in this stage of loading is marked, as recalled above, by severe internal matrix damage, especially near the fracture plane. Matrix plasticity and axially oriented matrix cracks within the stitch prevent large axial shear stresses developing, even under shear strains ~ 1.

2. The stitch debonds from the laminate over a zone that propagates a distance l_s from the fracture plane that is large compared to the stitch diameter. Axial sliding of the stitch relative to the laminate is opposed by friction, which is assumed to be characterized by a uniform shear traction, τ.
3. Deformation of the laminate in the z-direction is assumed to have a negligible effect on the mechanics of the stitch.
4. All deformation in the stitch is assumed to be either axial extension or axial shear, i.e., planes initially normal to the z-axis remain so. Bending effects are ignored. This approximation is justified by the presence of axial splitting cracks in the stitch, which separate it into thin segments which slide over one another without accumulating significant bending moments (Fig. 3).
5. Lateral ploughing of the stitch through the laminate (in the x-direction of Fig. 5) is assumed to follow the mechanics of a punch being pushed into a rigid/perfectly plastic medium in plane strain (Fig. 6). Thus the stitch is opposed by hydrostatic compression, σ_h, acting on its diameter D. The magnitude of σ_h is assumed to be independent of the lateral displacement of the stitch and uniform along that interval of the length of the stitch where nonzero lateral displacement has occurred.

The state of the stitch will be described in terms of only two independent variables, the displacements $u(z)$ and $w(z)$ of a slice of the stitch lying between z and $z+dz$. The axial strain, ε, and the rotation of its axis, θ, are given by

$$\varepsilon = \left[\left(\frac{\partial u}{\partial z} \right)^2 + \left(1 + \frac{\partial w}{\partial z} \right)^2 \right]^{1/2} - 1 \qquad (1a)$$

$$\theta = \left[\tan^{-1} \frac{\partial u}{\partial z} / \left(1 + \frac{\partial w}{\partial z} \right) \right] \tag{1b}$$

The axial stress in the stitch, σ_s, i.e., the stress component in the local fiber direction, is

$$\sigma_s = \varepsilon E_s \tag{2a}$$

$$\approx \varepsilon V_f E_f \tag{2b}$$

where E_s is the axial Young's modulus of the stitch, E_f that of the stitching fibers, and V_f the volume fraction of fibers within the stitch. The approximation of Eq. (2b) expresses the negligible contribution to E_s made by the matrix in advanced stages of damage.

Force equilibrium between the axial stress, σ_s, and the friction stress, τ, acting along the stitch leads in the shear lag approximation to the familiar result[1]

$$\frac{\partial \sigma_s}{\partial z} = \tau / R \tag{3a}$$

whence $$\sigma_s = \sigma_o - \tau \frac{z}{R} \qquad (z < l_s) \tag{3b}$$

$$l_s = R\sigma_0 / 2\tau \tag{3c}$$

where σ_0 is the value of σ_s on the fracture plane (z = 0), l_s is the slip length over which frictionally constrained sliding occurs, and

$$R \equiv 2A_s / s \tag{4}$$

[1] In deriving the force balance equation, a term of second order in θ, which arises because the boundary of the stitch stretches as it rotates, has been ignored for simplicity. This is consistent with our ignorance of the details of the friction process, which might involve other equally large but unknown variations with z.

with s the circumference of the stitch and A_s its cross-sectional area. For a stitch of circular cross-section, R is its radius.

The other equation of equilibrium for the stitch balances the lateral force generated by the axial stress in the stitch in concert with its curvature against the resistance of the laminate. Denoting by $\boldsymbol{F}(z)$ the axial force resultant in the stitch ($|\boldsymbol{F}| = \sigma_s A_s$; $\boldsymbol{F}$ oriented along the stitch) and by $\boldsymbol{P}$ the force of resistance of the laminate per unit length of the stitch:

$$|P| = 2R\sigma_h \quad , \tag{5a}$$

force balance for a slice of the stitch between z and $z + dz$ requires

$$\boldsymbol{F}(z + dz) - \boldsymbol{F}(z) + \boldsymbol{P}dz = 0 \quad . \tag{5b}$$

Here for simplicity the component P_x of $\boldsymbol{P}$ in the x-direction is assumed to be its only nonzero component and only leading order terms in θ are retained. Substituting (3b) into (5) yields

$$(\theta_o - 2\pi z / R)\frac{\partial \theta}{\partial z} = -P_x \quad . \tag{6}$$

Equation (6) is to be solved for $\theta(z)$ and σ_o subject to boundary conditions yet to be specified.

Given $\theta(z)$ and σ_o (and thence $\sigma_s(z)$ via Eq. (3b)), the displacement fields $u(z)$ and $w(z)$ follow from Eq. (1):

$$u(z) = \int_{z_0}^{z}\left[\frac{\sigma_s(z)\sin\theta}{E_s} + \sin\theta\right] dz \tag{7a}$$

$$w(z) = \int_{\sigma_0 R/2\pi}^{z}\left[\frac{\sigma_s(z)\cos\theta}{E_s} + \cos\theta - 1\right] dz \quad . \tag{7b}$$

The lower limit of Eq. (7a) will be defined below. The lower limit of integration in Eq. (7b) corresponds to the end of the debond/slip zone, $z = l_s$, where the displacements are zero.

The problem of interest here, i.e., predicting the mode II bridging traction law, requires calculation of the displacement, $u(0)$, for a specified magnitude, T, of the stress in the stitch resolved on the fracture plane, $z = 0$. Since only the axial stress, σ_s, in the fibers is treated as significant in the large displacement model, specifying T provides a boundary condition for $\sigma_o \equiv \sigma_s(0)$:[2]

$$T = \sigma_o \sin\theta \tag{8}$$

The system of model equations is closed by specifying the crack opening displacement, $w(0)$, for given axial stress, σ_0, in the stitch in a second boundary condition. Under general loading conditions, the relation between $w(0)$ and σ_0 depends on the far-field stress-displacement conditions for the delaminating structure, i.e., how the far-field stress, $\sigma_{ij}^{(ff)}$, depends on the crack sliding and opening displacements (Fig. 2). Such general conditions will be dealt with in subsequent work. For delamination cracks observed in End Notch Flexure (ENF) specimens, the opening displacement is always much smaller than the crack sliding displacement; the delamination cracks propagate in mode II [23]. For mode II conditions, the appropriate boundary condition is

$$w(0) = 0 \tag{9}$$

for all values of σ_0. This boundary condition is adopted here. However, there is not necessarily a solution to the problem which satisfies this condition. In fact, if the shear traction, T, is large enough, solutions can only be found with $w(0) < 0$; i.e., some mode I opening must be present. The critical value, T_0, of T marking this transition can be estimated quite well by solving the equations of state in the limit that $P_x/s\tau$ is large (the most common case in a polymer composite). Since $w(0)$ is a monotonically decreasing function of σ_0 for fixed T and σ_0 must satisfy $\sigma_0 \geq T$, T_0

is given by the value of T for which $w(0) = 0$ when $T = \sigma_0$. In the limit that $P_x/s\tau \gg 1$, one finds (Appendix A)

$$T_0 \approx (\pi - 2)\frac{\left(E_s/\tau\right)}{\left(P_x/s\tau\right)} \quad . \tag{10}$$

Solutions for Infinitely Thick Laminates

Equations (3) and (7) with the boundary conditions (8) and (9) are a nonlinear system and must be solved by iteration. From Eqs. (3b) and (6)

$$\theta = \sin^{-1}\left[T/\sigma_0\right] + \frac{P_x}{s\tau}\ln\left[1 - \frac{\tau}{\sigma}\frac{2z}{R}\right] \quad . \tag{10}$$

Following the sign convention chosen for θ in Fig. 5, θ is positive at the fracture plane ($z = 0$). It diminishes with increasing z and vanishes at $z = z_o$ given by

$$2z_0/R = \sigma_0/\tau\left\{1 - e^{-\sin^{-1}\left[T/\sigma_0\right]s\tau/P_x}\right\} \quad . \tag{11}$$

For $z > z_o$, θ is set identically to zero. There is no lateral deflection for $z > z_o$, i.e., $u(z>z_o) = 0$; and the lateral pressure, P_x, exerted on the stitch by the laminate is therefore also set to zero for $z > z_o$. Thus z_o appears as the lower limit in Equation (7a). Since $z_o < R\sigma_o/\tau_x$ (from Eq. (11)), one has $z_o < l_s$ always; slip always extends beyond the zone of stitch curvature.

The nonlinear system can be solved conveniently and with very modest computation as follows. For specified T, a value is guessed for σ_o and substituted into Eq. (10) to define $\theta(z)$. Then $w(0)$

[2] The shear stress in the stitch resolved on the fracture plane is $\sigma_0 \sin\theta\cos\theta$, while the sectional area of the stitch on

is evaluated from Eq. (7a) and iteration in σ_0 leads easily to the boundary condition Eq. (9). Once the correct value of σ_0 is determined, z_0 follows from Eq. (11) and $u(0)$ from Eq. (7a).

Representative results for all cases can be plotted succinctly by recognizing that the quantities T/τ, $P_x/s\tau$, E_s/τ, and R form a complete set of independent variables.

Solutions for Laminates of Finite Thickness

Let $2h$ denote the thickness of the laminate. If the laminate is sufficiently thin, the slip zone length will exceed the laminate half-thickness, i.e., $l_s > h$. In this case an important distinction arises between the cases of short rods and continuous stitches. For short rods, the condition $l_s = h$ marks the peak bridging traction. When the sliding displacement, $u(0)$, increases beyond the point where $l_s = h$, the condition $\sigma_s(h) = 0$ must be maintained, the rod will pull out of the laminate, and σ_0 and therefore the bridging traction must decrease. During this last phase of failure it is no longer appropriate to set $w(0) = 0$. More general solutions linked to the far-field conditions are required. These are deferred to a subsequent article.

For continuous stitches, $w(0)$ remains close to zero in ENF tests when $l_s > h$, but the problem must be modified to account for transfer of load from the through-thickness segment of the stitch to the segments lying along the laminate's outer surface (Fig. 7). Experiments show (as recalled in Section 2) that for high enough loads the surface segments of the stitch are pulled down into the laminate. Here this process will be modeled as an analogue of the response of the through-thickness segment of the stitch to shear tractions at the fracture plane. Each surface segment of the stitch will plough down into the laminate under the action of shear tractions, τ_h (Fig. 7). Equilibrium for the transition segment of the stitch (shaded in Fig. 7) implies that the shear tractions must have the average magnitude

$$\tau_h = \sigma_s(h) \tag{12}$$

---

the same plane is $A_s/\cos\theta$.

since the cross-sectional area of each surface segment is half that of the through-thickness segment. The mechanics of the deflecting surface segment of the stitch are assumed to be exactly the same as those of the through-thickness segment where the latter deflects at the fracture plane. Thus the surface segments of the stitch are assumed to debond from the laminate and slide relative to the laminate against the same friction stress, τ; and the ploughing displacement into the laminate is assumed to be opposed by the same hydrostatic pressure, σ_h. Results for the traction relation, $u[T]$, found for the through-thickness segment at the fracture plane can therefore be used as a boundary condition at $z = h$. Since the surface segment of the stitch has half the cross-sectional area of the through-thickness segment, its diameter, R, will be lower by the factor $1/\sqrt{2}$ if it has a similar shape. Since the deflection scales as R, the boundary condition for the axial displacement, $w(h)$, of the through-thickness stitch at $z = h$ becomes[3]

$$w(h) = u_\infty[\sigma_s(h)]/\sqrt{2} \quad . \tag{13}$$

Here the subscript in u_∞ signifies that the relation $u[T]$ to be used in the boundary condition is the one computed for an infinitely thick laminate. In other words, the debond/slip zone on the surface segment of the stitch is assumed to propagate as far as necessary without encountering any other features in the stitched laminate.

With the boundary condition Eq. (12) enforced, Eq. (7b) is replaced by

$$w(z) = \begin{cases} u_\infty[\sigma_s(h)]/\sqrt{2} + \int_h^z \left[\dfrac{\sigma_s(z)\cos\theta}{E_s} + \cos\theta - 1\right] dz & \left(h < \dfrac{\sigma_0 R}{2\tau}\right) \quad (14a) \\ \int_h^z \left[\dfrac{\sigma_s(z)\cos\theta}{E_s} + \cos\theta - 1\right] dz & \left(h > \dfrac{\sigma_0 R}{2\tau}\right) \quad (14b) \end{cases}$$

[3] While P_x and s also scale as $\sqrt{A_s}$, they appear in the equations of state only in the ratio, $P_x/s\tau$, and therefore contribute no further rescaling to the boundary condition.

Provided $z_o < h$, which is generally true for common cases, the other equations and boundary conditions remain unaltered.

4. ILLUSTRATIVE CALCULATIONS

Here some calculations are reported for a particular stitched laminate for which significant experimental data have already been published. This laminate consists of a quasi-isotropic lay-up (48 plies $[45/0/-45/90]_{ns}$), with an in-plane Young's modulus, E_1 = 44.6 GPa, transverse shear modulus, G_{13} = 2.6 GPa, and in-plane Poisson's ratios $\nu_{12} = \nu_{21} = 0.3$; stitches of doubled 3650 denier S-2 glass fiber tows on a square array of side 3.2 mm; individual stitch area A_s= 0.636 mm^2 and radius R = 0.45 mm; total stitch area fraction c_s = 0.062; and laminate half-thickness h = 3.6 mm [22,25]. Solutions will be discussed for a single stitch in a semi-infinite laminate of the same elastic properties and a single stitch in a laminate of finite thickness.

Figure 10 reproduces Turrettini's data for shear tests on single stitch specimens from [22]. The total shear load measured in [22] has been converted to an equivalent shear traction in the stitch on the fracture plane (the stitch providing the only mechanical connection across the fracture plane for all but very small loads). The measured sliding displacement has been taken as equivalent to $2u$, under the assumption that the global shear strain in the laminate remains relatively small, since the laminate is constrained by the gripping arrangement [22]. The maximum values of T in the data are just under 1 GPa, which loads are achieved when u = 0.5-0.6 μm. The curves are irregular but on average over the complete range of sliding displacements they indicate some softening.

Turrettini's data show pullout loads of ~ 70 MPa for the stitch following its rupture, which usually occurs some distance into the laminate. Taking $h/2$ as a typical distance of the site of tow rupture from the fracture plane in his experiments, shear lag analysis implies that the average friction stress must be $\tau = 70\, A_s/\pi Rh \approx 10$ MPa. This same value for τ is found for fiber tows in angle interlock weaves with similar resin matrices during pullout measurements [26]. Therefore τ = 10 MPa will be taken as a representative value in the following illustrations.

4.1 Finite Element Calculations for Small Displacements

4.2 Analytical Calculations for Large Displacements

Semi-Infinite Laminate. Calculations are reported first for a stitch in a semi-infinite laminate ($h \to \infty$), so that $w(z)$ is given by Eq. (14b). Computed bridging traction laws are shown in Fig. 9 for four values of $P_x/s\tau$ that are representative of polymer composites. The lower and left abscissa and ordinate labels show the sliding displacement and shear traction resolved on the fracture plane in normalized units. The upper and right axis labels show numerical examples when $\tau = 10$ MPa and $R = 0.45$ mm. The calculations were performed with $E_s/\tau = 5 \times 10^3$, which would be representative of a glass stitch ($E_s \approx 50$ GPa) when $\tau = 10$ MPa; and $E_s/\tau = 10^4$, which would be representative of a Kevlar fiber stitch ($E_s \approx 100$ GPa) for the same τ.

A solid circle symbol terminating a curve in Fig. 9 indicates the end of the regime where solutions exist for which the boundary condition Eq. (9) can be satisfied. (All the curves terminate in this way, but some beyond the range of the plot.) For higher values of T, solutions exist only for $w(0) < 0$; i.e., some mode I opening must develop.

In all cases (and for widely varying $P_x/s\tau$ and E_s/τ beyond the cases shown), $T(u)$ is a softening function. For the exemplary case, shear tractions ~ 1 GPa are achieved when the crack sliding displacement is $u \sim 0.5$ μm when $20 < P_x/s\tau < 60$ (Kevlar stitch) or $40 < P_x/s\tau < 80$ (glass stitch). This implies hydrostatic compression $\sigma_h \approx P_x/2R$ in the range 600 MPa $< \sigma_h <$ 1.8 GPa (Kevlar stitch) or 1.2 GPA $< \sigma_h <$ 2.4 GPa (glass stitch). Since the hydrostatic compression in the punch problem should be ~ three times the crush strength of the laminate, the latter is implied to be in the intervals (200 MPa, 600 MPa) for the Kevlar stitch and (400 MPa, 800 MPa) for the glass stitch, which are indeed typical of measured values for carbon/epoxy laminates.

Figure 10 shows the axial stress in the stitch at the fracture plane, σ_0, as a function of the shear traction, T. All curves are bounded above by the line $T = \sigma_0$, which represents the condition $\theta =$

$\pi/2$, i.e., the stitch lying parallel to the laminate at the fracture plane. At low T, σ_0 is considerably less than T, the stitch still lying nearly normal to the laminate. Termination of a curve at the bound $T = \sigma_0$ coincides with the end of the domain of T for which the boundary condition, $w(0) = 0$, can be satisfied. From Eq. (3c), the abscissa in Fig. 10 also indicates the sliding distance, l_s. For the exemplary set of material properties (scale at the top of Fig. 10), l_s rises to values that will easily exceed typical laminate thicknesses when $T \sim 20$ - 100 MPa.

Figure 11 shows the depth into the laminate over which the stitch develops nonzero curvature as a function of the shear traction, T. The depth diminishes with increasing $P_x/s\tau$. The right hand scale shows numerical values for the exemplary case. It remains quite small, ~ 1 mm, even for T ~ 1 GPa. This is consistent with experimental observations [22].

Laminate of Finite Thickness. Solutions of the traction law, $T(u)$, calculated with the boundary condition of Eq. (14) for a laminate thickness, $h = 3.6$ mm $= 8R$, are shown in Fig. 12. The solutions are superimposed over the equivalent family of curves for a semi-infinite laminate, copied from Fig. 9. Consideration of Fig. 10 shows that the slip zone along the stitch should reach the laminate surface very early in Fig. 12 ($T/\tau \sim 10$ MPa).

When the slip zone has reached the laminate surface, the traction law may show either hardening or softening relative to the law for the semi-infinite laminate. A competition arises between hardening due to the cessation of extension of the slip zone; and softening as the surface segment of the stitch is drawn down into the laminate. If the surface segment and surrounding laminate were infinitely rigid, hardening would occur, because the only change would be the loss of axial displacement of the stitch due to slip in the region $z > h$. If the surface segment and surrounding laminate were very compliant, softening would occur, because the stitch would then be less constrained at $z = h$ than in the semi-infinite case.

Figure 12 shows both hardening and softening, depending on the case and the load level. For low loads, curves for all values of $P_x/s\tau$ show softening relative to the semi-infinite case. As the load increases, hardening takes over. The curves for the finite laminate cross back over those for

the semi-infinite laminate at some critical load that increases with $P_x/s\tau$. For the exemplary laminate, hardening is not pronounced until $T > 1$ GPa in any case; and hardening is indeed absent from Turrettini's data (Fig. 10 and [22]).

The softening of the traction laws for the finite laminate imply that somewhat higher values of $P_x/s\tau$ would be required to match Turrettini's data than inferred in the preceding section: $P_x/s\tau \sim$ 60 - 80 for the glass stitch. This leads to inferred values of the crush strength of the laminate that are ~ 600 - 800 MPa, still close to experimental values.

4.3 Ultimate Failure of the Stitch

No prediction of ultimate failure of the stitch is attempted here, but some inferences for possible sites of stitch failure can be drawn. Since the slip distance, l_s, equals the laminate half-thickness quite early in the load history, at high loads the through-thickness segment of the stitch will experience axial stresses that are not far from uniform along its entire length. Therefore, failure of the stitch at locations far from the fracture plane must be possible. The failure location will be more strongly influenced by local degradation of the strength of the stitch, e.g., at the point near the laminate surface where it turns through a right angle, than by variations in the local stress state. Failures have been observed at variations locations [22].

5.0 CONCLUSIONS

The finite element calculations show that the response of the stitch and laminate to shear loading on the fracture plane is matrix dominated only for shear sliding displacements $u < 0.1$ mm, when the shear traction in the stitch is ~ 100 MPa. Larger loads observed at larger displacements can only be accounted for by considering the rotation of the fibers in the stitch near the fracture plane.

Instead of computationally intensive 3D finite element calculations in which the axes of symmetry for the constitutive properties of the stitch rotate during deformation, a simple one-

dimensional analytical model has been presented which incorporates the essential mechanisms observed in experiments. The model makes the following testable predictions.

The stiffness of the bridging traction law for a stitch in shear should rise with the axial modulus of the stitching fibers and with the crush strength of the reinforced laminate (which is correlated with the model parameter, P_x. The law will have decreasing slope for common values of laminate thickness in laminates reinforced by glass or Kevlar stitches.

If the stitch radius, R, is varied while the stitch area fraction on the fracture plane is held constant, there will be no change in the shear traction, T, in the stitch on the fracture plane for a fixed remote load. Furthermore, since P_x and the stitch circumference, s, both scale as R, the ratio $P_x/s\tau$ will be invariant under changes in R. Therefore, as illustrated in Fig. 9, the only change in the traction law will be that the sliding displacement, u, will scale directly as R. (This scaling arises from the fact that, as R rises, the slip length, l_s, rises, so that curvature must develop over a longer interval of the stitch.) Thus the stiffness of the law will rise if the stitch radius is decreased while the stitch area fraction is held constant.

For any stitch material and radius, pure shear displacement is possible up to some limiting traction, beyond which solutions exist only for non-zero opening displacements. In the exemplary laminate studied here, the limiting traction is not far below the ultimate strength of the stitch, so delamination crack growth under pure or near mode II conditions should be readily observed, as is indeed the case [23].

In common laminates of common thickness, the stitch will slip relative to the laminate all the way to the outer laminate surface when the shear traction in the stitch at the fracture plane is ~ 100 MPa or less. At loads above a few hundred MPa, the fibers in the stitch at the fracture plane will have rotated through large angles, gradually approaching the condition of being parallel to the fracture plane as the shear traction approaches 1 GPa. On the other hand, curvature in the stitch will be confined even at these highest loads to within ~ 1 mm of the fracture plane.

Acknowledgements

BNC was supported by AFOSR Contract No. F49620-94-C-0030, Program Monitors Dr. Walter Jones and Brian Sanders. The authors are indebted to Drs. André Turrettini, Robert McMeeking, Chang-Hung Kuo, and Roberta Massabò for helpful conversations.

References

1. Horton, R. E., and McCarty, J. E., "Damage Tolerance of Composites," in *Engineered Materials Handbook, Vol. 1: Composites*, ASM International, Metals Park, Ohio, 1987.

2. Smith, P. J., and Wilson, R. D., "Damage Tolerant Composite Wing Panels for Transport Aircraft," Boeing Commercial Airplane Company, NASA Contractor Report 3951, 1985.

3. Dow, M. B., and Smith, D. L., "Damage Tolerant Composite Materials Produced by Stitching Carbon Fabrics," *Int. SAMPE Technical Conf. Series* 1989, **21**, 595-605.

4. Dransfield, K., Baillie, C., and Mai, Y.-W., "Improving the Delamination Resistance of CFRP by Stitching - a Review," *Composite Science and Technology* 1994, **50**, 305-17.

5. Darbyshire, H. F., Bendix Aerospace-Electronics Company Report BDX-613-144 (1970).

6. Bradshaw, F. J., Dorey, G., and Sidey, G. R., "Impact Resistance of Carbon Fiber Reinforced Plastics," *Royal Aircraft Establishment Technical Report 72240*, Farnborough, England, 1973.

7. Krasnov, V. I., Kuznetsov, V. A., and Maksakov, A. Yu., "Automated Method of Transverse Reinforcement of Composites by Short Fibers," *Mekhanika Kompozitnykh Materialov*, **3**, 449-504, 1987.

8. Freitas, G., Fusco, T., Campbell, T., Harris, J., and Rosenberg, S., "Z-Fiber Technology and Products for Enhancing Composite Design," AGARD Conference, 1996.

9. Cox, B. N., Dadkhah, M. S., Morris, W. L., and Flintoff, J. G., "Failure Mechanisms of 3D Woven Composites in Tension, Compression, and Bending," *Acta Metall. Mater.*, 1994, **42**, 3967-84.

10. B. N. Cox and G. Flanagan, *Handbook of Analytical Methods for Textile Composites*, NASA Contractor Report Number 4750, NASA Langley Research Center, Hampton, Virginia, 1997.

11. Dickinson, L., "Effects of Stitching Parameters on Mechanical Properties and Damage Tolerance of Stitched/RTM Composites," *Fourth NASA/DoD Conference on Advanced Composites Technology*, Salt Lake City, Utah, 1993, ed. J. G. Davis, J. E. Gardner, and M. B. Dow, NASA, 1993.

12. Cox, B.N., (1992) Fundamental Concepts in the Suppression of Delamination Buckling by Stitching, in *Proc. 9th DoD/NASA/FAA Conf. On Fibrous Composites in Structural Design*, Lake Tahoe, Nevada, November 1991, ed. J. r. Soderquist, L. M. Neri, and H. L. Bohon. (U.S. Dept. Transportation), 1105-1110.

13. Cox, B. N. (1994), Delamination and Buckling in 3D Composites, *J. Comp. Mater.* **28**, 1114-26.

14. Jain, L.K., Mai, Y-W. (1994), Analysis of stitched laminated ENF specimens for interlaminar mode-II fracture toughness, , *Int. Journal of Fracture* **68**(3), 219-244.

15. Lu, T-J, and Hutchinson, J.W. (1995), Role of fiber stitching in eliminating transverse fracture in cross-ply ceramic composites, *J. of Am. Ceram. Soc.*, **78**(1), 251-253.

16. He, M.Y. and Cox, B.N. (1997), Crack bridging by through-thickness reinforcement in delaminating curved structures, *Composites*, in press.

17. Shu, D., and Mai, Y.-W., (1993), Effect of Stitching on Interlaminar Delamination Extension in composite Laminates, *Comp. Sci. Tech.* **49**, 165-71.

18. Mouritz, A. P., and Jain, L. K., "Interlaminar Fracture Properties of Stitched Fibreglass Composites," in *Proc. 11th Int. Conf. Composite Materials*, Gold Coast, Australia, 1997, ed. M. L. Scott (Woodhead Publishing, Melbourne, 1997).

19. Cox, B. N., Massabò, R., Mumm, D. R., Turrettini, A., and Kedward, K., "Delamination Fracture in the Presence of Through-Thickness Reinforcement," plenary paper in *Proc. 11th Int. Conf. Composite Materials*, Gold Coast, Australia, 1997, ed. M. L. Scott (Woodhead Publishing, Melbourne, 1997).

20. Rugg, K., Ward, K., and Cox, B. N., unpublished work.

21. Mumm, D. R., Harvard University, unpublished work.

22. Turrettini, A., "An Investigation of the Mode I and Mode II Stitch Bridging Laws in Stitched Polymer Composites," Masters Thesis, Department of Mechanical and Environmental Engineering, University of California, Santa Barbara, 1996.

23. Massabò, R., Mumm, D. R., and Cox, B. N., "Mode II Delamination Cracks in Stitched Composites," submitted to *Mechanics of Materials*.

24. Fleck, N. A., and Jelf, P. M., (1995), "Deformation and Failure of a Carbon Fiber Composite under Combined Shear and Transverse Loading," *Acta Metall. Mater.* **43**, 3001-7.

25. Dickinson, L., "Effects of Stitching Parameters on Mechanical Properties and Damage Tolerance of Stitched/RTM Composites," *Fourth NASA/DoD Conf. On Advanced Composites Technology*, Salt Lake City, Utah, 1993, ed. J. G. Davis, J. E. Gardner, and M. B. Dow, NASA, 1993.

APPENDIX A - Approximate Solutions to Analytical Model for Large $P_x/s\tau$

When $P_x/s\tau$ is large and T/σ_0 is not small (which is always the case for large T, where $\sigma_0 \to T$), Eq. (10) yields

$$\theta \to \sin^{-1}\left[\frac{T}{\sigma_0}\right] - \frac{P_x}{s\tau}\frac{\tau}{\sigma_0}\frac{2z}{R} \quad , \tag{A.1}$$

a linear function of z. Substituting according to (A.1) for θ, the integral in Eq. (7b) can be performed analytically; and in the limit $T \to \sigma_0$, there results

$$w(0) = \frac{\left(\frac{T}{\tau}\right)^2\left[8 - \pi^2 + (4\pi - 8)\left(\frac{P_x}{s\tau}\right) - 4\left(\frac{P_x}{s\tau}\right)^2\right] + (4\pi - 8)\left(\frac{T}{\tau}\right)\left(\frac{E_s}{\tau}\right)\left(\frac{P_x}{s\tau}\right)}{8\left(\frac{T}{\tau}\right)\left(\frac{P_x}{s\tau}\right)^2} \quad . \tag{A.2}$$

With only the leading terms in $P_x/s\tau$ retained, the condition $w(0) = 0$ leads to Eq. (10).

Figures

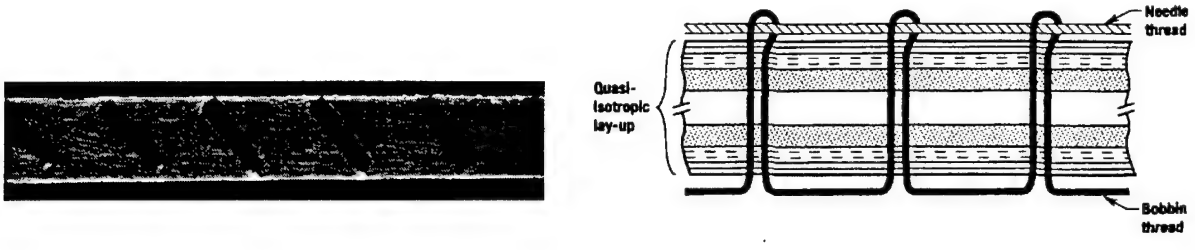

(a) (b)

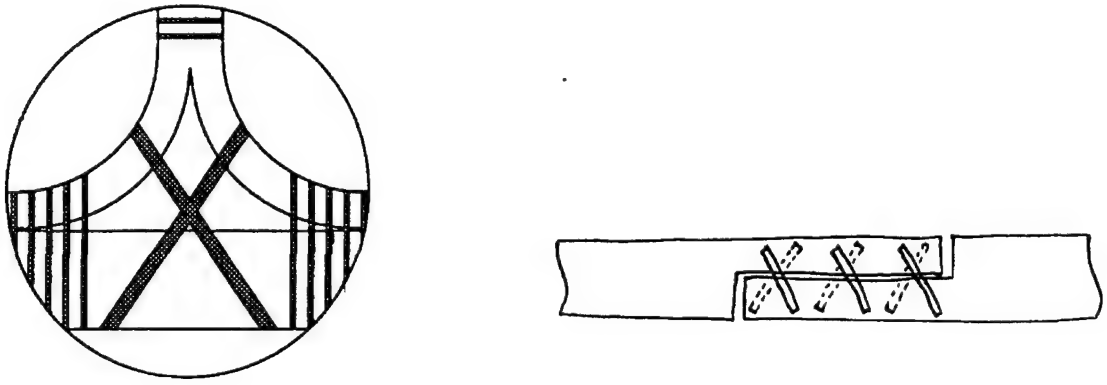

(c) (d)

1. Typical applications of through-thickness reinforcement. Skins reinforced to improve post-impact delamination resistance: (a) short rods and (b) stitching shown. Reinforced joints: (c) lap and (d) flange joints shown.

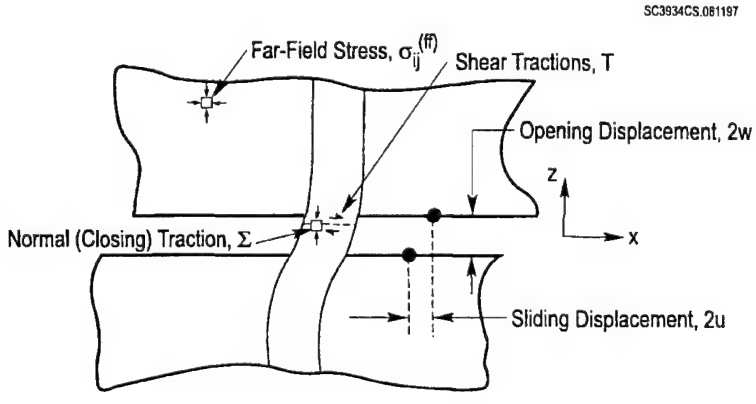

2. Bridging tractions and crack displacements.

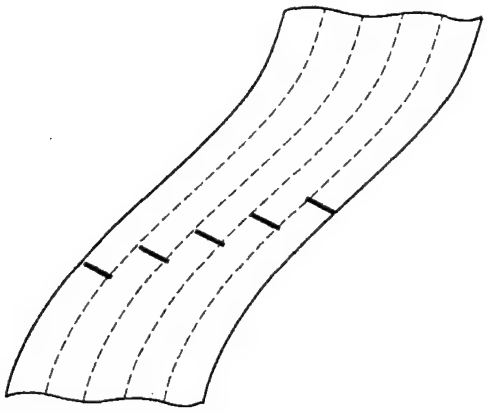

3. Schematic of splitting cracks in a stitch or short fibrous rod. The short line segments trace the separation of a single line in the undeformed stitch.

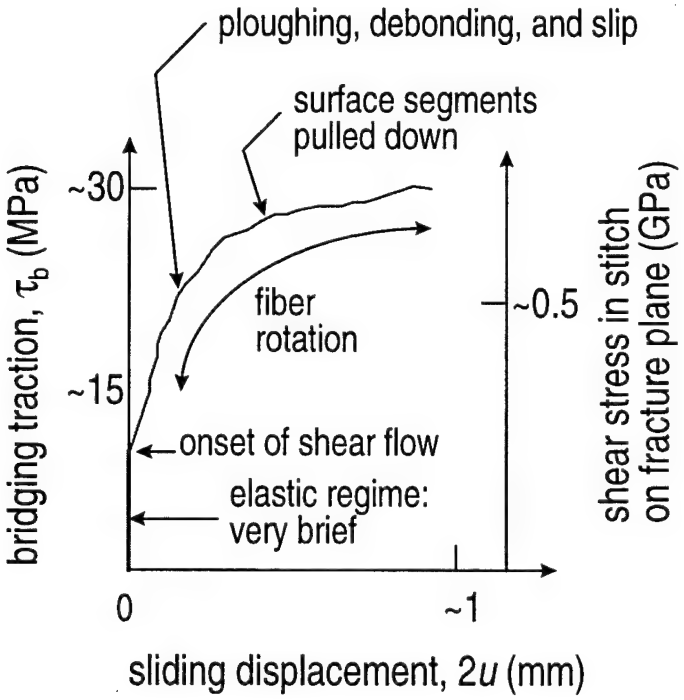

4. Summary of mechanisms and load levels in a single stitch loaded to failure in shear (from [18] and [22]).

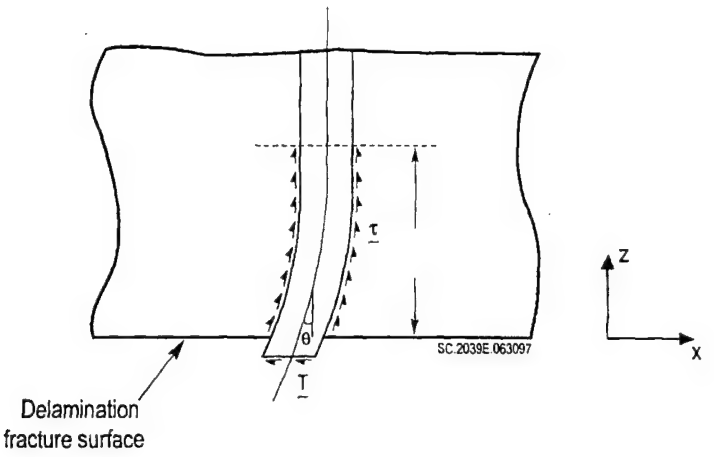

5. Nomenclature for the model for large displacements.

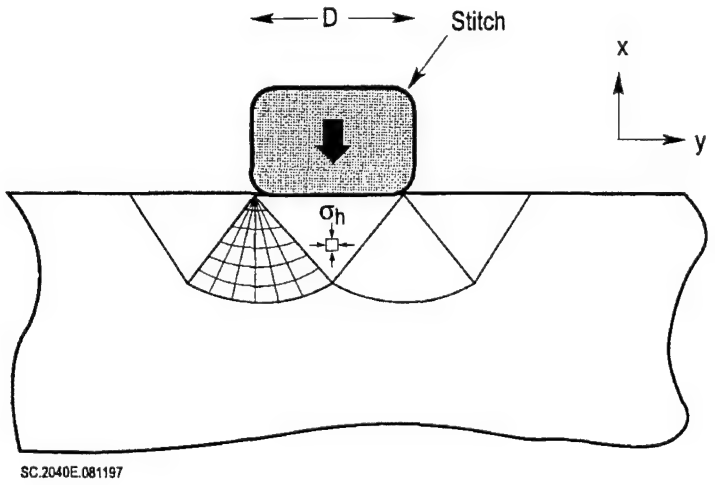

6. Lateral ploughing of a stitch through the laminate idealized as a punch problem in plane strain.

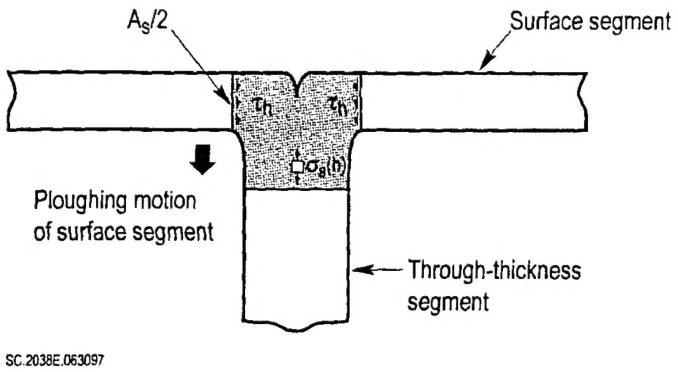

7. Force balance between the axial stress in a deformed stitch at the fracture plane and the boundary tractions acting on a representative element.

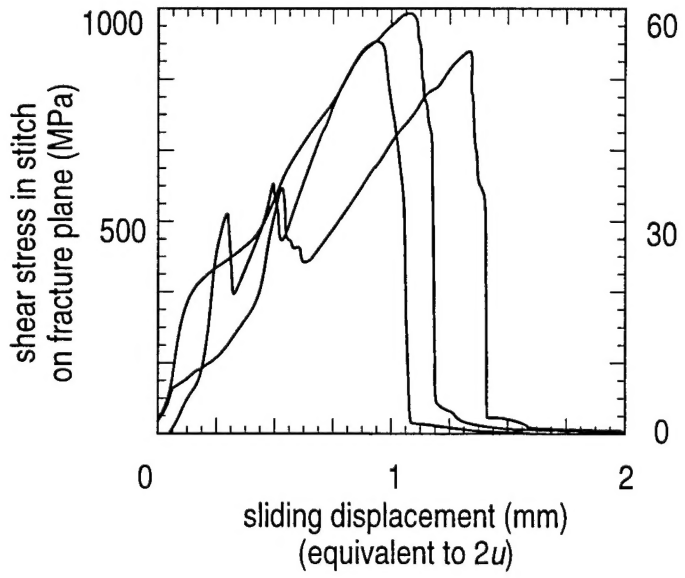

8. Shear traction-sliding displacement data from Turrettini [22] for carbon/epoxy laminate specimens containing a single stitch.

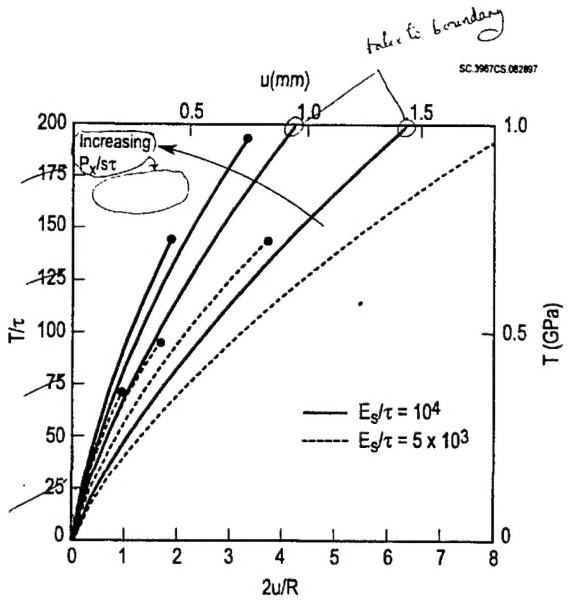

9. Shear traction-sliding displacement relation calculated for the two marked values of E_s/τ and for $P_x/s\tau = 20$, 40, 60, and 80. The lower and left axes show normalized variables (general cases); the right and upper axes, numbers for the particular material system defined in the text.

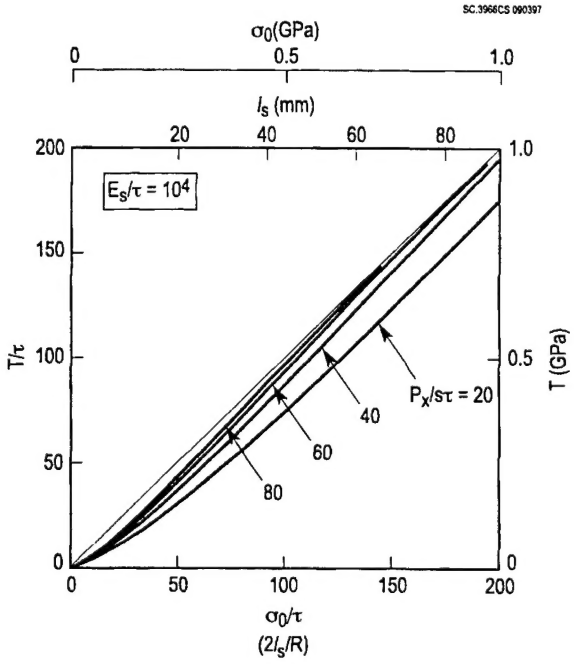

10. The shear traction on the fracture plane vs. the axial stress in the stitch at the fracture plane. The lower and left axes show normalized variables (general cases); the right and upper axes, numbers for the particular material system defined in the text. The upper axis has also been narked with the slip length, l_s, which is related to the axial stress by Eq. (3c).

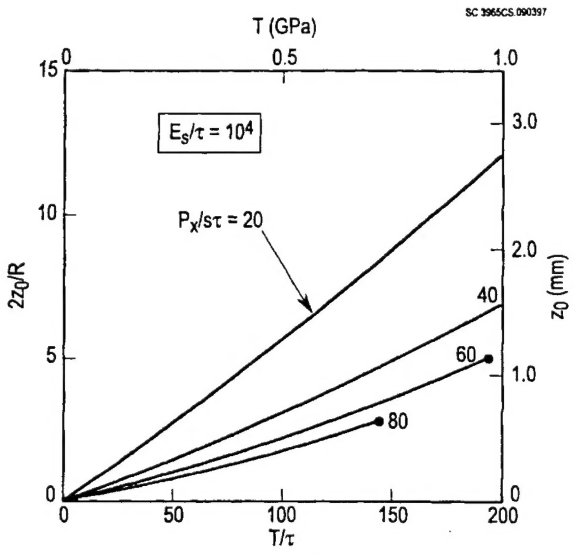

11. The maximum distance from the fracture plane over which curvature develops in the stitch as a function of the shear traction at the fracture plane. The lower and left axes show normalized variables (general cases); the right and upper axes, numbers for the particular material system defined in the text.

12. Traction law predicted for a laminate of finite thickness, $h = 4R$ (solid curves) superimposed over solutions for a semi-infinite laminate (dashed curves); for $P_x/s\tau = 20$, 40, 60, and 80; and $E_s/\tau = 10^4$.

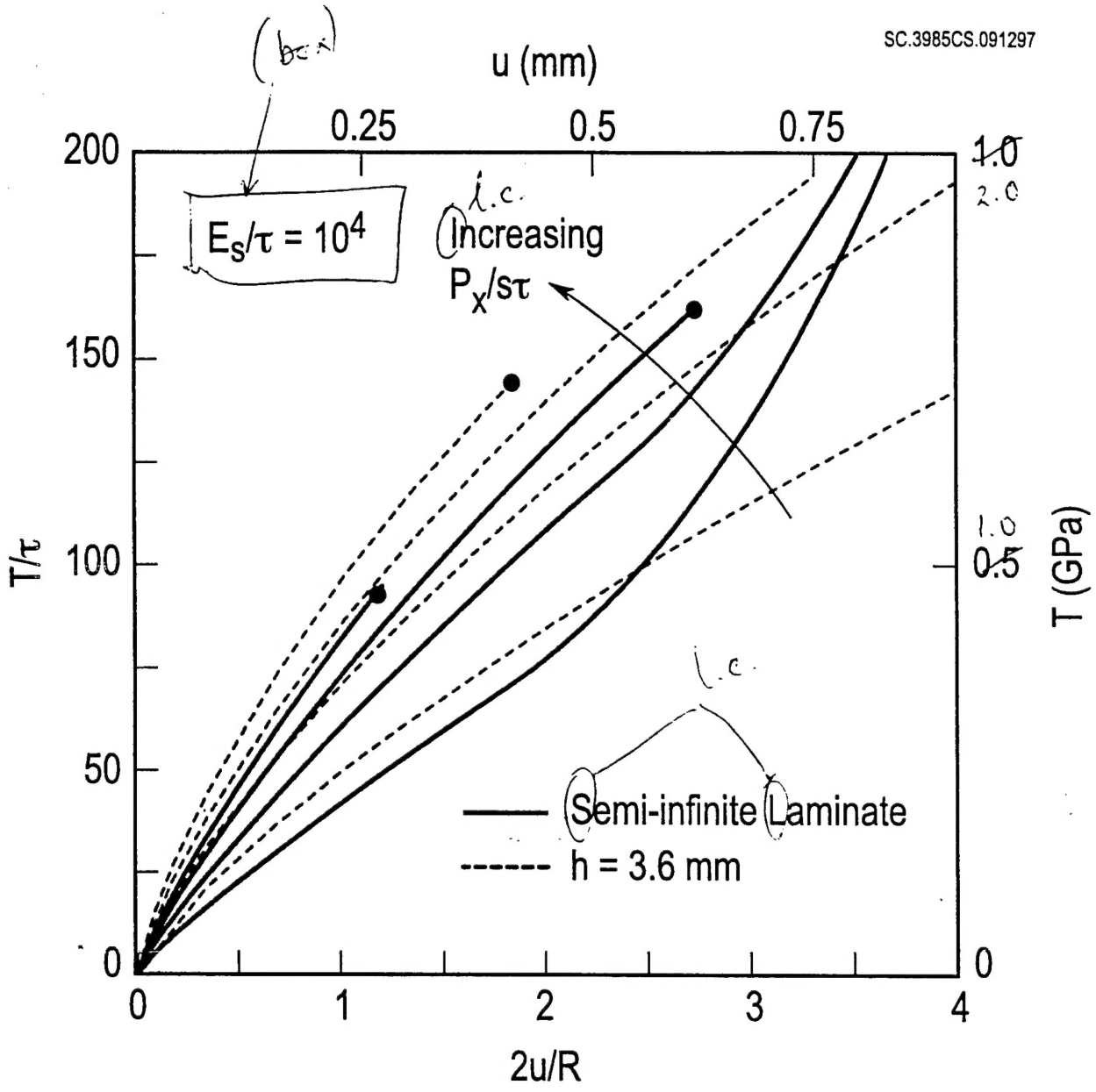
SC.3985CS.091297
u (mm)
0.25
0.5
0.75
200
150
100
50
0
T/τ
$E_s/\tau = 10^4$
Increasing
$P_x/s\tau$
1.0
2.0
1.0
0.5
T (GPa)
Semi-infinite Laminate
h = 3.6 mm
0
1
2
3
4
2u/R

12.